

Fractional relaxation noises, motions and the fractional energy balance equation

Shaun Lovejoy
Physics, McGill University,
3600 University st.
Montreal, Que. H3A 2T8
Canada

Abstract:

We consider the statistical properties of solutions of the stochastic fractional relaxation equation (a fractional Langevin equation) that has been proposed as a model for the ~~earth~~Earth's energy balance. In this equation, the (scaling) fractional derivative term models the energy storage processes that occur over a wide range of ~~space and time~~ scales. Up until now, stochastic fractional relaxation processes have ~~only~~ been considered with Riemann-Liouville fractional derivatives in the context of random walk processes where it yields highly nonstationary behaviour. ~~Instead, we consider~~ For our purposes we require the ~~stationary processes that are the~~stationary solutions of the Weyl fractional relaxation equations whose domain is $-\infty$ to t rather than 0 to t .

We ~~follow~~ develop a framework ~~developed~~ for handling the simplest fractional equations driven by Gaussian white noise forcings: fractional Gaussian noise (fGn) and fractional Brownian motion (fBm). ~~These more familiar processes are the high frequency limits. To avoid divergences, we follow the approach used in fractional Brownian motion (fBm): of The the~~ resulting fractional relaxation motions (fRm) and fractional relaxation noises (fRn) ~~generalize the more familiar fBm and fGn (fractional Gaussian noise). Since these processes are Gaussian, their properties are determined by their second order statistics; using Fourier and Laplace techniques, We we analytically determine both~~ develop power series as well as asymptotic expansions, ~~the small and large scale limits and We~~ show extensive analytic and numerical results on the autocorrelation functions, Haar fluctuations and spectra. We display sample realizations.

Finally, we discuss the prediction of fRn, fRm which – due to long memories is a *past* value problem, not an *initial* value problem (~~used for example in monthly and seasonal temperature forecasts~~). We develop an analytic formula for the fRn forecast skill and compare it to fGn. ~~Although T~~the large scale ~~white noise limit is attained in a slow power law manner is an (unpredictable) white noise that so that is attained in a slow power law manner;~~ when the temporal resolution of the series is small compared to the relaxation time (~~of the order of a few years in the Earth~~), fRn can mimic a long memory process with a wide range of exponents ~~wider than possible ranging from with~~ fGn ~~to or~~ fBm and beyond. We discuss the implications for monthly, seasonal, annual forecasts of the ~~earth~~Earth's temperature as well as for projecting the temperature to 2050 and 2100.

Style Definition: Normal: Font: Times New Roman, Indent: First line: 1.27 cm

Style Definition: Heading 1: Indent: Left: 0 cm, First line: 0 cm

Style Definition: Heading 2: Indent: Left: 0 cm, First line: 0 cm

Style Definition: MTDisplayEquation: Indent: First line: 0 cm

1. Introduction:

Over the last decades, stochastic approaches have rapidly developed and have spread throughout the geosciences. From early beginnings in hydrology and turbulence, stochasticity has made inroads in many traditionally deterministic areas. This is notably illustrated by stochastic parametrisations of Numerical Weather Prediction models, e.g. [Buizza *et al.*, 1999], and the “random” extensions of dynamical systems theory, e.g. [Chekroun *et al.*, 2010].

Pure stochastic approaches have developed primarily along two distinct lines. One is the classical (integer ordered, ~~linear~~) stochastic differential equation approach based on the Itô ~~or Stratonovich calculus~~ that goes back to the 1950’s (see the useful review [Dijkstra, 2013]). The other is the scaling strand that encompasses both linear (monofractal, [Mandelbrot, 1982]) and nonlinear (multifractal) models (see the review [Lovejoy and Schertzer, 2013]) ~~that are based on phenomenological scaling models, notably cascade processes~~. These and other stochastic approaches have played important roles in nonlinear Geoscience.

Up until now, the scaling and differential equation strands of stochasticity have had surprisingly little overlap. This is at least partly for technical reasons: integer ordered stochastic differential equations have exponential Green’s functions that are incompatible with wide range scaling. However, this shortcoming can – at least in principle – be easily overcome by introducing at least some derivatives of fractional order. Once the (typically) ad hoc restriction to integer orders is dropped, the Green’s functions are ~~based on~~ “generalized exponentials” ~~and these that are in turn~~ are based ~~instead on~~ fractional powers laws (see the review [Podlubny, 1999]). The integer-ordered stochastic equations that have received most attention are thus ~~the exceptional-special, nonscaling-special~~ cases. In physics they correspond to classical Langevin equations; in geophysics and climate modelling, they correspond to the Linear Inverse Modelling (LIM) approach that goes back to [Hasselmann, 1976] later elaborated notably by [Penland and Magorian, 1993], [Penland, 1996], [Sardeshmukh *et al.*, 2000], [Sardeshmukh and Sura, 2009] and [Newman, 2013]. Although LIM is not the only stochastic approach to climate, in two recent representative multi-author collections ([Palmer and Williams, 2010] and [Franzke and O’Kane, 2017]), all 32 papers shared the integer ordered assumption [Franzke and O’Kane, 2017], [Franzke and O’Kane, 2017] (the single exception being [Watkins, 2017], see also [Watkins *et al.*, 2020]).

Under the title “Fractal operators” [West *et al.*, 2003], reviews and emphasizes that in order to yield scaling behaviours, it suffices that stochastic differential equations contain fractional derivatives. However, when it is the time derivatives of stochastic variables that are fractional - fractional Langevin equations (FLE) - ~~then the~~ relevant processes are generally non-Markovian [Jumarie, 1993], so that there is no Fokker-Planck (FP) equation describing the ~~corresponding~~ probabilities of the corresponding fractional Langevin equation (see however [Schertzer *et al.*, 2001] for fractional spatial partial derivative equations). Furthermore, we expect that - as with the simplest scaling stochastic model - fractional Brownian motion (fBm, [Mandelbrot and Van Ness, 1968]) - that the solutions will not be semi-~~Martingales~~ martingales and hence that the Itô calculus used for integer ordered equations will not be applicable (see [Biagini *et al.*, 2008]). This may explain the relative paucity of mathematical literature on stochastic fractional equations (see however [Karczewska and Lizama, 2009]). In statistical physics, starting with [Mainardi and Pironi,

1996]. [Metzler and Klafter, 2000]. [Lutz, 2001] and helped with numerics, the FLE (and a more general “Generalized Langevin Equation” [Kou and Sunney Xie, 2004]. [Watkins et al., 2019]) has received a little more attention as a model for (nonstationary) particle diffusion (see [West et al., 2003] for an introduction, or [Vojta et al., 2019] for a more recent example).

These technical difficulties explain the apparent paradox of Continuous Time Random Walks (CTRW) and other approaches to anomalous diffusion that involve fractional equations. While CTRW probabilities are governed by the deterministic fractional ordered Generalized Fractional Diffusion equation (e.g. [Hilfer, 2000]. [Coffey et al., 2012]), the walks themselves are based on specific particle jump models rather than (stochastic) Langevin equations. Alternatively, a (spatially) fractional ordered Fokker-Planck equation may be derived from an integer-ordered but nonlinear Langevin equation for a diffusing particle driven by an (infinite variance) Levy motion [Schertzer et al., 2001]. [Kobeleev and Romanov, 2000b; Mainardi and Pironi, 1996; Vojta et al., 2019; West et al., 2003]

In nonlinear geoscience, it is all too common for mathematical models and techniques developed primarily for mathematical reasons, to be subsequently applied to the real world. This approach - effectively starting with a solution and then looking for a problem - occasionally succeeds, yet historically the converse has generally proved more fruitful. The proposal that an understanding of the Earth’s energy balance requires the Fractional Energy Balance Equation (FEBE, [Lovejoy et al., 2020b], announced in [Lovejoy, 2019b]) [Lovejoy, 2019b] is an example of the latter. First, the scaling exponent of macroweather (monthly, seasonal, interannual) temperature stochastic variability was determined ($H_I \approx -0.085 \pm 0.02$) and shown to permit skillful global temperature predictions, [Lovejoy, 2015], [Lovejoy et al., 2015], [Del Rio Amador and Lovejoy, 2019], [Del Rio Amador and Lovejoy, 2020a; Del Rio Amador and Lovejoy, 2020b]. Then, the multidecadal deterministic response to external (anthropogenic) forcing was shown to also obey a scaling law but with a different exponent [Hebert, 2017], [Lovejoy et al., 2017], [Procyk et al., 2020] ($H_F \approx -0.5 \pm 0.2$). It was only later that it was realized that the FEBE naturally accounts for both the high and low frequency exponents with $H = H_I + 1/2$ and $H_F = -H$ with the empirical exponents recovered with a FEBE of order $H \approx 0.42 \pm 0.02$. The realization that the FEBE fit the basic empirical facts motivated the present research into its statistical properties.

[Coffey et al., 2012; Hilfer, 2000]

In this paper, we consider the fractional energy balance equation (FEBE) which is a stochastic fractional relaxation equation ([Lovejoy et al., 2020a]), it is the FLE for the Earth’s temperature treated as a stochastic variable. The FEBE is a model determines of the earth’s global temperature where when the key energy storage processes are scaling and modelled by a fractional time derivative term. Whereas earlier approaches ([van Hateren, 2013], [Rypdal, 2012], [Hebert, 2017], [Lovejoy et al., 2017]) postulated that the climate response function itself is scaling, the FEBE instead situates the scaling in the energy storage processes [Hebert, 2017; Lovejoy et al., 2017; Rypdal, 2012; van Hateren, 2013].

The FEBE. The FEBE differs from the classical energy balance equation (EBE) in several ways. Whereas the EBE is integer ordered and describes the deterministic, exponential relaxation of the earth’s temperature to thermodynamic equilibrium (Newton’s law of cooling), the FEBE is both stochastic and of fractional order. The FEBE

unites the forcings due to internal and external variabilities. Whereas the former represents the forcing and response to the unresolved degrees of freedom - the “internal variability” - and is treated as a zero mean Gaussian noise, and the latter represents the external (e.g. anthropogenic) forcing and the forced response modelled as by the (deterministic) ensemble average of the total external forcing. Complementary work [Procyk et al., 2020] focuses on the deterministic FEBE equation and its application to projecting the Earth’s temperature to 2100.

An important but less obvious subtle EBE - FEBE difference is that whereas the former is an *initial* value problem whose initial condition is the earth’s temperature at $t = 0$, the FEBE is effectively a *past* value problem whose prediction skill improves with the amount of available past data and - depending on the parameters - it can have an enormous memory. To understand this, we recall that an important aspect of fractional derivatives is that they are defined as convolutions over various domains. To date, the main one that has been applied to physical problems is the Riemann-Liouville (RL, and the related Caputo) fractional derivative in which the domain of the convolution is the interval between an initial time $= 0$ and a later time t . This is the exclusive domain considered in Podlubny’s mathematical monograph on deterministic fractional differential equations [Podlubny, 1999] as well as in the stochastic fractional physics discussed in [West et al., 2003], [Herrmann, 2011], [Atanackovic et al., 2014], and most of the papers in [Hilfer, 2000] (with the partial exceptions of [Schuessel et al., 2000], and [Nonnenmacher and Metzler, 2000]). A key point of the FEBE is that it is instead based on Weyl fractional derivatives i.e. derivatives defined over semi-infinite domains, here from $-\infty$ to t . This is the natural range to consider for the Earth’s energy balance and it is needed to obtain statistically stationary responses. Although in some respects this semi-infinite domain is easy to handle the statistics of the resulting processes are not available in the literature.

Physically, in the EBE, the earth’s energy storage is modelled by a uniform slab of material implying that when perturbed, the temperature exponentially relaxes to a new thermodynamic equilibrium. whereas in However, the actual energy storage involves a hierarchy of mechanisms and the assumption that this storage is scaling the FEBE, is justified by the observed spatial scaling of atmospheric, oceanic and surface (e.g. topographic) structures (reviewed in [Lovejoy and Schertzer, 2013]). A consequence is that it is instead modelled by a scaling hierarchy of storage mechanisms so that the temperature relaxes to equilibrium in a power law rather than exponential manner.

This is the phenomenological justification for the FEBE developed in [Lovejoy et al., 2020b] where [Lovejoy and Schertzer, 2013] the fractional derivative of order H is an empirically determined parameter with $H = 1$ corresponding to the classical (exponential) exception. Alternatively, [Lovejoy, 2020a; b] [Lovejoy, 2019a] used Babenko’s operator method to show that the special $H = 1/2$ FEBE - the Half-ordered Energy Balance Equation (HEBE) - could be derived analytically from the classical Budyko-Sellers energy balance models ([Budyko, 1969], [Sellers, 1969]). To obtain the HEBE, it is only necessary to improve the mathematical treatment of the radiative boundary conditions in the classical energy transport equation. In other words, the $H = 1/2$ process discussed below is completely classical.

[Lovejoy, 2015] An important but less obvious EBE - FEBE difference is that whereas the former is an *initial* value problem whose initial condition is the earth’s temperature at

Field Code Changed

Formatted: Font: Italic

Formatted: Font: Italic

Formatted: Font: Italic

Formatted: Font: Italic

$t = 0$, the FEBE is effectively a *past* value problem whose prediction skill improves with the amount of available past data and — depending on the parameters — it can have an enormous memory. To understand this, we recall that an important aspect of fractional derivatives is that they are defined as convolutions over various domains. To date, the main one that has been applied to physical problems is the Riemann-Liouville (RL) fractional derivative in which the domain of the convolution is the interval between an initial time $= 0$ and a later time t . This is the exclusive domain considered in Podlubny's mathematical monograph on deterministic fractional differential equations [Podlubny, 1999] as well as in the stochastic fractional physics discussed in [West et al., 2003]. A key point of the FEBE is that it is instead based on Weyl fractional derivatives i.e. derivatives defined over semi infinite domains, here from $-\infty$ to t .

The purpose of this paper is to understand various statistical properties of the statistically stationary solutions of noise driven Weyl fractional relaxation - oscillation differential equations. We focus on the Weyl fractional relaxation equation that underpins the FEBE, particularly its stationary noise solution — “fractional Relaxation noise” (fRn) - and the its fRn integral “fractional Relaxation motion” (fRm) with stationary increments. These fRn, fRm are direct extensions of the widely studied fractional Gaussian noise (fGn) and fractional Brownian motion (fBm) processes. We derive the main statistical properties of both fRn and fRm including spectra, correlation functions and (stochastic) predictability limits needed for forecasting the earthEarth temperature ([Lovejoy et al., 2015], [Del Rio Amador and Lovejoy, 2019], [Del Rio Amador and Lovejoy, 2020a; Del Rio Amador and Lovejoy, 2020b]) or projecting it to 2050 or 2100 [Hébert et al., 2020], [Procyk et al., 2020].

The choice of a Gaussian white noise forcing was made both for theoretical simplicity but also for physical realism. While the temperature forcings in the (nonlinear) weather regime are highly intermittent, multifractal, in the lower frequency macroweather regime over which the FEBE applies it quite exceptional inasmuch as its intermittency is low so that the temperature anomalies are not far from Gaussian ([Lovejoy, 2018]). Responses to multifractal or Levy process FEBE forcings are likely however to be of interest elsewhere.

This paper is structured as follows. In section 2 we present the classical models of fractional Brownian motion and fractional Gaussian noise as solutions to fractional Langevin equations and define the corresponding fractional Relaxation motions (fRm) and fractional Relaxation noises (fRn) as generalizations. We develop a general framework for handling Gaussian noise driven linear fractional Weyl equations taking care of both high and low frequency divergence issues. Applying this to fBm, fRm we show that they both have stationary increments. Similarly, application of the framework to fGn and fRn shows that they are stationary noises (i.e. with small scale divergences). In section 3 we discuss analytic formulae for the second order statistics including autocorrelations, structure functions, Haar fluctuations and spectra that determine all the corresponding statistical properties (with many details in appendix A). In section 4 we discuss the problem of prediction — important for macroweather forecasting - deriving expressions for the theoretical prediction skill as a function of forecast lead time. In section 5 we conclude and in appendix B, we derive the properties of the HEBE special case.

Formatted: Indent: First line: 1 cm

2. Unified treatment of fBm and fRm:

2.1 fRn, fRm, fGn and fBm

In the introduction, we outlined physical arguments [Lovejoy et al., 2020a] argued that the ~~earth~~Earth's global energy balance could be well modelled by the (linearized) fractional energy balance equation, ~~more details will be published elsewhere~~. Taking T as the globally averaged temperature, τ_r as the characteristic time scale for energy storage/relaxation processes, ~~and~~ F as the (stochastic) forcing (energy flux; power per area), and λ the climate sensitivity (temperature increase per unit flux of forcing) the FEBE can be written in Langevin form as:

$$\tau_r^H \left({}_a^H D_t^H T \right) + T = \lambda F \quad (1)$$

Where ~~where (for $0 < H < 1$)~~ the Riemann-Liouville fractional derivative symbol ${}_a^H D_t^H$ is defined as:

$${}_a^H D_t^H T = \frac{1}{\Gamma(1-H)} \int_a^t (t-s)^{-H} T'(s) ds; \quad T' = \frac{dT}{ds}$$

$${}_a^H D_t^H T = \frac{1}{\Gamma(1-H)} \frac{d}{dt} \int_a^t (t-s)^{-H} T(s) ds; \quad 0 < H < 1 \quad (2)$$

Where Γ is the standard gamma function. Derivatives of order $\nu > 1$ can be obtained using $\nu = H + m$ where m is the integer part of ν , and then applying this formula to the m^{th} ordinary derivative. The main case studied in applications (e.g. random walks) is $a = 0$ so that Laplace transform techniques are often used; (alternatively, the somewhat different the “Riemann-Liouville-Caputo fractional derivative” ${}_0^H D_t^H$ is used). However, ~~here~~ we will be interested in $a = -\infty$; $a = -\infty$: the “Weyl fractional derivative” $_{-\infty}^H D_t^H$ which is naturally handled by Fourier techniques (section 3.5 and appendix A), and in this case, the distinction is unimportant. Although it is in many respects simpler, the statistical characterizations and prediction properties are not available in the literature justifying the following developments.

Since equation 1 is linear, by taking ensemble averages, it can be decomposed into deterministic and random components with: the former driven by the mean forcing ~~external to system~~ $\langle F \rangle_t$ - representing the forcing external to system - and the latter by the ~~fluctuating~~ stochastic ~~fluctuating~~ component $F - \langle F \rangle_t$ - representing the internal forcing due to the driving the internal internal-variability. In [Lovejoy et al., 2020a] Elsewhere we will primarily considered the deterministic part, in the following, we consider the simplest purely stochastic model in which $\langle F \rangle = 0$ and $F = \gamma$ where γ is a Gaussian “delta correlated” white noise:

$$\langle \gamma(s) \rangle = 0; \quad \langle \gamma(s) \gamma(u) \rangle = \delta(s-u) \quad (3)$$

In [Hebert, 2017], [Lovejoy et al., 2017], [Hébert et al., 2020], [Hébert et al., 2020] it was argued on the basis of an empirical study of ocean- atmosphere coupling that $\tau_r \approx 2$

Formatted: Font: Italic, Subscript

Field Code Changed

Formatted: Font: Symbol

Formatted: Font: Italic

years ([recent work indicates a value somewhat higher, \(\$\approx 5\$ years, \[Procyk et al., 2020\]\)](#) and in [Lovejoy et al., 2015] [Lovejoy et al., 2020a] and [Del Rio Amador and Lovejoy, 2019] that the value $H \approx 0.4$ reproduced both the [earthEarth's](#) temperature both at scales $\gg \tau_r$ as well as for macroweather scales (longer than the weather regime scales of about 10 days) but still $< \tau_r$.

When $0 < H < 1$, eq. 1 with $\gamma(t)$ replaced by a deterministic forcing is a fractional generalization of the usual ($H = 1$) relaxation equation; when $1 < H < 2$, it is a generalization of the usual ($H = 2$) oscillation equation, the “fractional oscillation equation”, see e.g. [Podlubny, 1999]. This classification is based on the deterministic equations; for the noise driven equations, we find that there are two critical exponents $H = 1/2$ and $H = 3/2$ and hence three ranges. Although we focus on the range $0 < H < 3/2$ (especially $0 < H < 1/2$), we also give results for the full range $0 < H < 2$ that includes the [strong](#) oscillation range.

To simplify the development, we use the relaxation time τ to nondimensionalize time i.e. to replace time by t/τ_r to obtain the canonical Weyl fractional relaxation equation:

$$(-\infty D_t^H + 1)U_H = \gamma; \quad U_H = \frac{dQ_H}{dt} \quad (-\infty D_t^H + 1)U_H = \gamma(t); \quad U_H = \frac{dQ_H}{dt} \quad (4)$$

for the [nondimensional](#) process U_H . The dimensional solution of eq. 1 with [nondimensional](#) $F = \gamma = \lambda F$ is simply $T(t) = \tau_r^{-1} U_H(t/\tau_r)$ so that in the nondimensional eq. 4, the characteristic transition “relaxation” time between dominance by the high frequency (differential) and the low frequency (U_H term) is $t = 1$. Although we give results for the full range $0 < H < 2$ - i.e. both the “relaxation” and “oscillation” ranges - for simplicity, we refer to the solution $U_H(t)$ as “fractional Relaxation noise” (fRn) and to $Q_H(t)$ as “fractional Relaxation motion” (fRm). Note that we take $Q_H(0) = 0$ so that Q_H is related to U_H via an ordinary integral from time = 0 to t and that fRn is only strictly a noise when $H \leq 1/2$.

In dealing with fRn and fRm, we must be careful of various small and large t divergences. For example, eqs. 1 and 4 are the fractional Langevin equations corresponding to generalizations of integer ordered stochastic diffusion equations: the solution with the classical $H = 1$ value is the Ornstein-Uhlenbeck process. Since $\gamma(t)$ is a “generalized function” - a “noise” - it does not converge at a mathematical instant in time, it is only strictly meaningful under an integral sign. Therefore, a [more](#) standard form of eq. 4 is obtained by integrating both sides by order H : (i.e. by differentiating by $-H$ and assuming that differentiation and integration of order H commute):

$$U_H(t) = -\infty D_t^{-H} U_H + -\infty D_t^{-H} \gamma = -\frac{1}{\Gamma(H)} \int_{-\infty}^t (t-s)^{H-1} U_H(s) ds + \frac{1}{\Gamma(H)} \int_{-\infty}^t (t-s)^{H-1} \gamma(s) ds \quad (5)$$

(see e.g. in [Karczewska and Lizama, 2009]). The white noise forcing in the above is statistically stationary; we show below that the solution for $U_H(t)$ is also statistically stationary. It is tempting to obtain an equation for the motion $Q_H(t)$ by integrating eq. 4 from $-\infty$ to t to obtain the fractional Langevin equation: $-\infty D_t^H Q_H + Q_H = W$ where W is Wiener process (a [usual-standard](#) Brownian motion) satisfying $dW = \gamma(t)dt$.

Formatted: Font: Symbol

Formatted: Font: Italic

Formatted: Font: Symbol

Formatted: Font: Italic

Formatted: Font: Not Italic

Formatted: MTDisplayEquation, Indent: First line: 0 cm

Unfortunately the Wiener process integrated $-\infty$ to t almost surely diverges, hence we relate Q_H to U_H by an integral from 0 to t .

In the high frequency limit, the derivative dominates and we obtain fRn and fRm are generalizations of fractional Gaussian noise (fGn, F_H) and fractional Brownian motion (fBm, B_H); this can be seen since the latter satisfy the simpler fractional Langevin equation:

$$-_{\infty} D_t^H F_H = \gamma(t); \quad F_H = \frac{dB_H}{dt} \quad (6)$$

Whose solution F_H is the fractional Gaussian noise process (fGn), and whose integral B_H is fractional Brownian motion (fBm). We thus anticipate that F_H and B_H are the high frequency limits of fRn, fRm. so that F_H is a Weyl fractional integration of order H of a white noise and if $H=0$, then F_H itself is a white noise and B_H is it's ordinary integral (from time $= 0$ to t), a usual Brownian motion, it satisfies $B_H(0) = 0$ (F_H is not to be confused with the forcing F).

Before continuing, a comment is necessary on the use of the symbol H that Mandelbrot introduced for fBm in honour of E. Hurst's-Hurst who pioneering-pioneered the study of long memory processes in Nile flooding [Hurst, 1951]. First, note that eq. 6 implies that the root mean square (RMS) increments of B_H over intervals Δt grow as

$$\left\langle \Delta B_H(\Delta t)^2 \right\rangle^{1/2} \propto \Delta t^{H+1/2} \text{ (see below). Since fBm is often defined by this scaling property,}$$

it is usual to use the fBm exponent $H_B = H+1/2$. In terms of H_B , from eq. 6, we see that fGn (F_H) is a fractional integration of a white noise of order $H = H_B - 1/2$, whereas fBm is an integral of order $H_B + 1/2$, the $1/2$ being a consequence of the fundamental scaling of the Wiener measure whose density is $\gamma(t)$. While the parametrization in terms of H_B is convenient for fGn and fBm, in this paper, we follow [Schertzer and Lovejoy, 1987] who more generally used H to denote an order of fractional integration. This more general usage includes the use of H as a general order of fractional integration in the Fractionally Integrated Flux (FIF) model [Schertzer and Lovejoy, 1987] which is the basis of space-time multifractal modelling (see the monograph [Lovejoy and Schertzer, 2013]). In the FIF generalization, the density of a Wiener measure (i.e. the white noise forcing in eq. 6) is replaced by the density of a (conservative) multifractal measure. The scaling of this multifractal measure is different from that of the Wiener measure so that the extra $1/2$ term does not appear. A consequence is that in multifractal processes, H simultaneously characterizes the order of fractional differentiation/integration ($H < 0$ or $H > 0$), and has a straightforward empirical interpretation as the "fluctuation exponent" that characterizes the rate at which fluctuations grow ($H > 0$) or decay ($H < 0$) with scale. In comparison, for fBm, the critical H distinguishing integration and differentiation is still zero, but $H > 0$ or $H < 0$ corresponds to fluctuation exponents $H_B > 1/2$ or $H_B < 1/2$; which for these Gaussian processes is termed "~~persistence~~-persistence" and "~~antipersistence~~antipersistence". There are therefore several H 's in the literature and in the paper below, we continue to denote the order of the fractional integration by H but we relate it to other exponents as needed.

2.2 Green's functions

As usual, we can solve inhomogeneous linear differential equations by using appropriate Green's functions:

Formatted: Font: Italic

Formatted: Font: Italic, Subscript

$$F_H(t) = \int_{-\infty}^t G_{0,H}^{(fGn)}(t-s) \gamma(s) ds$$

$$U_H(t) = \int_{-\infty}^t G_{0,H}^{(fRn)}(t-s) \gamma(s) ds$$
(7)

Where $G_{0,H}^{(fGn)}$ and $G_{0,H}^{(fRn)}$ are Green's functions for the differential operators corresponding respectively to D_t^H and $D_t^H + 1$.

$G_{0,H}^{(fGn)}$ and $G_{0,H}^{(fRn)}$ are the usual “impulse” (Dirac) response Green's functions (hence the subscript “0”). For the differential operator Ξ they satisfy:

$$\Xi G_{0,H}(t) = \delta(t)$$
(8)

Integrating this equation we find an equation for their integrals $G_{1,H}$ which are thus “step” (Heaviside, subscript “1”) response Green's functions satisfying:

$$\Xi G_{1,H}(t) = \Theta(t); \quad \Theta(t) = \int_{-\infty}^t \delta(s) ds$$

$$\frac{dG_{1,H}}{dt} = G_{0,H}$$
(9)

where Θ is the Heaviside (step) function. The inhomogeneous equation:

$$\Xi f(t) = F(t)$$
(10)

has a solution in terms of either an impulse or a step Green's function:

$$f(t) = \int_{-\infty}^t G_{0,H}(t-s) F(s) ds = \int_{-\infty}^t G_{1,H}(t-s) F'(s) ds; \quad F'(s) = \frac{dF}{ds}$$
(11)

the equivalence being established by integration by parts with the conditions $F(-\infty) = 0$ and $G_{1,H}(0) = 0$. The use of the step rather than impulse response is standard in the Energy Balance Equation literature since it gives direct information on energy balance and the approach to equilibrium (see e.g. [Lovejoy et al., 2020b]). The step response for the noise is also the basic impulse response function for the motion (although care is needed for the convergence, see below).

For fGn, the Green's functions are simply the kernels of Weyl fractional integrals:

$$F_H(t) = \frac{1}{\Gamma(H)} \int_{-\infty}^t (t-s)^{H-1} \gamma(s) ds$$
(12)

obtained by integrating both sides of eq. 6 by order H . We conclude:

Field Code Changed

Formatted: Font: Not Italic

Formatted: Font: Italic

$$G_{0,H}^{(fGn)} = \frac{t^{H-1}}{\Gamma(H)}; \quad -\frac{1}{2} \leq H < \frac{1}{2} \quad (13)$$

$$G_{1,H}^{(fGn)} = \frac{t^H}{\Gamma(H+1)};$$

Similarly, appendix A shows that for fRn, dDue to the statistical stationarity of the white noise forcing $\gamma(t)$, that the Riemann-Liouville Green's functions can be used:

$$U_H(t) = \int_{-\infty}^t G_{0,H}^{(fRn)}(t-s) \gamma(s) ds \quad (14)$$

with:

$$G_{0,H}^{(fRn)}(t) = \sum_{n=1}^{\infty} (-1)^{n+1} \frac{t^{nH-1}}{\Gamma(nH)} \quad 0 < H \leq 2 \quad (15)$$

$$G_{1,H}^{(fRn)}(t) = \sum_{n=1}^{\infty} (-1)^{n+1} \frac{t^{nH}}{\Gamma(nH+1)}$$

so that $G_{0,H}^{(fGn)}$, $G_{1,H}^{(fGn)}$ are simply the first terms in the power series expansions of the corresponding fRn, fRm Green's functions.

We now recall some classical results useful in geophysical applications. First, These these Green's functions are often equivalently written in terms of Mittag-Leffler functions ("generalized exponentials"), $E_{\alpha,\beta}$:

$$G_{0,H}^{(fRn)}(t) = t^{H-1} E_{H,H}(-t^H) \quad E_{\alpha,\beta}(z) = \sum_{n=0}^{\infty} \frac{z^n}{\Gamma(\alpha n + \beta)}$$

$$G_{1,H}^{(fRn)}(t) = t^H E_{H,H+1}(-t^H) \quad H \geq 0 \quad (16)$$

By taking integer H , the Γ functions reduce to factorials and $G_{0,H}$, $G_{1,H}$ reduce to exponentials hence, $G_{0,H}^{(fRn)}$, $G_{1,H}^{(fRn)}$ are sometimes called "generalized exponentials". Finally Second, we note that at the origin, for $0 < H < 1$, $G_{0,H}$ is singular whereas $G_{1,H}$ is regular so that it is often may be advantageous to use the latter (step) response function (for example in the numerical simulations in section 4). These Green's function responses are shown in figure 1. When $0 < H \leq 1$, the step response is monotonic; in an energy balance model, this would correspond to relaxation to thermodynamie equilibrium. When $1 < H < 2$, we see that there is overshoot and oscillations around the long term value; it is therefore (presumably) outside the physical range of an equilibrium process.

In order to understand the relaxation process – i.e. the approach to the asymptotic value 1 in fig. 1 for the step response $G_{1,H}$ – we need the asymptotic expansions:

Formatted: Indent: First line: 1 cm

Commented [SL1]: check: is this term for the ML or for the GReen?

Field Code Changed

Formatted: MTDisplayEquation

Commented [SL2]: check: is this term for the ML or for the GReen?

$$G_{\zeta,H}^{(fRn)}(t) = \sum_{n=0}^{\infty} \frac{(-1)^n}{\Gamma(\zeta - nH)} t^{\zeta-1-nH}; \quad t \gg 1 \quad (17)$$

Where $G_{\zeta,H}(t)$ is the ζ order (fractionally) integrated impulse response $G_{0,H}$. Specifically, for $\zeta = 0, 1$ we obtain the special cases corresponding to impulse and step responses:

$$G_{0,H}^{(fRn)}(t) = H \sum_{n=1}^{\infty} (-1)^{n+1} \frac{t^{-1-nH}}{\Gamma(1-nH)}; \quad t \gg 1$$

$$G_{0,H}^{(fRn)}(t) = \sum_{n=0}^{\infty} (-1)^n \frac{t^{-1-nH}}{\Gamma(-nH)}; \quad t \gg 1$$

$$G_{1,H}^{(fRn)}(t) = \sum_{n=0}^{\infty} (-1)^n \frac{t^{-nH}}{\Gamma(1-nH)}; \quad t \gg 1 \quad (18)$$

($0 < H < 1$, $1 < H < 2$; note that the $n = 0$ terms are 0, 1 for $G_{0,H}^{(fRn)}$, $G_{1,H}^{(fRn)}$ respectively)

[Podlubny, 1999], i.e. power laws in t^H rather than t^H . According to this, the asymptotic approach to the step function response (bottom row in fig. 1) is a slow, power law process. In the FEBE, this implies for example that the classical CO₂ doubling experiment would yield a power law rather than exponential approach to a new thermodynamic equilibrium. Comparing this to the EBE, i.e. the special case $H = 1$, we have:

$$G_{0,1}(t) = e^{-t}; \quad G_{1,1}(t) = 1 - e^{-t} \quad (19)$$

so that when $H = 1$, the asymptotic step response is instead approached exponentially fast. There are also analytic formulae for fRn when $H = 1/2$ (the HEBE) discussed in appendix C notably involving logarithmic corrections.

Formatted: MTDisplayEquation, Indent: First line: 0 cm

Field Code Changed

Formatted: Font: Symbol

Formatted: Font: Italic

Formatted: Subscript

Formatted: Font: Italic, Subscript

Formatted: Font: Symbol

Commented [SL3]: Corrected sign! -1**n not -1**(n+1)

Field Code Changed

Field Code Changed

Formatted: Font: Italic

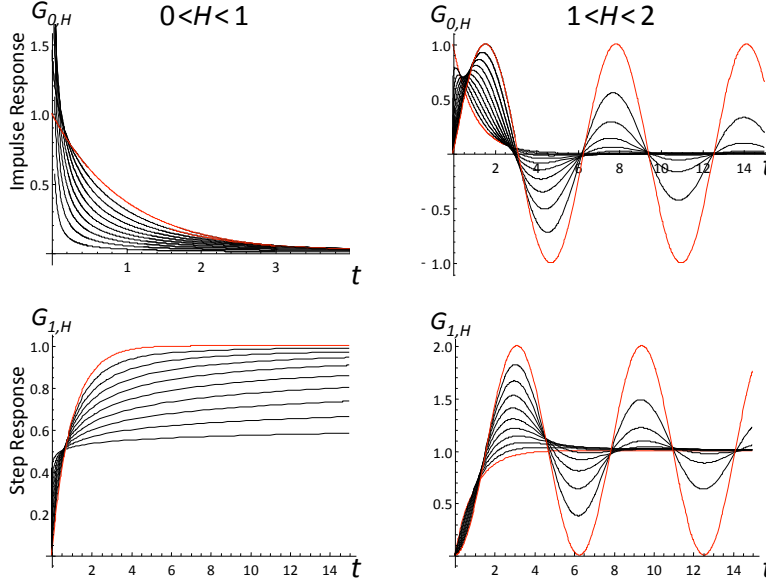


Fig. 1: The impulse (top) and step response functions (bottom) for the fractional relaxation range ($0 < H < 1$, left, red is $H = 1$, the exponential), the black curves, bottom to top are for $H = 1/10, 2/10, \dots, 9/10$) and the fractional oscillation range ($1 < H < 2$, red are the integer values $H = 1$, bottom, the exponential, and top, $H = 2$, the sine function, the black curves, bottom to top are for $H = 11/10, 12/10, \dots, 19/10$).

2.3 A family of Gaussian noises and motions:

In the above, we discussed fGn, fRn and their integrals fBm, fRm, but these are simply special cases: ~~a of a more general theory valid for a wide family variety of Green's functions that lead to convergent noises and motions could be used. We expect for example we expect our that our approach also to applies to the stochastic Basset's equation which could be regarded as a natural extension of the stochastic relaxation equation (see discussed in [Karczewska and Lizama, 2009] for the more general case of finite and complex vector-valued processes), which could be regarded as an extension of the stochastic relaxation equation.~~

With the motivation outlined in the previous sections, ~~and following~~ [Mandelbrot and Van Ness, 1968] (see also [Biagini et al., 2008]), the simplest way to proceed is to start by defining the general motion $Z_H(t)$ as:

$$Z_H(t) = N_H \int_{-\infty}^t G_{1,H}(t-s) \gamma(s) ds - N_H \int_{-\infty}^0 G_{1,H}(-s) \gamma(s) ds \quad (2019)$$

where N_H is a normalization constant and H is an index. It is advantageous to rewrite this in standard notation (e.g. [Biagini et al., 2008]) as:

$$Z_H(t) = N_H \int_{\mathbb{R}} (G_{1,H}(t-s)_+ - G_{1,H}(-s)_+) \gamma(s) ds \quad (2120)$$

where the “+” subscript indicates that the argument is $\rightarrow 0$, and the range of integration is over all the real axis \mathbb{R} . Here and throughout, the Green’s functions need only be specified for $t > 0$ corresponding to their causal range.

The advantage of starting with the motion Z_H is that it is based on the step response $G_{1,H}$ which is finite at small t ; the disadvantage is that integrals may diverge at large scales. The second (constant) term in eq. 20 was introduced by [Mandelbrot and Van Ness, 1968] for fBm precisely in order to avoid large scale divergences in fBm. ~~As discussed in appendix A,~~ The introduction of this constant physically corresponds to considering the long-time behaviour of the fractional random walks discussed in [Kobayashi and Romanov, 2000a] and [West et al., 2003]. The physical setting of the random walk applications is a walker ~~with position $X(t)$ and velocity $V(t)$. Assuming that the walker starts at the origin~~ ~~corresponds to~~ ~~corresponding~~ to a fractionally diffusing particle ~~whose velocity obeying~~ ~~obeys~~ the fractional Riemann-Liouville relaxation equation.

From the definition (eq. 19-20 or 2021), we have:

$$\langle Z_H(0) \rangle = 0; \quad Z_H(0) = 0 \quad Z_H(0) = 0; \quad \langle Z_H(0) \rangle = 0 \quad (2224)$$

Hence, the origin plays a special role, so that the $Z_H(t)$ process is nonstationary.

The variance $V_H(t)$ of Z_H (not to be confused with the velocity of a random walker) is:

$$V_H(t) = \langle Z_H^2(t) \rangle = N_H^2 \int_{\mathbb{R}} (G_{1,H}(t-s)_+ - G_{1,H}(-s)_+)^2 ds \quad (2322)$$

Equivalently, with an obvious change of ~~change of~~ variable:

$$V_H(t) = N_H^2 \int_0^\infty (G_{1,H}(s+t) - G_{1,H}(s))^2 ds + N_H^2 \int_0^t G_{1,H}(s)^2 ds \quad (2423)$$

so that $V_H(0) = 0$. Z_H will converge in a root mean square sense if V_H converges. If ~~$G_{1,H}$ is~~ ~~a power-law~~ at large scales: ~~$G_{1,H} \propto t^{H_l}$; $t \gg 1$~~ then $H_l < 1/2$ is required for

convergence. Similarly, if at small scales ~~$G_{1,H} \propto t^{H_h}$; $t \ll 1$~~ , then convergence of V_H requires $H_h > -1/2$. We see that for fBm (eq. 13), $H_l = H_h = H$ so that this restriction implies $-1/2 < H < 1/2$ which is equivalent to the usual range $0 < H_B < 1$ with $H_B = H + 1/2$. Similarly, for fRm, using $G^{(fRn)}_{1,H}(t)$, we have $H_h = H$, (eq. 15) and $H_l = -H$, (eq. 187) so that fRm converges for $H > -1/2$, i.e. over the entire range $0 < H < 2$ discussed in this paper. Since the small scale limit of fRm is fBm, we see that ~~the~~ range $0 < H < 2$ overlaps with the range of fBm and extends it at large H .

From eq. 2049 we can consider the statistics of the increments:

$$\begin{aligned} Z_H(t) - Z_H(u) &= N_H \int_{\mathbb{R}} (G_{1,H}(t-s)_+ - G_{1,H}(u-s)_+) \gamma(s) ds \\ &= N_H \int_{\mathbb{R}} (G_{1,H}(t-u-s')_+ - G_{1,H}(-s')_+) \gamma(s') ds'; \quad s' = s - u \end{aligned} \quad (2524)$$

Formatted: Subscript, Lowered by 6 pt

Formatted: Lowered by 6 pt

where we have used the fact that $\gamma(s') \stackrel{d}{=} \gamma(s)$ where $\stackrel{d}{=}$ means equality in a probability sense.

This shows that:

$$Z_H(t) - Z_H(u) \stackrel{d}{=} Z_H(t-u) - Z_H(0) = Z_H(t-u) \quad (2625)$$

so that the increments $Z_H(t)$ are stationary. From this, we obtain the variance of the increments $\Delta Z_H(\Delta t) = Z_H(t) - Z_H(t-\Delta t)$:

$$\langle \Delta Z_H(\Delta t)^2 \rangle = V_H(\Delta t); \quad \Delta t = t - u \quad (2726)$$

Since $Z_H(t)$ is a mean zero Gaussian process, its statistics are determined by the covariance function:

$$C_H(t, u) = \langle Z_H(t) Z_H(u) \rangle = \frac{1}{2} (V_H(t) + V_H(u) - V_H(t-u)) \quad (2827)$$

The noises are the derivatives of the motions and as we mentioned, depending on H , we only expect their finite integrals to converge. Let us therefore define the resolution τ noise $Y_{H,\tau}$ corresponding to the mean increments of the motions:

$$Y_{H,\tau}(t) = \frac{Z_H(t) - Z_H(t-\tau)}{\tau} \quad (2928)$$

The noise, $Y_H(t)$ can now be obtained as the limit $\tau \rightarrow 0$:

$$Y_H(t) = \frac{dZ_H(t)}{dt} \quad (3029)$$

Applying eq. 2627, we obtain the variance:

$$\langle Y_{H,\tau}(t)^2 \rangle = \langle Y_{H,\tau}^2 \rangle = \tau^{-2} V_H(\tau) \quad (3130)$$

since $\langle Y_{H,t}(0) \rangle = 0$, $Y_{H,\tau}(t)$ could be considered as the anomaly fluctuation of Y_H , so that $\tau^{-2} V_H(\tau)$ is the anomaly variance at resolution τ .

From the covariance of Z_H (eq. 2728) we obtain the correlation function:

$$\begin{aligned} R_{H,\tau}(\Delta t) &= \langle Y_{H,\tau}(t) Y_{H,\tau}(t-\Delta t) \rangle = \tau^{-2} \langle (Z_H(t) - Z_H(t-\tau))(Z_H(t-\Delta t) - Z_H(t-\Delta t-\tau)) \rangle \\ &= \tau^{-2} \frac{1}{2} (V_H(\Delta t - \tau) + V_H(\Delta t + \tau) - 2V_H(\Delta t)) \quad \Delta t \geq \tau \end{aligned}$$

$$R_{H,\tau}(0) = \langle Y_{H,\tau}(t)^2 \rangle = \tau^{-2} V_H(\tau); \quad \Delta t = 0 \quad (3231)$$

Alternatively, taking time in units of the resolution $\lambda = \Delta t/\tau$:

$$\begin{aligned} R_{H,\tau}(\lambda\tau) &= \langle Y_{H,\tau}(t) Y_{H,\tau}(t-\lambda\tau) \rangle = \tau^{-2} \langle (Z_H(t) - Z_H(t-\tau))(Z_H(t-\lambda\tau) - Z_H(t-\lambda\tau-\tau)) \rangle \\ &= \tau^{-2} \frac{1}{2} (V_H((\lambda-1)\tau) + V_H((\lambda+1)\tau) - 2V_H(\lambda\tau)) \quad \lambda \geq 1 \end{aligned}$$

$$R_{H,\tau}(0) = \langle Y_{H,\tau}(t)^2 \rangle = \tau^{-2} V_H(\tau); \quad \lambda = 0 \quad (3332)$$

Formatted: Lowered by 6 pt

Formatted: Indent: First line: 0 cm

Formatted: Lowered by 6 pt

Formatted: Lowered by 6 pt

Formatted: Lowered by 6 pt

Formatted: Lowered by 6 pt

$R_{H,\tau}$ can be conveniently written in terms of centred finite differences:

$$R_{H,\tau}(\lambda\tau) = \frac{1}{2} \Delta_\tau^2 V_H(\lambda\tau) \approx \frac{1}{2} V_H''(\Delta t); \quad \Delta_\tau f(t) = \frac{f(t+\tau/2) - f(t-\tau/2)}{\tau} \quad (3433)$$

The finite difference formula is valid for $\Delta t \geq \tau$. For finite τ , it allows us to obtain the correlation behaviour by replacing the second difference by a second derivative, an approximation [that](#) is very good except when Δt is close to τ .

Taking the limit $\tau \rightarrow 0$ in eq. [343](#) to obtain the second derivative of V_H , and after some manipulations, we obtain the following simple formula for the limiting function $R_H(\Delta t)$:

$$R_H(\Delta t) = \frac{1}{2} \frac{d^2 V_H(\Delta t)}{d\Delta t^2} = N_H^2 \int_0^\infty G_{0,H}(s + \Delta t) G_{0,H}(s) ds; \quad G_{0,H} = \frac{dG_{1,H}}{ds} \quad (3534)$$

If the integral for V_H converges, this integral for $R_H(\Delta t)$ will also converge except possibly at $\Delta t = 0$ (in the examples below, when $H \leq 1/2$).

Eq. [354](#) shows that R_H is the correlation function of the noise:

$$Y_H(t) = \int_{-\infty}^t G_{0,H}(t-s) \gamma(s) ds \quad Y_H(t) = N_H \int_{-\infty}^t G_{0,H}(t-s) \gamma(s) ds \quad (3635)$$

This result could have been derived formally from:

$$Y_H(t) = Z_H'(t) = \frac{dZ_H(t)}{dt} = \frac{d}{dt} \int_{-\infty}^t G_{1,H}(t-s) \gamma(s) ds;$$

$$= \int_{-\infty}^t G_{0,H}(t-s) \gamma(s) ds$$

$$Y_H(t) = Z_H'(t) = \frac{dZ_H(t)}{dt} = N_H \frac{d}{dt} \int_{-\infty}^t G_{1,H}(t-s) \gamma(s) ds$$

$$= N_H \int_{-\infty}^t G_{0,H}(t-s) \gamma(s) ds \quad (3736)$$

but [our-the above](#) derivation explicitly handles the convergence issues.

A useful statistical characterization of the processes is by the statistics of ~~its~~ [their](#) Haar fluctuations over an interval Δt . For an interval Δt , Haar fluctuations are the differences between the averages of the first and second halves of an interval. For the noise Y_H , the Haar fluctuation is:

$$\Delta Y_H(\Delta t)_{Haar} = \frac{2}{\Delta t} \int_{t-\Delta t/2}^t Y_H(s) ds - \frac{2}{\Delta t} \int_{t-\Delta t}^{t-\Delta t/2} Y_H(s) ds$$

([3837](#))

In terms of $Z_H(t)$:

Field Code Changed

Field Code Changed

Formatted: MTDisplayEquation

Field Code Changed

$$\Delta Y_H(\Delta t)_{Haar} = \frac{2}{\Delta t} (Z_H(t) - 2Z_H(t - \Delta t/2) + Z_H(t - \Delta t))$$

(3938)

Therefore:

$$\begin{aligned} \langle \Delta Y_H(\Delta t)_{Haar}^2 \rangle &= \left(\frac{2}{\Delta t} \right)^2 \left(2 \langle \Delta Z_H(\Delta t/2)^2 \rangle - 2 \langle Y_{H,\Delta t/2}(t) Y_{H,\Delta t/2}(t - \Delta t/2) \rangle \right) \\ &= \left(\frac{2}{\Delta t} \right)^2 (4V_H(\Delta t/2) - V_H(\Delta t)) \end{aligned}$$

(4039)

This formula will be useful below.

3 Application to fBm, fGn, fRm, fRn:

3.1 fBm, fGn:

The above derivations were for noises and motions derived from differential operators whose impulse and step Green's functions had convergent $V_H(t)$. Before applying them to fRn, fRm, we illustrate this by applying them first to fBm and fGn.

The fBm results are obtained by using the fGn step Green's function (eq. 13) in eq. 243 to obtain:

$$V_H^{(fBm)}(t) = N_H^2 \left(\frac{2 \sin(\pi H) \Gamma(-1-2H)}{\pi} \right) t^{2H+1}, \quad -\frac{1}{2} \leq H < \frac{1}{2}$$

(4140)

The standard normalization and parametrisation is:

$$\begin{aligned} N_H = K_H &= \left(\frac{\pi}{2 \sin(\pi H) \Gamma(-1-2H)} \right)^{1/2} \\ &= \left(-\frac{\pi}{2 \cos(\pi H_B) \Gamma(-2H_B)} \right)^{1/2}; \end{aligned} \quad H_B = H + \frac{1}{2}; \quad 0 \leq H_B < 1$$

(4241)

This normalization turns out to be convenient ~~for both not only for fBm and fRm but also for fRm~~ so that we use it below to obtain:

$$V_{H_B}^{(fBm)}(t) = t^{2H+1} = t^{2H_B}; \quad 0 \leq H_B < 1$$

(4342)

so that:

$$\langle \Delta B_H(\Delta t)^2 \rangle^{1/2} = \Delta t^{H_B}; \quad \Delta B_H(\Delta t) = B_H(t) - B_H(t - \Delta t)$$

(4443)

so – as mentioned earlier – H_B is the fluctuation exponent for fBm. Note that fBm is usually defined as the Gaussian process with V_H given by eq. 43 i.e. with this normalization (e.g. [Biagini et al., 2008]).

We can now calculate the correlation function relevant for the fGn statistics. With the normalization ~~$N_H = K_H$~~ :

Formatted: Indent: First line: 0 cm

Commented [SL4]: Note the -ve sign removed!

Field Code Changed

Commented [SL5]: Changed sign and removed bad numerator factor

Field Code Changed

Formatted: Font: Italic

Formatted: Font: Italic

Formatted: Font: Italic, Subscript

$$R_{H,\tau}^{(fGn)}(\lambda\tau) = \frac{1}{2}\tau^{2H-1}\left((\lambda+1)^{2H+1} + (\lambda-1)^{2H+1} - 2\lambda^{2H+1}\right); \quad \lambda \geq 1; \quad -\frac{1}{2} < H < \frac{1}{2}$$

$$R_{H,\tau}^{(fGn)}(0) = \tau^{2H-1}$$

$$R_{H_B,\tau}^{(fGn)}(\lambda\tau) \approx H(2H+1)(\lambda\tau)^{2H-1} = H_B(2H_B-1)(\lambda\tau)^{2(H_B-1)}; \quad -\frac{1}{2} < H < \frac{1}{2}, \quad \lambda \gg 1 \quad (4544)$$

the bottom ~~line~~-approximations are valid for large scale ratios λ . We note the difference in sign for $H_B > 1/2$ (“persistence”), and for $H_B < 1/2$ (“antipersistence”). When $H_B = 1/2$, the noise corresponds to usual-standard Brownian motion, it is uncorrelated.

3.2 fRm, fRn

3.2.1 $V_H(t)$

Since fRm, fRn are Gaussian, their properties are determined by their second order statistics, by $V_H(t)$, $R_H(t)$. These statistics are second order in $G_{0,H}(t)$ and can most easily be determined using the Fourier representation of $G_{0,H}(t)$, (section 3.5, appendix A). The development is challenging because unlike the $G_{0,H}(t)$ functions that are entirely expressed in series of fractional powers of t , $V_H(t)$ and $R_H(t)$ involve mixed fractional and integer power expansions, the details are given in appendix A, here we summarize the main results. To lighten the notation, we drop the superscripts “fRn”, “fRm” and use the unnormalized functions ($N_H = 1$).

First, for the motions, we have:

$$V_H(t) = 2 \sum_{n=2}^{\infty} D_n \Gamma(-1-Hn) t^{1+Hn} + 2 \sum_{j=1, \text{odd}}^{\infty} F_j \frac{t^{j+1}}{\Gamma(j+2)}; \quad 0 < H < 2$$

$$D_n = (-1)^n \frac{\sin\left(nH\frac{\pi}{2}\right) \sin\left((n-1)H\frac{\pi}{2}\right)}{2\pi \sin\left(H\frac{\pi}{2}\right)}$$

$$F_j = -\frac{1}{\pi H} \cot\left(\frac{\pi H}{2}\right) \left(\Phi\left(-1, 1, 1 - \frac{j}{H}\right) + \Phi\left(-1, 1, \frac{j}{H}\right) \right)$$

where Φ is the Hurwitz-Lerch phi function $\Phi(z, s, a) = \sum_{n=0}^{\infty} z^n (n+a)^{-s}$. When $0 < H < 1/2$,

then the leading term is t^{1+Hn} with $n = 2$, so that the coefficient can be used for normalization: $N_H^{-2} = K_H^{-2} = 2D_2\Gamma(-1-2H)$ (the fBm normalization). When $1/2 < H < 2$, then this becomes negative, so that it cannot be used, however in this case, the leading term is t^2 and its coefficient may be used for normalization:

Formatted: Normal

Formatted: Font: Italic

Formatted: Font: Italic

Formatted: Font: Italic

Formatted: Font: Italic, Subscript

Formatted: MTDisplayEquation, Indent: First line: 0 cm

$$N_H^{-2} = F_1 = -\frac{1}{\pi H} \cot\left(\frac{\pi H}{2}\right) \left(\Phi\left(-1, 1, 1 - \frac{1}{H}\right) + \Phi\left(-1, 1, \frac{1}{H}\right) \right) = \int_0^\infty G_{0,H}(s)^2 ds; \quad 1/2 < H < 2$$

(4746)

(see section 3.5 A for the relation with $G_{0,H}$). Since $\Phi\left(-1, 1, 1 - \frac{j}{H}\right)$ diverges for all integer

j/H and since we sum over odd integer j , the expansion only converges for irrational H . Therefore, the convergence properties are not clear, but due to the presence of the Γ functions they appear to converge for all t although the convergence is slow (see the numerical results in appendix A, and also for a slightly different expansion that converges more rapidly, useful in applications).

For multidecadal global climate projections, the relaxation time has been estimated at ≈ 5 years ([Procyk et al., 2020]), so that we are interested in the long time behaviour (exploited for example in [Hébert et al., 2020]). For this, asymptotic expansions are useful, in appendix A we show that:

$$V_H(t) = t + a_H - 2 \sum_{n=1}^{\infty} D_{-n} \Gamma(-1 + nH) t^{1-nH} + 2P_{H,-}(t); \quad t \gg 1$$

(4847)

where we have included the term:

$$P_{H,\pm}(t) = 0; \quad 0 < H < 1$$

$$P_{H,\pm}(t) = -e^{i \cos(\frac{\pi}{H})} \frac{\sin\left(\pm \frac{\pi}{H} + \frac{H\pi}{2} + t \sin\left(\frac{\pi}{H}\right)\right)}{H \sin\left(\frac{\pi H}{2}\right)}; \quad 1 < H < 2$$

(4948)

for $1 < H < 2$, $\cos(\pi/H) < 0$ so that at large t , $P_H(t)$ is subdominant, however it explains the oscillations visible in fig. 2. The constant a_H can be determined numerically if needed.

For convenience, the leading terms of the normalized V_H are:

$$V_H^{(norm)}(t) = t^{1+2H} + O(t^{1+3H}) + O(t^2); \quad N_H = K_H = (2D_2 \Gamma(-1-2H))^{-1/2}; \quad 0 < H < 1/2$$

(5049)

and for $1/2 < H < 2$, using $N_H = (F_1)^{-1/2}$:

$$V_H^{(norm)}(t) = t^2 - \frac{2\Gamma(-1-2H) \sin(\pi H)}{\pi F_1} t^{1+2H} + O(t^{1+3H}); \quad 1/2 < H < 3/2$$

(5150)

$$V_H^{(norm)}(t) = t^2 + \frac{F_3}{12F_1} t^4 + O(t^{2H+1}); \quad 3/2 < H < 2$$

Formatted: Font: Not Italic

Formatted: Font: Italic

Note that for $3/2 < H < 2$, $F_3 = -\int_0^\infty G'_{0,H}(s)^2 ds$ (appendix A). The change in normalization for $H > 1/2$ is necessary since $K_H^2 < 0$ for this range. Fig. 2 shows plots of $V^{(norm)}_H(t)$, the small t^2 behaviour for $H > 1/2$ corresponds to fRm increments $\langle \Delta Q_H^2(\Delta t) \rangle^{1/2} = (V_H^{(norm)}(\Delta t))^{1/2} \approx \Delta t$ i.e. to a smooth process, differentiable of order 1; see section 3.4.

Since $\langle \Delta Q_H(\Delta t)^2 \rangle = V_H(\Delta t)$, the corrections imply that at large scales $\langle \Delta Q_H(\Delta t)^2 \rangle^{1/2} < \Delta t^{1/2}$ so that the fRm process Q_H appears to be anti-persistent at large scales.

3.2.2 $R_H(t)$

The formulae for R_H can be obtained from the above using $R_H(t) = (1/2) d^2 V_H(t) / dt^2$ (eq. 35, appendix A):

$$R_H(t) = \sum_{n=2}^{\infty} D_n \Gamma(1-Hn) t^{-1+Hn} + \sum_{j=1, \text{ odd}}^{\infty} F_j \frac{t^{j-1}}{\Gamma(j)} \quad (5251)$$

The normalized autocorrelation functions are thus:

$$R_H^{(norm)}(t) = H(1+2H)t^{-1+2H} + O(t^{-1+3H}); \quad t \ll 1; \quad 0 < H < 1/2$$

$$R_H^{(norm)}(t) = 1 - \frac{\Gamma(1-2H) \sin(\pi H)}{\pi F_1} t^{-1+2H} + O(t^{-1+3H}); \quad t \ll 1; \quad 1/2 < H < 3/2$$

$$R_H^{(norm)}(t) = 1 + \frac{t^2}{2F_1} F_3 + O(t^{-1+2H}) \dots; \quad t \ll 1; \quad 3/2 < H < 2 \quad (5352)$$

(note $F_3 < 0$ for $3/2 < H < 2$).

The asymptotic expansions are:

$$R_H(t) = -\sum_{n=1}^{\infty} D_{-n} \Gamma(1+nH) t^{-(1+nH)} + P_{H,+}(t); \quad t \gg 1 \quad (5453)$$

(when $0 < H < 1/2$, for $t \approx \tau$ we must use the exact resolution τ fGn formula, eq. 45, top, note the absolute value sign for $1/2 < H < 3/2$). For large t :

$$R_H(t) = -\frac{1}{\Gamma(-H)} t^{-1-H} + O(t^{-1-2H}); \quad 0 < H < 2; \quad t \gg 1. \quad (5554)$$

Note that for $0 < H < 1$, $\Gamma(-H) < 0$ so that $R > 0$ over this range (fig. 3). Formulae 53 shows that there are three qualitatively different regimes: $0 < H < 1/2$, $1/2 < H < 3/2$, $3/2 < H < 2$;

Formatted: Indent: First line: 0 cm

Formatted: MTDisplayEquation

Formatted: MTDisplayEquation

Formatted: Indent: First line: 0 cm

this is in contrast with the deterministic relaxation and oscillation regimes ($0 < H < 1$ and $1 < H < 2$). We return to this in section 3.4.

Now that we have worked out the behaviour of the correlation function, we can comment on the issue of the memory of the process. Starting in turbulence, there is the notion of “integral scale” that is conventionally defined as the long time integral of the correlation function. When the integral scale diverges, the process is conventionally termed a “long memory process”. With this definition, if the long time exponent of R_H is ≥ -1 , then the process has a long memory. Eq. 55 shows that the long time exponent $= -(1+H)$ so that for all H considered here, the integral scale converges. However, it is of the order of the relaxation time which may be much larger than the length of the available sample series. For example, eq. 55 shows that when $H < 1/2$, the effective exponent $2H-1$ implies (in the absence of a cut-off), a divergence at long times, so that up to the relaxation scale, fRn mimics a long memory process.

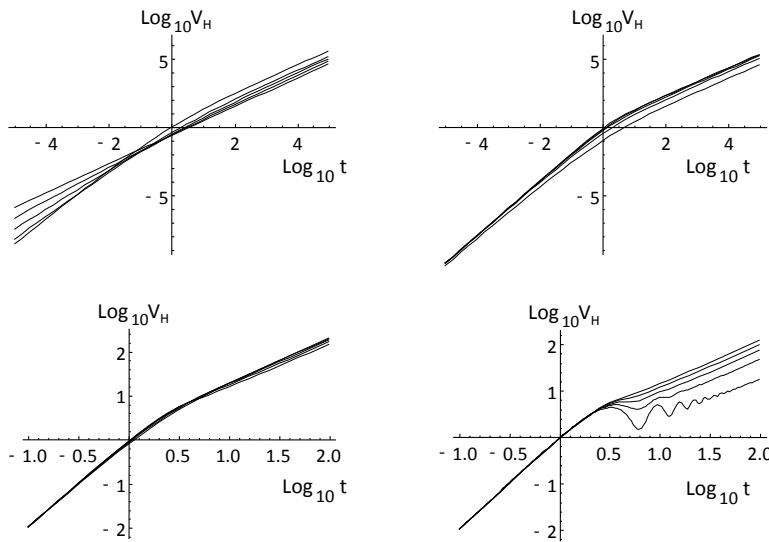


Fig. 2: The normalized V_H functions for the various ranges of H for fRn. The plots from left to right, top to bottom are for the ranges $0 < H < 1/2$, $1/2 < H < 1$, $1 < H < 3/2$, $3/2 < H < 2$. Within each plot, the lines are for H increasing in units of $1/10$ starting at a value $1/20$ above the plot minimum; overall, H increases in units of $1/10$ starting at a value $1/20$, upper left to $39/20$, bottom right (ex. for the upper left, the lines are for $H = 1/20, 3/10, 5/20, 7/20, 9/20$). For all H 's the large t behaviour is linear (slope = 1, although note the oscillations for the lower right hand plot for $3/2 < H < 2$). For small t , the slopes are $1+2H$ ($0 < H < 1/2$) and 2 ($1/2 < H < 2$).

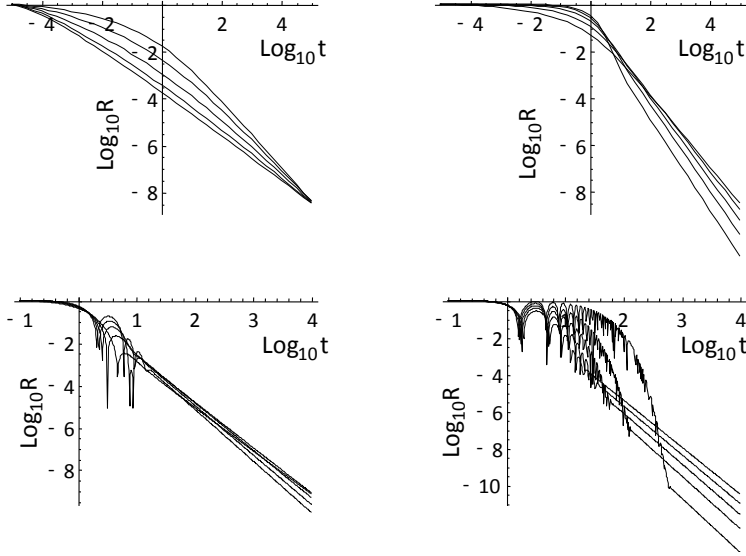


Fig. 3: The normalized correlation functions R_H for fRn corresponding to the V_H function in fig. 2 $0 < H < 1/2$ (upper left) $1/2 < H < 1$ (upper right), $1 < H < 3/2$ lower left, $3/2 < H < 2$ lower right. In each plot, the curves correspond to H increasing from bottom to top in units of $1/10$ starting from $1/20$ (upper left) to $39/20$ (bottom right). For $H < 1/2$, the resolution is important since $R_{H,\tau}$ diverges at small τ . In the upper left figure, $R_{H,\tau}$ is shown with $\tau = 10^{-5}$; they were normalized to the value at resolution $\tau = 10^{-5}$, for $H > 1/2$, the curves are normalized with $N_H = F_3^{-1/2}$. In all cases, the large t slope is $-1-H$.

uncorrelated:

3.2 fRm, fRn

There are various cases to consider, appendix B gives some of the mathematical details including a small t series expansions for $0 < H < 3/2$; the leading terms are:

(45)

$$V_H^{(fRm)}(t) = t^2 - \frac{2\Gamma(-1-2H)\sin(\pi H)}{\pi C_H^2} t^{1+2H} + O(t^{1+3H}); \quad N_H = C_H^{-1}, \quad 1/2 < H < 3/2$$

$$V_H^{(fRm)}(t) = t^2 - \frac{t^4}{12C_H^2} \int_0^\infty G_{0,H}^{(fRm)}(s)^2 ds + O(t^{2H+1}); \quad 3/2 < H < 2$$

$$C_H^2 = \int_0^\infty G_{0,H}^{(fRm)}(s)^2 ds$$

All for $t \ll 1$. The change in normalization for $H > 1/2$ is necessary since $K_H^2 < 0$ for this range. Similarly, the $H > 1/2$ normalization cannot be used for $H < 1/2$ since C_H diverges for $H < 1/2$. See fig. 2 for plots of $V_H^{(fRm)}(t)$. Note that the small t^2 behaviour for $H > 1/2$ corresponds to fRm increments $\langle \Delta Q_H^2(\Delta t) \rangle^{1/2} = \left(V_H^{(fRm)}(\Delta t) \right)^{1/2} \approx \Delta t$ i.e. to a smooth process, differentiable of order 1; see section 3.4.

For large t , we have:

$$\begin{aligned} V_H^{(fRm)}(t) &= N_H^2 \left[t - \frac{2t^{1-H}}{\Gamma(2-H)} + a_H + O(t^{1-2H}) \right]; & H < 1 \\ V_H^{(fRm)}(t) &= N_H^2 \left[t + a_H - \frac{2t^{1-H}}{\Gamma(2-H)} + O(t^{1-2H}) \right]; & H > 1 \end{aligned}$$

(46)

where a_H is a constant, the above is valid for $t \gg 1$. Since $\langle \Delta Q_H(\Delta t)^2 \rangle = V_H(\Delta t)$, the corrections imply that at large scales $\langle \Delta Q_H(\Delta t)^2 \rangle^{1/2} < \Delta t^{1/2}$ so that the fRm process Q_H appears to be anti-persistent at large scales.

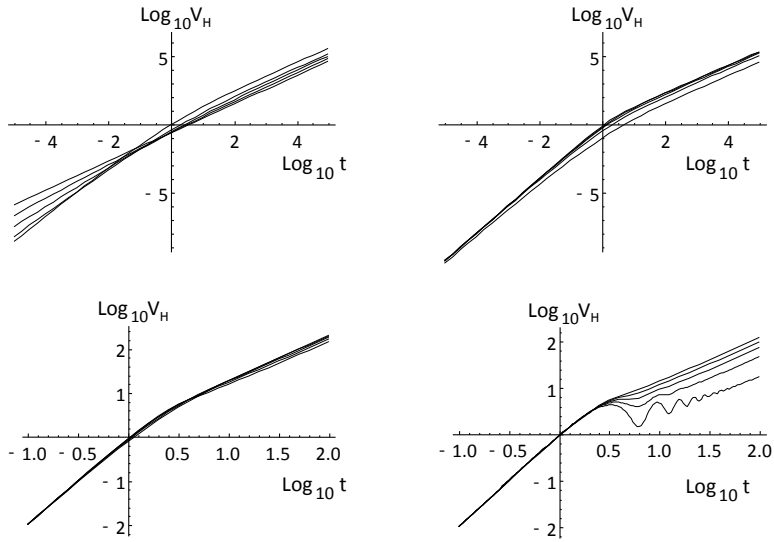


Fig. 2: The V_H functions for the various ranges of H for fRm (these characterize the variance of fRm). The plots from left to right, top to bottom are for the ranges $0 < H < 1/2$, $1/2 < H < 1$, $1 < H < 3/2$, $3/2 < H < 2$. Within each plot, the lines are for H increasing in units of $1/10$ starting at a value $1/20$ above the plot minimum (ex. for the upper left, the lines are for $H = 1/20, 3/10, 5/20, 7/20, 9/20$). For all H 's the large t behaviour is linear (slope = one, although note the oscillations for $3/2 < H < 2$). For small t , the slopes are $1+2H$ ($0 < H \leq 1/2$) and 2 ($1/2 \leq H < 2$).

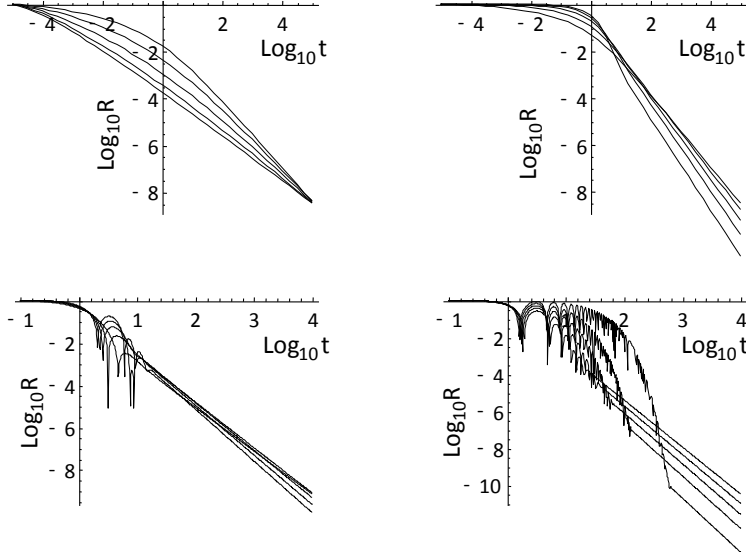


Fig. 3: The correlation functions R_H for fRn corresponding to the V_H function in fig. 2. $0 < H < 1/2$ (upper left), $1/2 < H < 1$ (upper right), $1 < H < 3/2$ (lower left), $3/2 < H < 2$ (lower right). In each plot, the curves correspond to H increasing from bottom to top in units of $1/10$ starting from $1/20$ (upper left) to $39/20$ (bottom right). For $H < 1/2$, the $R_{H,\tau}$ are shown with $\tau = 10^{-5}$; they were normalized to the value at resolution $\tau = 10^{-5}$. For $H > 1/2$, the curves are normalized with $N_H = 1/C_H$; for $H < 1/2$, they were normalized to the value at resolution $\tau = 10^{-5}$. In all cases, the large t slope is $-1-H$.

The formulae for R_H can be obtained by differentiating the above results for V_H twice (eqs. 45, 46), see appendix B for details and Padé approximants):

$$R_H^{(fRn)}(t) = 1 - \frac{\Gamma(1-2H)\sin(\pi H)}{\pi C_H^2} t^{-1+2H} + O(t^{-1+3H}); \quad t \ll 1; \quad 1/2 < H < 3/2$$

$$R_H^{(fRn)}(t) = 1 - \frac{t^2}{2C_H^2} \int_0^\infty G'_{0,H}(s)^2 ds + O(t^{-1+2H}) \dots; \quad t \ll 1; \quad 3/2 < H < 2 \quad (47)$$

(when $0 < H < 1/2$, for $t \approx \tau$ we must use the resolution τ fGn formula, eq. 44, top).
For large t :

$$R_H^{(fRn)}(t) = -\frac{N_H^2}{\Gamma(-H)} t^{-1-H} + O(t^{-1-2H}): \quad 0 < H < 2 \quad ; \quad t \gg 1 \quad (48)$$

Note that for $0 < H < 1$, $\Gamma(-H) < 0$ so that $R > 0$ over this range (fig. 3). Also, when $H < 1/2$, we see (eq. 47) that $R_H(t)$ diverges in the small scale limit so that we must use $R_{H,\tau}(t)$ and the corresponding small t formula above is only valid for $1 \gg t \gg \tau$. When $t \approx \tau$, the exact formula (eq. 31) must be used. Formulae 45, 47 show that there are three qualitatively different regimes: $0 < H < 1/2$, $1/2 < H < 3/2$, $3/2 < H < 2$; this is in contrast with the deterministic relaxation and oscillation regimes ($0 < H < 1$ and $1 < H < 2$). We return to this in section 3.4.

Now that we have worked out the behaviour of the correlation function, we can comment on the issue of the memory of the process. Starting in turbulence, there is the notion of “integral scale” that is conventionally defined as the long time integral of the correlation function. When the integral scale diverges, the process is conventionally termed a “long memory process”. With this definition, if the long time exponent of R_H is > -1 , then the process has a long memory. Eq. 48 shows that the long time exponent is $-1-H$ so that for all H considered here, the integral scale converges. However, it is of the order of the relaxation time which may be much larger. For example, eq. 47 shows that when $H < 1/2$, the effective exponent $2H-1$ implies (in the absence of a cut-off), a divergence at long times, so that fRn mimics a long memory process.

3.3 Haar fluctuations

Using eq. 4039 we can determine the behaviour of the RMS Haar fluctuations.

Applying this equation to fGn we obtain $\left\langle \Delta F_H(\Delta t)_{Haar}^2 \right\rangle^{1/2} \propto \Delta t^{H_{Haar}}$ with $H_{Haar} = H - 1/2$

(the subscript “Haar” indicates that this is not a difference/increment fluctuation but rather a Haar fluctuation). For the motion, the Haar exponent is equal to the exponents of the

increments (eq. 4344) so that $\left\langle \Delta B_H(\Delta t)_{Haar}^2 \right\rangle^{1/2} \propto \Delta t^{H_{Haar}}$ with $H_{Haar} = H_B = H + 1/2$ (both

results were obtained in [Lovejoy et al., 2015]). Therefore, from an empirical viewpoint if we have a scaling Gaussian process and (up to the relaxation time scale) when $-1/2 < H_{Haar} < 0$, it has the scaling of an fGn and when $0 < H_{Haar} < 1/2$, it scales as an fBm.

Using eq. 3940, we can determine the Haar fluctuations for fRn $\left\langle \Delta U_H(\Delta t)_{Haar}^2 \right\rangle^{1/2}$.

With the small and large t approximations for $V_H(t)$, we can obtain the small and large Δt behaviour of the Haar fluctuations. Therefore, the leading terms for small Δt are:

$$\left\langle \Delta U_H(\Delta t)_{Haar}^2 \right\rangle^{1/2} = \Delta t^{H_{Haar}} \quad \begin{array}{l} H_{Haar} = H - 1/2; \quad 0 < H < 3/2 \\ H_{Haar} = 1; \quad 3/2 < H < 2 \end{array} \quad ; \quad \Delta t \ll 1 \quad (5655)$$

where the $\Delta t^{H-1/2}$ behaviour comes from terms in $V_H \approx t^{1+2H}$ and the Δt behaviour from the $V_H \approx t^4$ terms that arise when $H > 3/2$. Note (eq. 3940) that $\left\langle \Delta U_H(\Delta t)_{Haar}^2 \right\rangle^{1/2}$ depends on $4V_H(\Delta t/2) - V_H(\Delta t)$ so that quadratic terms in $V_H(t)$ cancel. The $H_{Haar} = 1$ behaviour from the $V_H \approx t^4$ terms that arise when $H > 3/2$.

As H increases past the critical value $H = 1/2$, the sign of H_{Haar} changes so that when $1/2 < H < 3/2$, we have $0 < H_{Haar} < 1$ so that over this range, the small Δt behaviour mimics that of fBm rather than fGn (discussed in the next section).

For large Δt , the corresponding formula is:

$$\left\langle \Delta U_{Haar}^2(\Delta t) \right\rangle^{1/2} \propto \Delta t^{-1/2}; \quad \Delta t \gg 1; \quad 0 < H < 2 \quad (5756)$$

This white noise scaling is due to the leading behavior $V_H(t) \approx t$ over the full range of H (eq. 487), see fig. 4a.

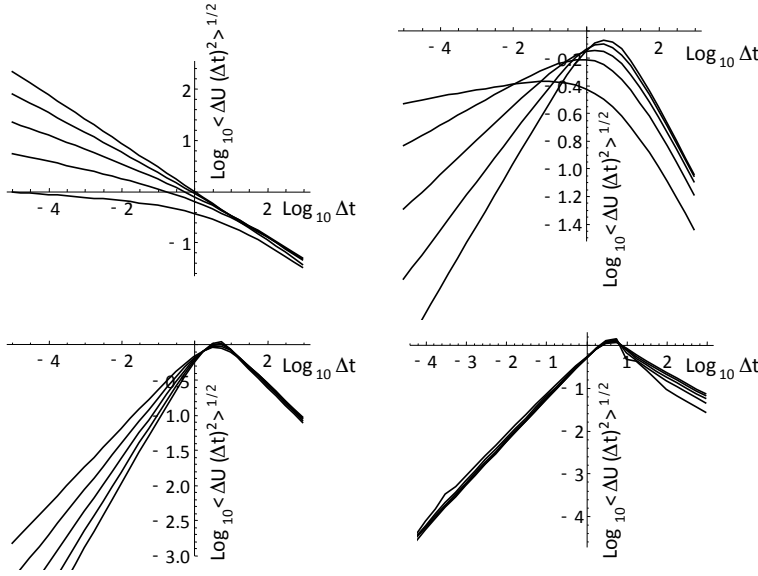


Fig. 4a: The RMS Haar fluctuation plots for the fRn process for $0 < H < 1/2$ (upper left), $1/2 < H < 1$ (upper right), $1 < H < 3/2$ (lower left), $3/2 < H < 2$ (lower right). The individual curves correspond to those of fig. 2, 3. The small Δt slopes follow the theoretical values $H - 1/2$ up to $H = 3/2$ (slope = 1); for larger H , the small t slopes all = 1. Also, at large t due to dominant $V \approx t$ terms, in all cases we obtain slopes $t^{-1/2}$.

3.4 fBm, fRm or fGn?

Our analysis has shown that there are three regimes with qualitatively different small scale behaviour, let us compare them in more detail. The easiest way to compare the different regimes is to consider their increments. Since fRn is stationary, we can use:

$$\langle \Delta U_H(\Delta t)^2 \rangle = \langle (U_H(t) - U_H(t - \Delta t))^2 \rangle = 2(R_H^{(fRn)}(0) - R_H^{(fRn)}(\Delta t)). \quad (5857)$$

Over the various ranges for small Δt , ($\tau \ll 1$ is the resolution) recall that we have:

$$\langle \Delta U_{H,\tau}(\Delta t)^2 \rangle \approx 2\tau^{-1+2H} - 2H(2H+1)\Delta t^{-1+2H}; \quad 1 \gg \Delta t \gg \tau; \quad 0 < H < 1/2$$

$$\langle \Delta U_H(\Delta t)^2 \rangle \approx \Delta t^{-1+2H}; \quad 1/2 < H < 3/2 \quad (5958)$$

$$\langle \Delta U_H(\Delta t)^2 \rangle \approx \Delta t^2; \quad 3/2 < H < 2$$

(when $H > 1/2$ the resolution is not important, the index is dropped). We see that in the small H range, the increments are dominated by the resolution τ , the process is a noise that does not converge point-wise, hence the τ dependence. In the middle ($1/2 < H < 3/2$) regime, the process is point-wise convergent (take the limit $\tau \rightarrow 0$) although it cannot be differentiated by any positive integer order. Finally, the largest H regime ($3/2 < H < 2$), the

process is smoother: $\lim_{\Delta t \rightarrow 0} \langle (\Delta U_H(\Delta t) / \Delta t)^2 \rangle = 1$, so that it is almost surely differentiable of

order 1. — Since the fRm are simply order one integrals of fRn, their orders of differentiability are simply augmented by one.

Considering the first two ranges i.e. $0 < H < 3/2$, we therefore have several processes with the same small scale statistics and this may lead to difficulties in interpreting empirical data that cover ranges of time scales smaller than the relaxation time. For example, we already saw that over the range $0 < H < 1/2$ that at small scales we could not distinguish fRn from the corresponding fGn; they both have anomalies (averages after the removal of the mean) or Haar fluctuations that decrease with time scale with exponent $H - 1/2$, (eq. 4956). This similitude was not surprising since they both were generated by Green's functions with the same high frequency term. From an empirical point of view, with data only available over scales much smaller than the relaxation time, it might be impossible to distinguish the two since over scales much smaller than the relaxation time, their statistics can be very close.

The problem is compounded when we turn to increments or fluctuations that increase with scale. To see this, note that in the middle range ($1/2 < H < 3/2$), the exponent $-1 + 2H$ spans the range 0 to 2. This is the same overlaps the range 1 to 2 spanned by fRm (Q_H) with $0 < H < 1/2$:

$$\langle \Delta Q_H(\Delta t)^2 \rangle = V_H^{(fRm)}(\Delta t) \propto \Delta t^{1+2H}; \quad \Delta t \ll 1; \quad 0 < H < 1/2 \quad (6059)$$

and with fBm (B_H) over the same H range (but for all Δt):

$$\langle \Delta B_H(\Delta t)^2 \rangle = V_H^{(fBm)}(\Delta t) = \Delta t^{1+2H}; \quad 0 < H < 1/2 \quad (6160)$$

Formatted: Font: Symbol

Field Code Changed

Formatted: Font: Italic

Formatted: Indent: First line: 0 cm

Formatted: Font: Italic

If we use the usual fBm exponent $H_B = H + 1/2$, then, over the range $0 < H < 1/2$ we may not only compare fBm with fRm with the same H_B , but also with an fRn process with an H larger by unity, i.e. with $H_B = H - 1/2$ in the range $1/2 < H < 3/2$. In this case, we have:

$$\begin{aligned}
 \left\langle \Delta U_H(\Delta t)^2 \right\rangle &\propto \Delta t^{2H_B}; \quad \Delta t \ll 1; \quad 0 < H_B < 1 \\
 &\propto 2 \left(1 - a \Delta t^{-H_B - 3/2} \right); \quad \Delta t \gg 1 \\
 \left\langle \Delta Q_H(\Delta t)^2 \right\rangle &\propto \Delta t^{2H_B}; \quad \Delta t \ll 1; \quad 1/2 < H_B < 1 \\
 &\propto \Delta t - b \Delta t^{3/2 - H_B}; \quad \Delta t \gg 1 \\
 \left\langle \Delta B_H(\Delta t)^2 \right\rangle &= \Delta t^{2H_B}; \quad 0 < H_B < 1
 \end{aligned} \tag{626+}$$

where a, b are constants (section 3.2). Over the entire range $0 < H_B < 1$, we see that the only difference between fBm, ~~and fRn, and fRn-fRm~~ is their different large scale ~~corrections to the small scale~~ Δt^{2H_B} behaviours. Therefore, if we found a process that over a finite range was scaling with exponent $1/2 < H_B < 1$, then over that range, we could not tell the difference between fRn, fRm, fBm, see fig. 4b for an example with $H_B = 0.95$.

Formatted: Indent: First line: 0 cm

Field Code Changed

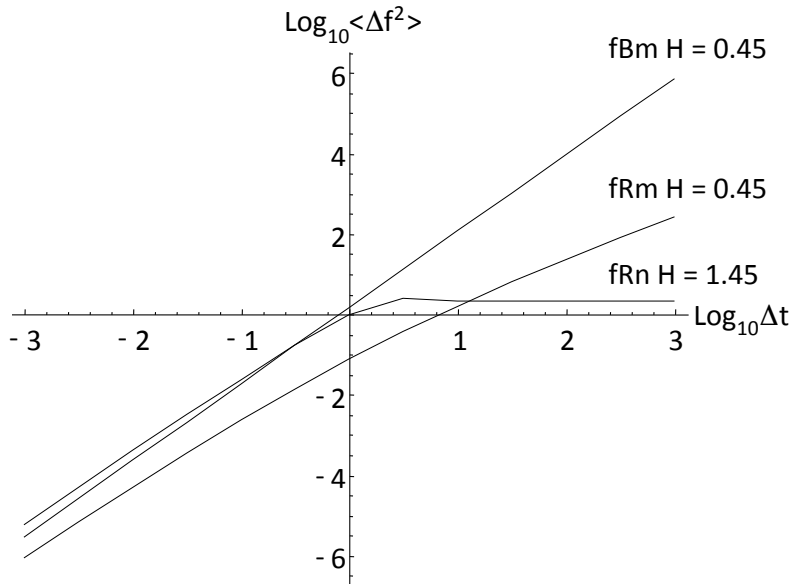


Fig. 4b: A comparison of fRn with $H = 1.45$, fRm with $H = 0.45$ and fBm with $H = 0.45$. For small Δt , they all have RMS increments with exponent $H_B = 0.95$ and can only be distinguished by their behaviours at Δt larger than the relaxation time ($\log_{10} \Delta t = 0$ in this plot).

3.5 Spectra:

Since $Y_H(t)$ is stationary process, its spectrum is the Fourier transform of the correlation function $R_H(t)$ (the Wiener-Khintchin theorem). However, it is easier to determine it directly from the fractional relaxation equation using the fact that the Fourier transform (F.T., indicated by the tilde) of the Weyl fractional derivative is simply

$F.T.[-D_t^H Y_H] = (i\omega)^H \tilde{Y}_H(\omega)$ (e.g. [Podlubny, 1999], this is simply the extension of the usual rule for the F.T. of integer-ordered derivatives). Therefore take the F.T. of eq. 4 (the fRn), to obtain:

$$\left((i\omega)^H + 1 \right) \tilde{U}_H = \tilde{\gamma}. \quad (6362)$$

so that the Fourier transform of $G_{0,H}$ is:

$$\tilde{G}_{0,H}(\omega) = \frac{1}{1 + (i\omega)^H} \quad (64)$$

And the spectrum of Y_H is:

Formatted: Indent: First line: 0 cm

Field Code Changed

Field Code Changed

Formatted: Font: Italic

Formatted: Subscript

Formatted: Font: Italic, Subscript

Formatted: MTDisplayEquation

Formatted: Subscript

$$E_U(\omega) = \left\langle \left| \widetilde{U}_H(\omega) \right|^2 \right\rangle = \left\langle \left| \widetilde{G}_{0,H}(\omega) \right|^2 \left| \widetilde{\gamma}(\omega) \right|^2 \right\rangle = \frac{1}{\left(1 + (-i\omega)^H \right) \left(1 + (i\omega)^H \right)} \quad (6563)$$

$$= \left(1 + 2\cos\left(\frac{\pi H}{2}\right) \omega^H + \omega^{2H} \right)^{-1}$$

(since the Gaussian white noise was normalized such that $\left\langle \left| \widetilde{\gamma}(\omega) \right|^2 \right\rangle = 1$). Due to the Wiener-Khinchin theorem, the spectrum is the Fourier transform of the autocorrelation function, hence:

$$R_H(t) = \frac{1}{2\pi} \int_{-\infty}^{\infty} e^{i\omega t} E_U(\omega) d\omega = \frac{1}{2\pi} \int_{-\infty}^{\infty} \frac{e^{i\omega t}}{\left(1 + (i\omega)^H \right) \left(1 + (-i\omega)^H \right)} d\omega \quad (66)$$

We use this relationship extensively in appendix A in order to derive the main fRn, fRm statistical properties that were discussed above.

From eq. 66 we already can immediately obtain some basic results. First, due to Parseval's theorem:

$$R_H(0) = \frac{1}{2\pi} \int_{-\infty}^{\infty} \left| \widetilde{G}_{0,H}(\omega) \right|^2 d\omega = \int_0^{\infty} G_{0,H}(s)^2 ds \quad (67)$$

When $H < 1/2$ this is divergent, but when $H > 1/2$, this can be used to normalize R_H .

We may easily obtain the asymptotic high and low frequency behaviours are therefore;

$$E_U(\omega) = \begin{cases} \omega^{-2H} + O(\omega^{-3H}); & \omega \gg 1 \\ 1 - 2\cos\left(\frac{\pi H}{2}\right) \omega^H + O(\omega^{2H}) & \omega \ll 1 \end{cases} \quad (6864)$$

This corresponds to the scaling regimes determined by direct calculation above:

$$R_H(t) \propto \begin{cases} t^{-1+2H} & t \ll 1 \\ t^{-1-H} & t \gg 1 \end{cases} \quad (6965)$$

($H \neq 1$). Note that the usual (Orenstein-Uhlenbeck) result for $H = 1$ has no ω^H term, hence no t^{-1-H} term; it has an exponential rather than power law decay at large t .

From the spectrum of U , we can easily determine the spectrum of the stationary Δt increments of the fRm process Q_H :

$$E_{\Delta Q}(\omega) = \left(\frac{2\sin\frac{\omega\Delta t}{2}}{\omega} \right)^2 E_U(\omega); \quad \Delta Q(\Delta t) = \int_{t-\Delta t}^t U(s) ds \quad (66)$$

Field Code Changed

Formatted: MTDisplayEquation

Formatted: Indent: First line: 1 cm

Formatted: English (CAN)

Formatted: Indent: First line: 1 cm

Formatted: Font: Italic

3.6 Sample processes

It is instructive to view some samples of fRn, fRm processes. For this purpose, we can use the solution for fRn in the form of a convolution (eq. 35), and use numerical convolution algorithms. For simulations, both the small and large scale divergences must be considered. Starting with the approximate methods developed by [Mandelbrot and Wallis, 1969], it took some time for exact fBm, and fGn simulation techniques to be developed [Hipel and McLeod, 1994], [Palma, 2007]. Fortunately, for fRm, fRn, the low frequency situation is easier since the long time memory is much smaller than for fBm, fGn. Therefore, as long as we are careful to always simulate series a few times the relaxation time and then to throw away the earliest 2/3 or 3/4 of the simulation, the remainder will have accurate correlations. With this procedure to take care of low frequency issues, we can therefore use the solution for fRn in the form of a convolution (eqs. 19, 35, 36), and use standard numerical convolution algorithms.

However, we still must be careful about the high frequencies since the impulse response Green's functions $G_{0,H}$ are singular for $H < 1$. In order to avoid singularities, Simulations-simulations of fRn are best made by first simulating the motions Q_H and then taking finite differences using: $Q_H = G_{1,H} * \gamma$ $Q_H \approx G_{1,H} * \gamma$ (* denotes a Weyl convolution)

and obtain the resolution τ fRn, using $U_{H,\tau}(t) = (Q_H(t + \tau) - Q_H(t)) / \tau$. Numerically, thisThis allows us to use the smoother (nonsingular) G_1 in the convolution rather than the singular G_0 . The simulations shown in figs. 5, 6 follow this procedure and the Haar fluctuation statistics were analyzed verifying the statistical accuracy of the simulations.

[Hipel and McLeod, 1994; Mandelbrot and Wallis, 1969; Palma, 2007]

In order to clearly display the behaviours, recall that when $t \gg 1$, we showed that all the fRn converge to Gaussian white noises and the fRm to Brownian motions (albeit in a slow power law manner). At the other extreme, for $t \ll 1$, we obtain the fGn and fBm limits (when $0 < H < 1/2$) and their generalizations for $1/2 < H < 2$.

Fig. 5a shows three simulations, each of length 2^{19} , pixels, with each pixel corresponding to a temporal resolution of $\tau = 2^{-10}$. so that the unit (relaxation) scale is 2^{10} elementary pixels. Each simulation uses the same random seed but they have H 's increasing from $H = 1/10$ (top set) to $H = 5/10$ (bottom set). The fRm at the right is from the running sum of the fRn at the left. Each series has been rescaled so that the range (maximum - minimum) is the same for each. Starting at the top line of each group, we show 2^{10} points of the original series degraded by a factor 2^9 . The second line shows a blow-up by a factor of 8 of the part of the upper line to the right of the dashed vertical line. The line below is a further blow-up by factor of 8, until the bottom line shows 1/512 part of the full simulation, but at full resolution. The unit scale indicating the transition from small to large is shown by the horizontal red line in the middle right figure. At the top (degraded by a factor 2^9), the unit (relaxation) scale is 2 pixels so that the top line degraded view of the simulation is nearly a white noise (left), (ordinary) Brownian motion (right). In contrast, the bottom series is exactly of length unity so that it is close to the fGn limit with the standard exponent $H_B = H + 1/2$. Moving from bottom to top in fig. 5a, one effectively transitions from fGn to fRn (left column) and fBm to fRm (right).

If we take the empirical relaxation scale for the global temperature to be 2^7 months (≈ 10 years, [Lovejoy et al., 2017]) and we use monthly resolution temperature anomaly data, then the nondimensional resolution is 2^{-7} corresponding to the second series from the

Formatted: Font: Italic

Formatted: Subscript

Formatted: Font: Italic, Subscript

Formatted: Font: Italic

Field Code Changed

Field Code Changed

Formatted: Superscript

Formatted: Superscript

Formatted: Not Superscript/ Subscript

top (which is thus 2^{10} months \approx 80 years long). Since $H \approx 0.42 \pm 0.02$ ([Del Rio Amador and Lovejoy, 2019]), the second series from the top in the bottom set is the most realistic, we can make out the low frequency undulations that are mostly present at scales $1/8$ of the series (or less).

Fig. 5b shows realizations constructed from the same random seed but for the extended range $1/2 < H < 2$ (i.e. beyond the fGn-range). Over this range, the top (large scale, degraded resolution) series is close to a white noise (left) and Brownian motion (right). For the bottom series, there is no equivalent fGn or fBm process, the curves become smoother although the rescaling may hide this somewhat (see for example the $H = 13/20$ set, the blow-up of the far right $1/8$ of the second series from the top shown in the third line. For $1 < H < 2$, also note the oscillations with wavelength-frequency $2\pi / \sin(\pi / H)$ (eq. 49) of order-unity, this is the fractional oscillation range.

Fig. 6a shows simulations similar to fig. 5a (fRn on the left, fRm on the right) except that instead of making a large simulation and then degrading and zooming, all the simulations were of equal length (2^{10} points), but the relaxation scale was changed from 2^{15} pixels (bottom) to 2^{10} , 2^5 and 1 pixel (top). Again the top is white noise (left), Brownian motion (right), and the bottom is (nearly) fGn (left) and fBm (right), fig. 6b shows the extensions to $1/2 < H < 2$.

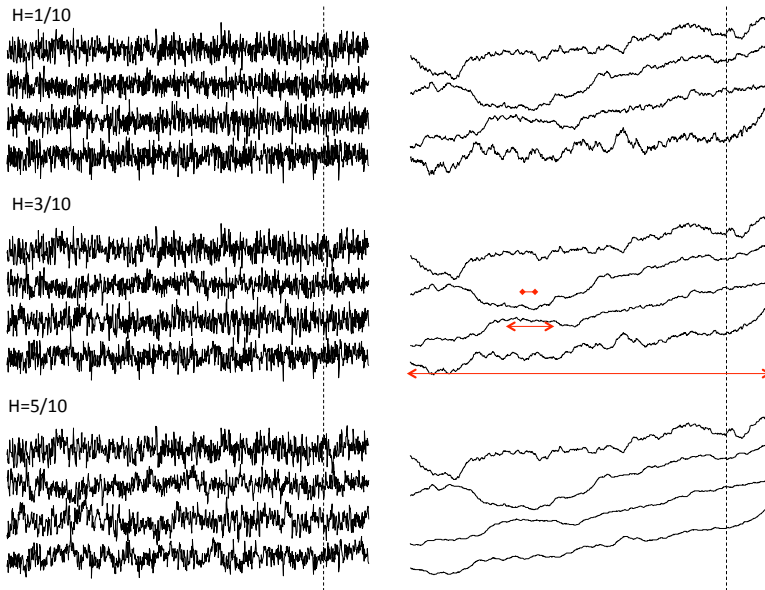


Fig. 5a: fRn and fRm simulations (left and right columns respectively) for $H = 1/10, 3/10, 5/10$ (top to bottom sets) i.e. the exponent range that overlaps with fGn and fBm. There are three simulations, each of length 2^{19} pixels, each use the same random seed with the unit scale equal to

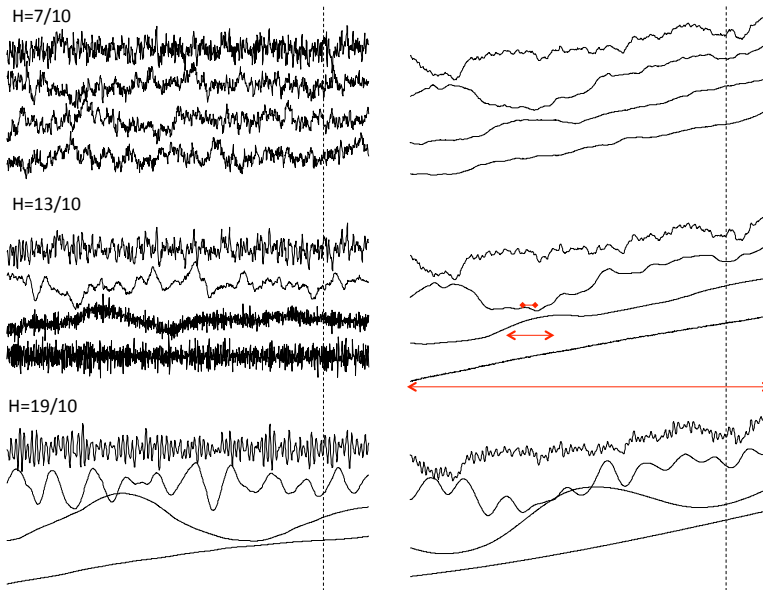
Formatted: Superscript

Formatted: Font: Italic

2^{10} pixels (i.e. a resolution of $\tau = 2^{-10}$). The entire simulation therefore covers the range of scale 1/1024 to 512 units. The fRm at the right is from the running sum of the fRn at the left.

Starting at the top line of each groupset, we show 2^{10} points of the original series degraded in resolution by a factor 2^9 . Since the length is $l = 2^9$ units long, each pixel has resolution $\tau = 1/2$. The second line of each set takes shows a blow-up by a factor of 8 of the part segment of the upper line lying to the right of the dashed vertical line, 1/8 of its length. It therefore spans $t=0$ to $t = 2^9/8 = 2^6$ but resolution was taken as $\tau = 2^{-4}$, hence it is still 2^{10} pixels long (note, each series was rescaled so that its range between maximum and minimum was the same). Since each pixel has a resolution of 2^{-4} , the unit scale is 2^4 pixels long, this is shown in red in the second series from the top (middle set). The process of taking 1/8 and blowing up by a factor of 8 line below each is a further blow up by factor of 8, continues to the third line (length $l = 2^3$, resolution $\tau = 2^{-7}$, unit scale $= 2^7$ pixels (shown by the red arrows in the third series) until the bottom line-series which spans the range $l = 0$ to $t = 1$ and a resolution $\tau = 2^{-10}$ shows 1/512 part of the full simulation, but at full resolution, with unit scale 2^{10} pixels (the whole series displayed). Each series was rescaled in the vertical so that its range between maximum and minimum was the same.

The unit relaxation scales indicating indicated by the red arrows mark the transition from small to large scale. Since this is shown by the horizontal red line in the middle-right figure. At the top series in each set has a (degraded by a factor 2^9), the unit scale is of $2 \cdot 2$ (degraded) pixels (too small to be shown in red) so that the strongly degraded view at the top of each simulation is nearly a white noise (left), or (ordinary) Brownian motion (right). In contrast, the bottom series is exactly of length unity $l = 1$ so that it is close to the fGn and fBm limits (left and right) with the standard exponent $H_B = H + 1/2$. As indicated in the text, the second series from the top in the bottom set is most realistic for monthly temperature anomalies.



Formatted: Font: Italic

Formatted: Font: Symbol

Formatted: Font: Italic

Formatted: Font: Symbol

Formatted: Superscript

Formatted: Superscript

Formatted: Superscript

Formatted: Superscript

Formatted: Font: Italic

Formatted: Font: Symbol

Formatted: Superscript

Formatted: Font: Italic

Formatted: Font: Not Italic

Formatted: Font: Not Italic

Formatted: Indent: First line: 1 cm

Formatted: Font: 10.5 pt

Formatted: Font: 11 pt

Formatted: Font: 11 pt

Fig. 5b: The same as fig. 5a but for $H = 7/10$, $13/10$ and $19/10$ (top to bottom). Over this range, the top (large scale, degraded resolution) series is close to a white noise (left) and Brownian motion (right). For the bottom series, there is no equivalent fGn or fBm process, the curves become smoother although the rescaling may hide this somewhat (see for example the middle $H = 13/20$ set, the blow-up of the far right 1/8 of the second series from the top shown in the third line). Also note for the bottom two sets with $1 < H < 2$, the oscillations that have frequency $2\pi / \sin(\pi / H)$ wavelengths of order unity, this is the fractional oscillation range.

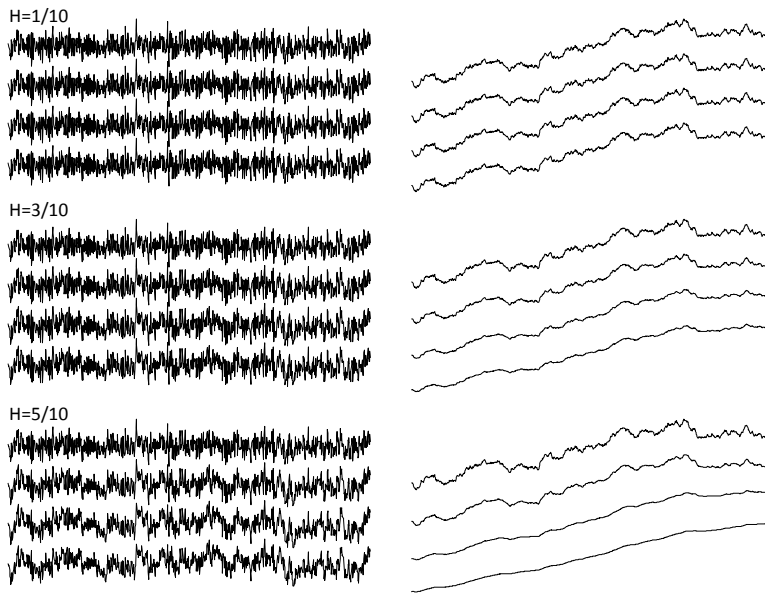


Fig. 6a: This set of simulations is similar to fig. 5a (fRn on the left, fRm on the right) except that instead of making a large simulation and then degrading and zooming, all the simulations were of equal length (2^{10} points), but resolutions $\tau = 2^{-15}, 2^{-10}, 2^{-5}$ the, 1 (bottom to top). The simulations therefore spanned the ranges of scale 2^{-15} to 2^{-5} ; 2^{-10} to 1; 2^{-5} to 2^5 ; 1 to 2^{10} and the same random seed was used in each so that we can see how the structures slowly change when the relaxation scale changes. The bottom fRn, $H = 5/10$ set is the closest to that observed for the Earth's temperature, and since the relaxation scale is of the order of a few years, the second series from the top of this set (with one pixel = one month) is close to that of monthly global temperature anomaly series. In that case the relaxation scale would be 32 months and the entire series would be $2^{10}/12 \approx 85$ years long.

unit scale (the relaxation time) was changed from 2^{15} pixels (bottom row of each set) to 2^{10} , 2^5 and 1 pixel (top). The top series (of total length 2^{10} relaxation times) is (nearly) a white noise (left), and Brownian motion (right), and the bottom is (spanning a range of scales from 2^{-15} to 2^{-5} relaxation times) is (nearly) an fGn (left) and fBm (right). The total range of scales covered here

Formatted: Font: 11 pt

Formatted: Superscript

Formatted: Superscript

Formatted: Font: Italic

Formatted: Superscript

Formatted: Indent: First line: 1 cm

($2^{10} \times 2^{15}$) is larger than in fig. 5a and allows one to more clearly distinguish the high and low frequency regimes.

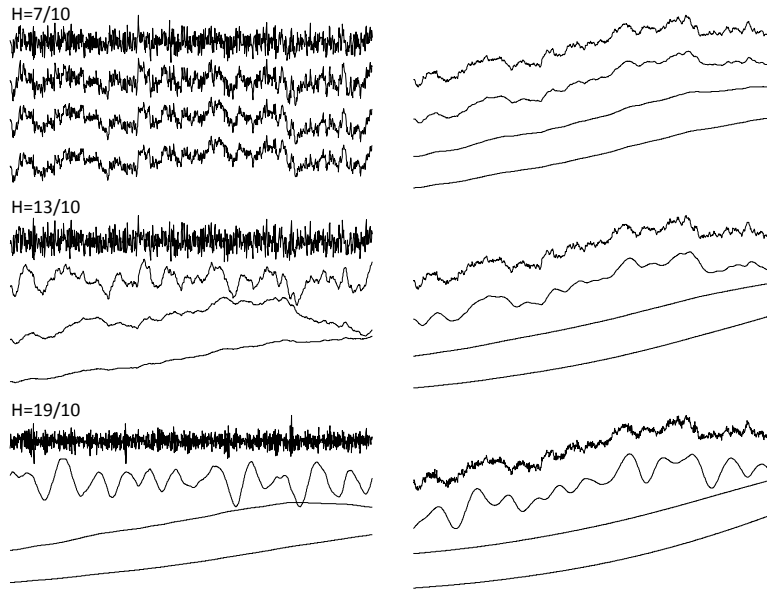


Fig. 6b: The same fig. 6a but for larger H values; see also fig. 5b.

4. Prediction

The initial value for Weyl fractional differential equations is effectively at $t = -\infty$, so that for fRn it is not directly relevant at finite times (although the ensemble mean is assumed = 0; for fRm, $Q_H(0)=0$ is important). The prediction problem is thus to use past data (say, for $t < 0$) in order to make the most skilful prediction of the future noises and motions at $t > 0$. We are therefore dealing with a *past value* rather than a usual *initial value* problem. The emphasis on past values is particularly appropriate since in the fGn limit, the memory is so large that values of the series in the distant past are important. Indeed, prediction of fGn with a finite length of past data involves placing strong (mathematically singular) weights on the most ancient data available (see [Gripenberg and Norros, 1996], [Del Rio Amador and Lovejoy, 2019], [Del Rio Amador and Lovejoy, 2020b]). This is quite different from standard stochastic predictions that are based on short memory (exponential) auto-regressive or moving average type processes that are not much different from initial value problems.

Formatted: Font: Italic

Formatted: Font: Italic, Subscript

In general, there will be small scale divergences (for fRn, when $0 < H \leq 1/2$) so that it is important to predict the finite resolution fRn: $Y_{H,\tau}(t)$. Using eq. 288 for $Y_{H,\tau}(t)$, we have:

$$Y_{H,\tau}(t) = \frac{N_H}{\tau} \left[\int_{-\infty}^t G_{1,H}(t-s)\gamma(s)ds - \int_{-\infty}^0 G_{1,H}(-s)\gamma(s)ds \right] - \frac{N_H}{\tau} \left[\int_{-\infty}^{t-\tau} G_{1,H}(t-\tau-s)\gamma(s)ds - \int_{-\infty}^0 G_{1,H}(-s)\gamma(s)ds \right] \quad (7067)$$

$$= \frac{N_H}{\tau} \left[\int_{-\infty}^t G_{1,H}(t-s)\gamma(s)ds - \int_{-\infty}^{t-\tau} G_{1,H}(t-\tau-s)\gamma(s)ds \right]$$

Let us ~~Defining~~ define the predictor for $t \geq 0$ (indicated by a circumflex):

$$\hat{Y}_\tau(t) = \frac{N_H}{\tau} \left[\int_{-\infty}^0 G_{1,H}(t-s)\gamma(s)ds - \int_{-\infty}^0 G_{1,H}(t-\tau-s)\gamma(s)ds \right] \quad (7168)$$

To show that it is indeed the optimal predictor, consider ~~We see that~~ the error $E_\tau(t)$ in the predictor is:

$$E_\tau(t) = Y_\tau(t) - \hat{Y}_\tau(t) = N_H \tau^{-1} \left[\int_{-\infty}^t G_{1,H}(t-s)\gamma(s)ds - \int_{-\infty}^{t-\tau} G_{1,H}(t-\tau-s)\gamma(s)ds \right] - N_H \tau^{-1} \left[\int_{-\infty}^0 G_{1,H}(t-s)\gamma(s)ds - \int_{-\infty}^0 G_{1,H}(t-\tau-s)\gamma(s)ds \right] \quad (7269)$$

$$= N_H \tau^{-1} \left[\int_0^t G_{1,H}(t-s)\gamma(s)ds - \int_0^{t-\tau} G_{1,H}(t-\tau-s)\gamma(s)ds \right]$$

Eq. 63-72 shows that the error depends only on $\gamma(s)$ for $s > 0$ whereas the predictor (eq. 6271) only depends on $\gamma(s)$ so that for $s < 0$, hence they are orthogonal:

$$\langle E_\tau(t) \hat{Y}_\tau(t) \rangle = 0 \quad (7370)$$

Hence ~~this is a sufficient condition for~~, $\hat{Y}_\tau(t)$ ~~is to be~~ the minimum square predictor which is the optimal predictor for Gaussian processes, (e.g. [Papoulis, 1965]). The prediction error variance is:

$$\langle E_\tau(t)^2 \rangle = N_H^2 \tau^{-2} \left[\int_0^{t-\tau} (G_{1,H}(t-s) - G_{1,H}(t-\tau-s))^2 ds + \int_{t-\tau}^t G_{1,H}(t-s)^2 ds \right] \quad (7471)$$

or with a change of variables:

$$\langle E_\tau(t)^2 \rangle = \tau^{-2} V_H(\tau) - N_H^2 \tau^{-2} \left[\int_{t-\tau}^\infty (G_{1,H}(u+\tau) - G_{1,H}(u))^2 du \right] \quad (7572)$$

where we have used $\langle Y_\tau^2 \rangle = \tau^{-2} N_H^2 V_H(\tau)$ (the unconditional variance).

Field Code Changed

Field Code Changed

Field Code Changed

Field Code Changed

Field Code Changed

Using the usual definition of forecast skill (also called the Minimum Square Skill Score or MSSS) we obtain:

$$S_{k,\tau}(t) = 1 - \frac{\langle E_\tau(t)^2 \rangle}{\langle E_\tau(\infty)^2 \rangle} = \frac{N_H^2 \int_{t-\tau}^{\infty} (G_{1,H}(u+\tau) - G_{1,H}(u))^2 du}{V_H(\tau)}$$

$$= \frac{\int_{t-\tau}^{\infty} (G_{1,H}(u+\tau) - G_{1,H}(u))^2 du}{\int_0^{\infty} (G_{1,H}(u+\tau) - G_{1,H}(u))^2 du + \int_0^{\tau} G_{1,H}(u)^2 du} \quad (7673)$$

When $H < 1/2$ and $G_{1,H}(t) = G_{1,H}^{(fGn)}(t) = \frac{t^H}{\Gamma(1+H)}$, we can check that we obtain the

fGn result:

$$\int_{t-\tau}^{\infty} (G_{1,H}(u+\tau) - G_{1,H}(u))^2 du \approx \frac{\tau^{1+2H}}{\Gamma(1+H)^2} \int_{\lambda-1}^{\infty} ((v+1)^H - v^H)^2 dv; \quad v = u/\tau; \quad \lambda = t/\tau \quad (7774)$$

[Lovejoy et al., 2015]. This can be expressed in terms of the function:

$$\xi_H(\lambda) = \int_0^{\lambda-1} ((u+1)^H - u^H)^2 du \quad (7875)$$

So that the usual fGn result (independent of τ) is:

$$S_k = \frac{\xi_H(\infty) - \xi_H(\lambda)}{\xi_H(\infty) + \frac{1}{2H+1}} \quad (7976)$$

To survey the implications, let's start by showing the τ independent results for fGn, shown in fig. 7 which is a variant on a plot published in [Lovejoy et al., 2015]. We see that when $H \approx 1/2$ ($H_B \approx 1$) that the skill is very high, indeed, in the limit $H \rightarrow 1/2$, we have perfect skill for fGn forecasts (this would of course require an infinite amount of past data to attain).

Field Code Changed

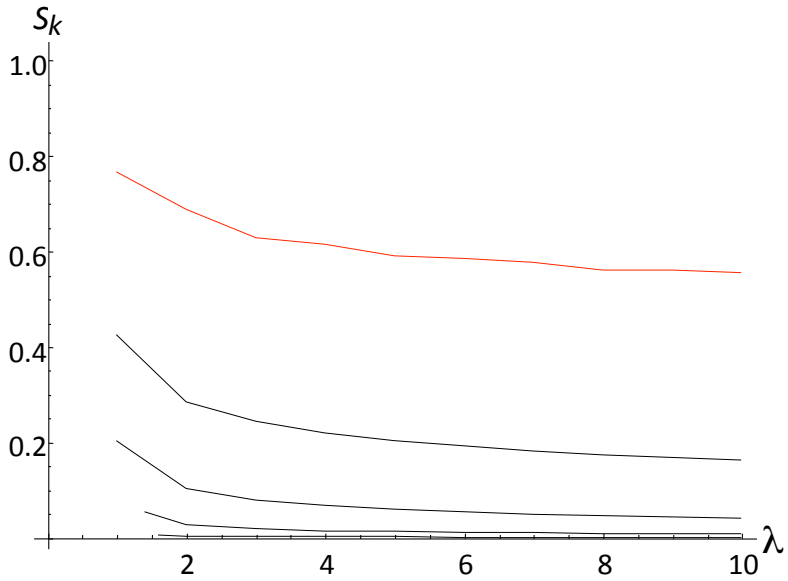


Fig. 7: The prediction skill (S_k) for pure fGn processes for forecast horizons up to $\lambda = 10$ steps (ten times the resolution). This plot is non-dimensional, it is valid for time steps of any duration. From bottom to top, the curves correspond to $H = 1/20, 3/10, \dots, 9/20$ (red, top, close to the empirical H).

Formatted: Font: 11 pt

Formatted: Font: 11 pt, Italic

Formatted: Font: 11 pt

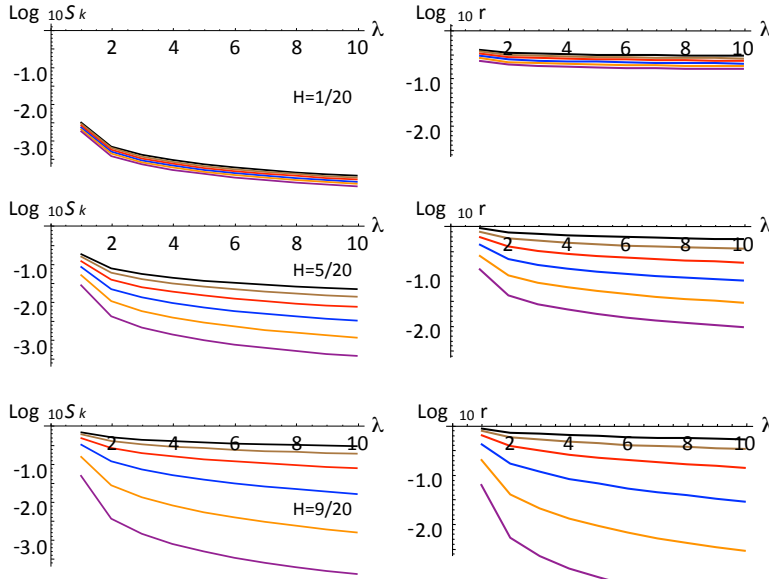


Fig. 8: The left column shows the skill (S_k) of fRn forecasts (as in fig. 7 for fGn) for fRn skill with $H = 1/20, 5/20, 9/20$ (top to bottom set); λ is the forecast horizon, the number of steps of resolution τ forecast into the future. The right hand column shows the ratio (r) of the fRn to corresponding fGn skill.

Here the result depends on τ ; each curve is for different values increasing from 10^{-4} (top, black) to 10 (bottom, purple) increasing by factors of 10 (the red set in the bottom plots with $\tau = 10^{-2}$, $H = 9/20$ are closest to the empirical values). The right hand column shows the ratio (r) of the fRn to corresponding fGn skill.

Now consider the fRn skill. In this case, there is an extra parameter, the resolution of the data, τ . Figure 8 shows curves corresponding to fig. 7 for fRn with forecast horizons integer multiples (λ) of τ i.e. for times $t = \lambda\tau$ in the future, but with separate curves, one for each of five τ values increasing from 10^{-4} to 10 by factors of ten. When τ is small, the results should be close to those of fGn, i.e. with potentially high skill, and in all cases, the skill is expected to vanish quite rapidly for $\tau > 1$ since in this limit, fRn becomes an (unpredictable) white noise (although there are scaling corrections to this).

To better understand the fGn limit, it is helpful to plot the ratio of the fRn to fGn skill (fig. 8, right column). We see that even with quite small values $\tau = 10^{-4}$ (top, black curves), that some skill has already been lost. Fig. 9 shows this more clearly, it shows one time step and ten time step skill ratios. To put this in perspective, it is helpful to compare this using some of the parameters relevant to macroweather forecasting. According to [Lovejoy et al., 2015] and [Del Rio Amador and Lovejoy, 2019], the relevant empirical Haar exponent is \approx

Formatted: Font: 11 pt

Formatted: Font: Symbol, 11 pt

Formatted: Font: 11 pt

Formatted: Indent: First line: 1 cm

Formatted: Font: Symbol, 11 pt

Formatted: Font: 11 pt

Formatted: Font: 11 pt, Superscript

Formatted: Font: 11 pt

Formatted: Font: 11 pt, Italic

Formatted: Font: 11 pt

1014 ~~-0.08~~ values for the global temperature H is ≈ 0.45 over the range 1 month to 10 years, (i.e.
 1015 the empirical RMS Haar exponent is ≈ -0.05 so that the $H = -0.05 + 1/2 - 0.08 \approx 0.42$).
 1016 Although direct empirical estimates of the relaxation time, are difficult since the responses
 1017 to anthropogenic forcing begin to dominate over the internal variability after ≈ 10 years
 1018 [Procyk et al., 2020] have used the deterministic response to estimate a global relaxation time
 1019 of ≈ 5 years. Also, according to [Hébert et al., 2020], the transition scale is ≈ 2 years
 1020 (although the uncertainty is large), so that for monthly resolution forecasts, the non-
 1021 dimensional resolution is $\tau \approx 1/24100$. With these values, we see (red curves) that we may
 1022 have lost $\approx 2530\%$ of the fGn skill for one month forecasts and $\approx 8085\%$ for ten month
 1023 forecasts. Comparing this with fig. 7 we see that this implies about 60% and 10% skill (see
 1024 also the red curve in fig. 8, bottom set).

1025 Going beyond the $0 < H < 1/2$ region that overlaps fGn, fig. 10 clearly shows that the
 1026 skill continues to increase with H . We already saw (fig. 4) that the range $1/2 < H < 3/2$ has
 1027 RMS Haar fluctuations that for $\Delta t < 0$ mimic fBm and these do indeed have higher skill,
 1028 approaching unity for H near 1 corresponding to a Haar exponent $\approx 1/2$, i.e. close to an
 1029 fBm with $H_B = 1/2$, i.e. a regular Brownian motion. Recall that for Brownian motion, the
 1030 increments are unpredictable, but the process *itself* is predictable (persistence).

1031 Finally, in figure 11a, b, we show the skill for various H 's as a function of resolution
 1032 τ . Fig. 11a for the $H < 3/2$ shows that for all H , the skill decreases rapidly for $\tau > 1$. Fig.
 1033 11b in the fractional oscillation equation regime shows that the skill also oscillates.

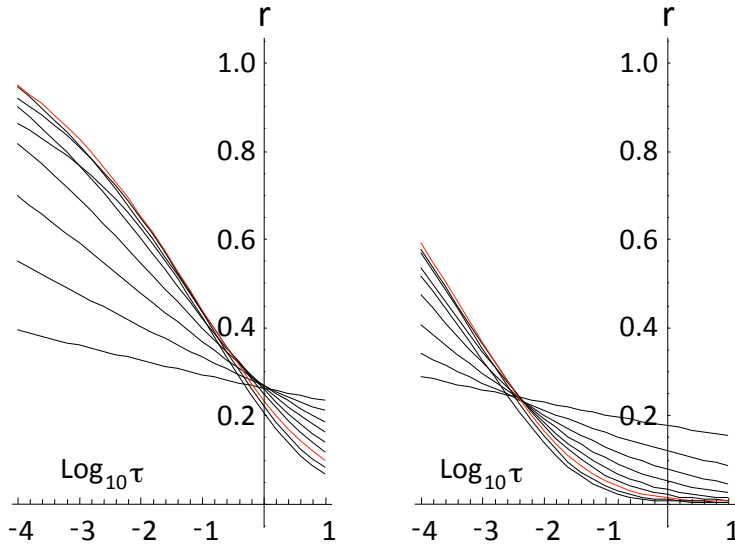


Fig. 9: The ratio of fRn skill to fGn skill (left: one step horizon, right: ten step forecast horizon) as a function of resolution τ for H increasing from (at left) bottom to top ($H = 1/20, 2/20, 3/20 \dots 9/20$); the $H = 9/20$ curves (close to the empirical value) is shown in red.

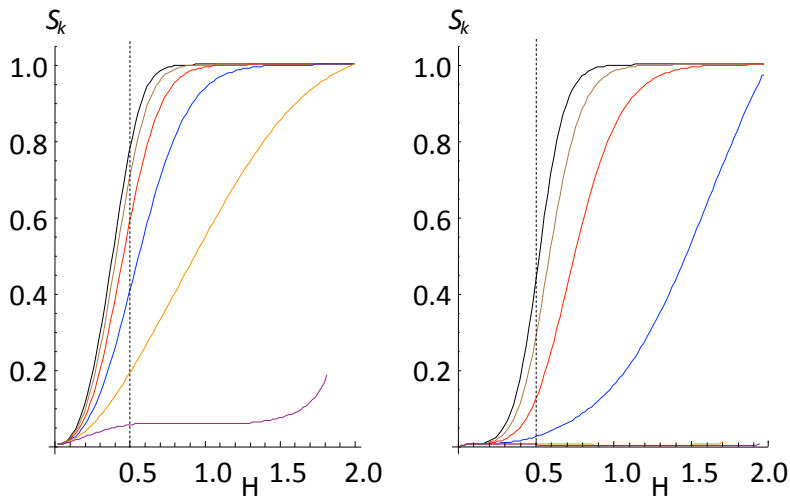


Fig. 10: The one step (left) and ten step (right) fRn forecast skill as a function of H for various resolutions (τ) ranging from $\tau = 10^{-4}$ (black, left of each set) through $\tau = 10^{-3}$ (brown) 10^{-2} (red), 0.1 (blue), 1 (orange), to $\tau = 10$ (purple). In the right set (right of each set, purple, for the right set the $\tau = 1$ (orange), 10 (purple) lines are nearly on top of the $S_k = 0$ line. Again red ($\tau = 10^{-2}$) is the more empirical relevant value for monthly data). Recall that the regime $H < 1/2$ (to the left of the vertical dashed lines) corresponds to the overlap with fGn.

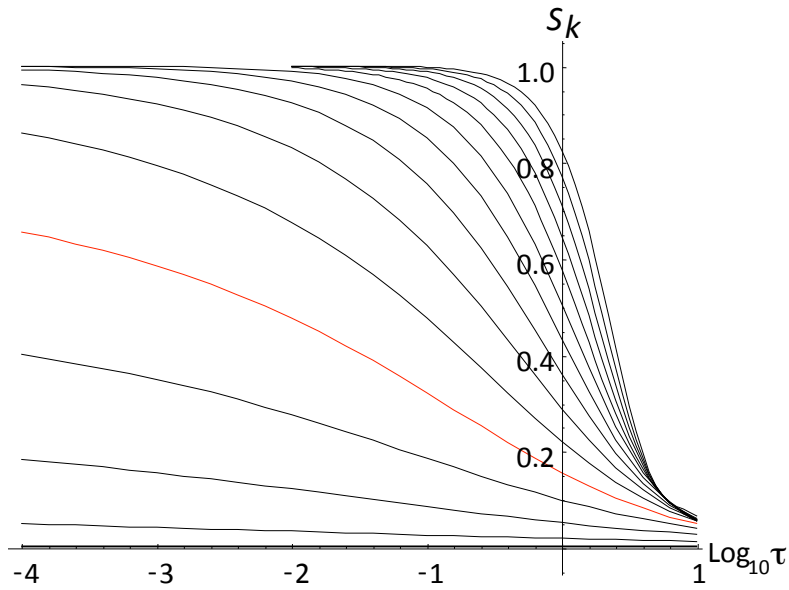


Fig. 11a: One step fRn prediction skills as a function of resolution for H 's increasing from $1/20$ (bottom) to $29/20$ (top), every $1/10$. Note the rapid transition to low skill, (white noise) for $\tau > 1$. The curve for $H = 9/20$ is shown in red.

Formatted: Font: 11 pt

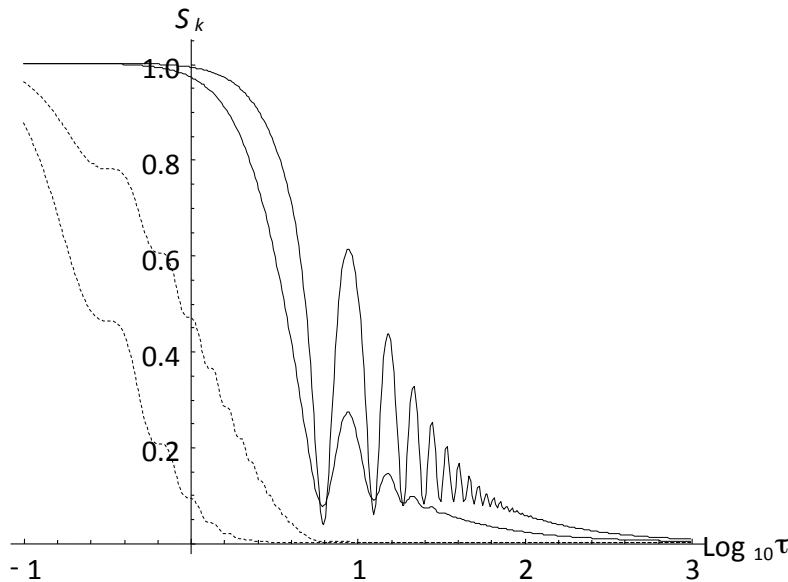


Fig. 11b: Same as fig. 11a except for $H = 37/20, 39/20$ showing the one step skill (black), and the ten step skill (dashed). The right hand dashed and right hand solid lines, are for $H = 39/20$, they clearly show that the skill oscillates in this fractional oscillation equation regime. The corresponding left lines are for $H = 37/20$.

4. Conclusions:

Ever since [Budyko, 1969] and [Sellers, 1969], the energy balance between the earth and outer space has been modelled by the Energy Balance Equation (EBE) which is an ordinary first order differential equation for the temperature (Newton's law of cooling). In the EBE, the integer ordered derivative term accounts for energy storage. Physically, it corresponds to storage in a uniform slab of material. To increase realism, one may introduce a few interacting slabs (representing for example the atmosphere and ocean mixed layer; the Intergovernmental Panel on Climate Change recommends two such components [IPCC, 2013]). However due to spatial scaling, a more realistic model involves a continuous hierarchy of storage mechanisms and this can easily be modelled by using fractional rather than integer ordered derivatives: the Fractional Energy Balance Equation (FEBE). [Lovejoy, 2019b; 2019c; Lovejoy et al., 2020b].

The FEBE is a fractional relaxation equation that generalizes the EBE. When forced by a Gaussian white noise, it is also a generalization of fractional Gaussian noise (fGn) and its integral generalizes fractional Brownian motion (fBm). Over the

Formatted: Font: 11 pt

Formatted: Heading 2, Indent: First line: 0 cm

parameter range $0 < H < 1/2$ (H is the order of the fractional derivative), the high frequency FEBE limit (fGn) has been used as the basis of monthly and seasonal temperature forecasts [Lovejoy et al., 2015], [Del Rio Amador and Lovejoy, 2019], [Del Rio Amador and Lovejoy, 2020a; Del Rio Amador and Lovejoy, 2020b]. For multidecadal time scales the low frequency limit has been used as the basis of climate projections through to the year 2100 [Hebert, 2017], [Lovejoy et al., 2017], [Hébert et al., 2020], [Procyk et al., 2020]. The success of these two applications with different exponents but with values predicted by the FEBE with the same empirical underlying $H \approx 0.4$, is what originally motivated the FEBE, and the work reported here. The statistical characterizations – correlations, structure functions Haar fluctuations and spectra as well as the predictability properties are important for these and other FEBE applications.

While the deterministic fractional relaxation equation is classical, various technical difficulties arise when it is generalized to the stochastic case: in the physics literature, it is a Fractional Langevin Equation (FLE) that has almost exclusively been considered as a model of diffusion of particles starting at an origin. This requires $t = 0$ (Riemann-Liouville) initial conditions that imply that the solutions are strongly nonstationary. In comparison, the Earth's temperature fluctuations that are associated with its internal variability are statistically stationary. This can easily be modelled by Weyl fractional derivatives, i.e. initial conditions at $t = -\infty$.

Beyond the proposal that the FEBE is a good model for the Earth's temperature, the key novelty of this paper is therefore to consider the FEBE as a Weyl fractional Langevin equation and proceed to give the fundamental statistical properties including series expansions about the origin and infinity (asymptotic), as well as the theoretical predictability skill. When driven by Gaussian white noises, the solutions are a new stationary process – fractional Relaxation noise (fRn). Over the range $0 < H < 1/2$, we show that the small scale limit is a fractional Gaussian noise (fGn) – and its integral – fractional Relaxation motion (fRm) – has stationary increments and which generalizes fractional Brownian motion (fBm). Although at long enough times, the fRn tends to a Gaussian white noise, and fRm to a standard Brownian motion, this long time convergence is slow (it is a power law).

The deterministic FEBE has two qualitatively different cases: $0 < H < 1$ and $1 < H < 2$ corresponding to fraction relaxation and fractional oscillation processes respectively. In comparison, the stochastic FEBE has three regimes: $0 < H < 1/2$, $1/2 < H < 3/2$, $3/2 < H < 2$, with the lower ranges ($0 < H < 3/2$) having anomalous high frequency scaling. For example, it was found that fluctuations over scales smaller than the relaxation time can either decay or grow with scale – with exponent $H - 1/2$ (section 3.5) – the parameter range $0 < H < 3/2$ has the same scaling as the (stationary) fGn ($H < 1/2$) and the (nonstationary) fBm ($1/2 < H < 3/2$), so that processes that have been empirically identified with either fGn or fBm on the basis of their scaling, may in fact turn out to be (stationary) fRn processes; the distinction is only clear at time scales beyond the relaxation time.

Although the basic approach could be more applied to a range of FLEs, we focused on the fractional relaxation-oscillation equation. Much of the effort was to deduce the asymptotic small and large scale behaviours of the autocorrelation

Formatted: Font: Italic

Field Code Changed

Formatted: Font: Italic

functions that determine the statistics and in verifying these with extensive numeric simulations. An interesting exception was the $H = 1/2$ special case which for fGn corresponds to an exactly $1/f$ noise. Here, we were able to find exact mathematical expressions for the full correlation functions, showing that they had logarithmic dependencies at both small and large scales. The resulting Half order EBE (HEBE) has an exceptionally slow transition from small to large scales (a factor of a million or more is needed) and empirically, it is quite close to the global temperature series over scales of months, decades and possibly longer.

Beyond improved monthly, seasonal temperature forecasts and multidecadal projections, the stochastic FEBE opens up several paths for future research. One of the more promising of these is to follow up on the special value $H = 1/2$ that is very close to that found empirically and that can be analytically deduced from the classical Budyko-Sellers energy transport equation by improving the mathematical treatment of the radiative boundary conditions [Lovejoy, 2020a; b]. [Lovejoy, 2019a]. In the latter case, one obtains a partial fractional differential equation for the horizontal space-time variability of temperature anomalies over the Earth's surface, allowing regional forecasts and projections. Generalizations include the nonlinear albedo-temperature feedbacks needed for modelling of transitions between different past climates. In geophysics, the two main stochastic approaches are stochastic differential equations and stochastic scaling models. In the former, the equations are typically assumed to be of integer order. As a consequence they have exponential Green's functions and they are handled mathematically using the Itô calculus. In contrast, scaling models are typically constructed to directly satisfy scaling symmetries, the usual ones are the linear (monofractal) fBm, fGn and their Levy extensions [Watkins, 2017] or the nonlinear stochastic models (cascades, multifractals).

In this paper we combine both the scaling and differential equation approaches by allowing the time derivatives to be of fractional order. Fractional derivatives are convolutions with power laws, in Fourier space they are power law filters, they are scaling. In this paper, we considered fractional Langevin equations in which the fractional time (not space) terms are scaling. For technical reasons, these fractional time processes are non-Markovian so that they do not have Fokker-Plank equations nor are they semi-martingales, they are not amenable to the Itô calculus. These technical issues may explain why the stochastic relaxation equations of interest in this paper have barely been considered. Indeed, the closest that have been considered up until now are the stochastic Riemann-Liouville fractional relaxation equations that are relevant in fractional random walks. However, these walks are nonstationary whereas we require stationary processes that are obtained as solutions of stochastic Weyl fractional equations. Our motivation is the proposal by [Lovejoy et al., 2020a] that the Fractional Energy Balance Equation (FEBE) is a good model of the earth's radiative equilibrium with the sun and outer space. In this model, the

Formatted: Indent: First line: 1 cm

fractional term in the equation phenomenologically accounts for scaling, hierarchical energy storage mechanisms. The deterministic FEBE models the response of the earth to changing external forcings (solar, volcanic, anthropogenic) whereas the noise driven FEBE discussed here models the climate system's response to internal variability that has been acting for a very long time.

The FEBE is a fractional relaxation equation that generalizes Newton's law of cooling, it is also a generalization of fractional Gaussian noise (fGn) and its integral fractional Brownian motion (fBm). Over the parameter range $0 < H < 1/2$ (H is the order of the fractional derivative), the high frequency FEBE limit (fGn) has been used as the basis of monthly and seasonal temperature forecasts [Lovejoy *et al.*, 2015], [Del Rio Amador and Lovejoy, 2019]. For multidecadal time scales — with the same value $H \approx 0.4$ — it has been used as the basis of climate projections [Hébert *et al.*, 2020]. The success of these two applications with a unique exponent makes it plausible that the FEBE is a good model of the earth's energy budget.

When the order of the fractional derivative H is in the range $0 < H < 1$, the equation is called the fractional relaxation equation, the value $H = 1$ corresponds to standard integer ordered (exponential) relaxation: for deterministic temperatures it is Newton's law of cooling, for the noise driven case, it yields Ornstein–Uhlenbeck processes. In the range $1 < H < 2$ (the maximum discussed here), the character of the deterministic equation changes, over this range it is called the fractional oscillation equation. In the stochastic case, there are three qualitatively distinct regimes not two: $0 < H < 1/2$, $1/2 < H < 3/2$, $3/2 < H < 2$ with the lower ranges ($0 < H < 3/2$) having anomalous high frequency scaling. For example, we found that fluctuations over scales smaller than the relaxation time can either decay or grow with scale — with exponent $H - 1/2$ (section 3.5) — the parameter range $0 < H < 3/2$ has the same scaling as the (stationary) fGn ($H < 1/2$) and the (nonstationary) fBm ($1/2 < H < 3/2$), so that processes that have been empirically identified with either fGn or fBm on the basis of their scaling, may in fact turn out to be (stationary) fRn processes; the distinction is only clear at time scales beyond the relaxation time.

Since the Riemann–Liouville fractional relaxation equation had already been studied, the main challenge was to implement the Weyl fractional derivative while avoiding divergence issues. The key was to follow the approach used in fBM, i.e. to start by defining fractional motions and then the corresponding noises as the (ordinary) derivatives of the motions. Over the range $0 < H < 1/2$, the noises fGn and fRn diverge in the small scale limit: like Gaussian white noise, they are generalized functions that are strictly only defined under integral signs; they can best be handled as differences of motions.

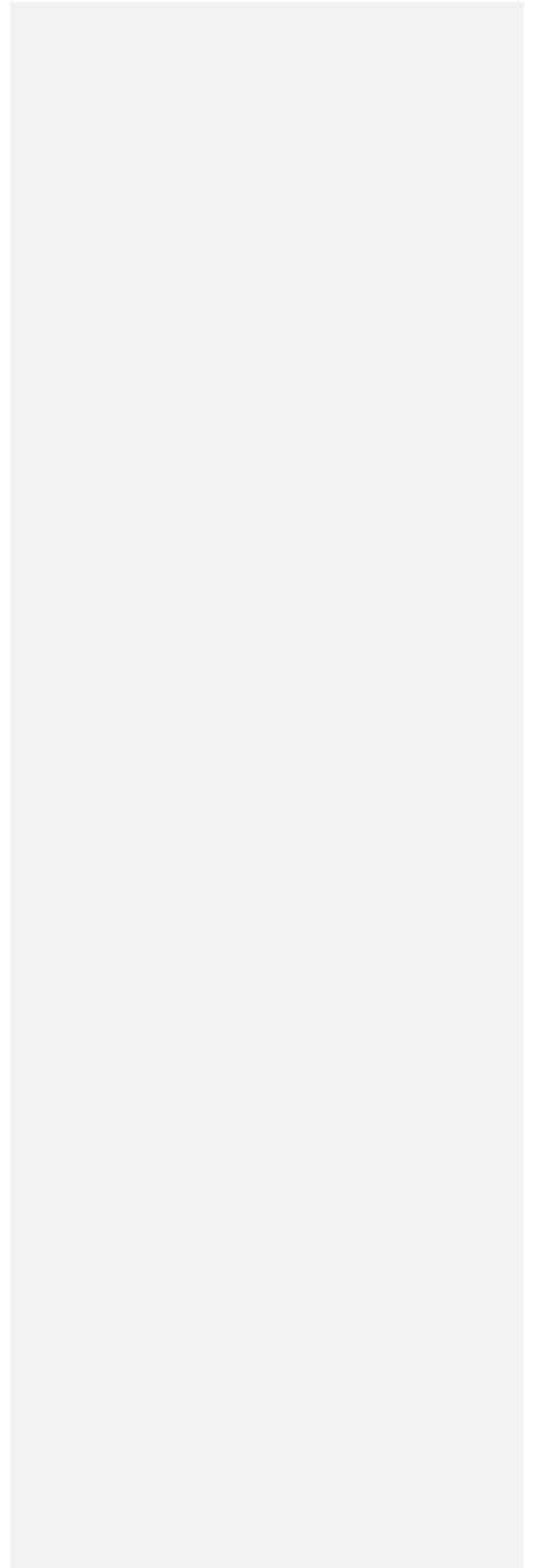
Although the basic approach could be applied to a range of fractional operators, we focused on the fractional relaxation equation. Much of the effort was to deduce the asymptotic small and large scale behaviours of the autocorrelation functions that determine the statistics and in verifying these with extensive numeric simulations. An interesting exception was the $H = 1/2$ special case which for fGn corresponds to an exactly $1/f$ noise. Here, we were able to find exact mathematical expressions for the full correlation functions, showing that they had logarithmic dependencies at both small and large scales. The value $1/2$ is very close to that found empirically for the earth's temperature and the exceptionally slow transition from small to large scales (a factor of a million or more is needed) suggests that this may be a good model for regional temperatures since the variation of the apparent

~~(local) exponents (estimated over a range of 100 to 1000 in scale), may simply be a consequence of varying relaxation time scales rather than regionally varying exponents.~~

Acknowledgements:

I thank L. Del Rio Amador, R. Procyk, ~~and~~ R. Hébert, C. Penland, N. Watkins for discussions. I also acknowledge an exchange with ~~N. Watkins and~~ K. Rypdal. This work was unfunded, there were no conflicts of interest.

μ_{12}
 μ_{13}



Appendix A: Random walks and the Weyl fractional Relaxation equation

The usual fractional derivatives that are considered in physical applications are defined over the interval from 0 to t ; this includes the Riemann–Liouville (“R-L”; e.g. the monographs by [Miller and Ross, 1993], and [West et al., 2003]) and the Caputo fractional derivatives [Podlubny, 1999]. The domain 0 to t is convenient for initial value problems and can notably be handled by Laplace transform techniques. However, many geophysical applications involve processes that have started long ago and are most conveniently treated by derivatives that span the domain $-\infty$ to t , i.e. that require the semi-infinite Weyl fractional derivatives.

It is therefore of interest to clarify the relationship between the Weyl and R-L stochastic fractional equations and Green’s functions when the systems are driven by stationary noises. In this appendix, we consider the stochastic fractional relaxation equation for the velocity V of a diffusing particle. This was discussed by [Kobelev and Romanov, 2000a] and [West et al., 2003] in a physical setting where V corresponds to the velocity of a fractionally diffusing particle. The fractional Langevin form of the equation is:

$${}_0D_t^H V + V = \gamma \quad (71)$$

where γ is a white noise and we have used the R-L fractional derivative. This equation can be written in a more standard form by integrating both sides by order H :

$$V(t) = -{}_0D_t^{-H} V + {}_0D_t^{-H} \gamma = -\frac{1}{\Gamma(H)} \int_0^t (t-s)^{H-1} V(s) ds + \frac{1}{\Gamma(H)} \int_0^t (t-s)^{H-1} \gamma(s) ds \quad (72)$$

The position $X(t) = \int_0^t V(s) ds + X_0$ satisfies:

$${}_0D_t^H X + X = W \quad (73)$$

where $dW = \gamma(s) ds$ is a Wiener process.

The solution for $X(t)$ is obtained using the Green’s function $G_{0,H}$:

$$X(t) = \int_0^t G_{0,H}(t-s) W(s) ds + X_0 E_{1,H}(-t^H); \quad G_{0,H}(t) = t^{H-1} E_{H,H}(-t^H) \quad (74)$$

where E is a Mittag-Leffler function (eq. 16). Integrating by parts and using $G_{1,H}(0) = 0$, $W(0) = 0$ we obtain:

$$\int_0^t G_{0,H}(t-s) W(s) ds = \int_0^t G_{1,H}(t-s) \gamma(s) ds; \quad dW = \gamma(s) ds; \quad G_{1,H}(t) = \int_0^t G_{0,H}(s) ds \quad (75)$$

This yields:

$$X(t) = \int_0^t G_{1,H}(t-s) \gamma(s) ds + X_0 E_{1,H}(-t^H) \quad (76)$$

$X(t)$ is clearly nonstationary: its statistics depend strongly on t . The first step in extracting a stationary process is to take the limit of very large t , and consider the process

over intervals that are much shorter than the time since the particle began diffusing. We will show that the increments of this new process are stationary.

Define the new process $Z_{t'}(t)$ over a time interval t that is short compared to the time elapsed since the beginning of the diffusion (t'):

$$Z_{t'}(t) = X(t') - X(t' - t) = \int_0^{t'} G_{0,H}(t' - s) \gamma(s) ds - \int_0^{t'-t} G_{0,H}(t' - t - s) \gamma(s) ds \quad (77)$$

(for simplicity we will take $X_0 = 0$, but since $E_{1,H}(-t'^H)$ rapidly decreases to zero, at large t' this is not important). Now use the change of variable $s' = s - t' + t$:

$$Z_{t'}(t) = \int_{-t'+t}^t G_{1,H}(t - s') \gamma(s' + t' - t) ds' - \int_{-t'+t}^0 G_{1,H}(-s') \gamma(s' + t' - t) ds' \quad (78)$$

Now, use the fact that $\gamma(s' + t' - t) = \gamma(s')$ (equality in a probability sense) and take the limit $t' \rightarrow \infty$. Dropping the prime on s we can write this as:

$$Z(t) = Z_{\infty}(t) = \int_{-\infty}^t G_{1,H}(t - s) \gamma(s) ds - \int_{-\infty}^0 G_{1,H}(-s) \gamma(s) ds \quad (79)$$

—where we have written $Z(t)$ for the limiting process.

Since $Z(0) = 0$, $Z(t)$ is still nonstationary. But now consider the process $Y(t)$ given by its derivative:

$$Y(t) = \frac{dZ(t)}{dt} = \int_{-\infty}^t G_{0,H}(t - s) \gamma(s) ds; \quad G_{0,H}(t) = \frac{dG_{1,H}(t)}{dt} \quad (80)$$

(since $G_1(0) = 0$). $Y(t)$ is clearly stationary.

We now show that $Y(t)$ satisfies the Weyl version of the relaxation equation. Consider the shifted function: $Y_{t'}(t) = Y_0(t + t')$ and take Y_0 as a solution to the Riemann-Liouville fractional equation:

$${}_0D_t^H Y_0 + Y_0 = \gamma \quad (81)$$

or equivalently in integral form:

$$Y_0(t) = -{}_0D_t^{-H} Y_0 + {}_0D_t^{-H} \gamma = -\frac{1}{\Gamma(H)} \int_0^t (t-s)^{H-1} Y_0(s) ds + \frac{1}{\Gamma(H)} \int_0^t (t-s)^{H-1} \gamma(s) ds \quad (82)$$

With solution:

$$Y_0(t) = \int_0^t G_{0,H}(t-s) \gamma(s) ds \quad (83)$$

(with $Y_0(0) = 0$).

Now shift the time variable so as to obtain:

$$Y_{t'}(t) = -\frac{1}{\Gamma(H)} \int_0^{t+t'} (t+t'-s)^{H-1} Y_0(s) ds + \frac{1}{\Gamma(H)} \int_0^{t+t'} (t+t'-s)^{H-1} \gamma(s) ds \quad (84)$$

(with $Y_{t'}(-t') = 0$). Now make the change of variable $s' = s - t'$:

$$Y_{t'}(t) = -\frac{1}{\Gamma(H)} \int_{-t'}^t (t-s')^{H-1} Y_{t'}(s') ds' + \frac{1}{\Gamma(H)} \int_{-t'}^t (t-s')^{H-1} \gamma(s') ds'; \quad \gamma(s'+t') \stackrel{d}{=} \gamma(s')$$
(85)

We see that $Y_{t'}$ is therefore the solution of:

$$-_{t'} D_t^H Y_{t'} + Y_{t'} = \gamma$$
(86)

However, since $Y_{t'}$ is the shifted Y_0 we have the solution:

$$Y_{t'}(t) = Y_0(t+t') = \int_0^{t+t'} G_0(t+t'-s) \gamma(s) ds = \int_{-t'}^t G_0(t-s') \gamma(s'+t') ds'$$
(87)

Again, using $\gamma(s'+t') \stackrel{d}{=} \gamma(s')$ and dropping the primes, we obtain:

$$Y_{t'}(t) = \int_{-t'}^t G_0(t-s) \gamma(s) ds$$
(88)

Finally, taking the limit $t' \rightarrow \infty$ we have the equation and solution for

$$Y(t) = Y_\infty(t) :$$

$$-_{\infty} D_t^H Y + Y = \gamma; \quad Y(t) = \int_{-\infty}^t G_0(t-s) \gamma(s) ds; \quad Y(t) = Y_\infty(t)$$
(89)

with $Y(-\infty) = 0$.

The conclusion is that as long as the forcings are statistically stationary we can use the R-L Green's functions to solve the Weyl fractional derivative equation. Although we have explicitly derived the result for the fractional relaxation equation, we can see that it is of wider generality.

Appendix **BA**: The small and large scale fRn, fRm statistics:

A.1 $R_H(t)$ as a Laplace transform

In section 2.3, we derived general statistical formulae for the auto-correlation functions of motions and noises defined in terms of Green's functions of fractional operators. Since the processes are Gaussian, autocorrelations fully determine the statistics. While the autocorrelations of fBm and fGn are well known (and discussed in section 3.1), those for fRm and fRn are new and are not so easy to deal with since they involve quadratic integrals of Mittag-Leffler functions.

In this appendix, we derive the basic power law expansions valid as well as large t (asymptotic) expansions, and we numerically investigate their accuracy. For simplicity, we consider the unnormalized autocorrelation and V functions.

It seems simplest to start with the Fourier expression for the autocorrelation function for the unit white noise forcing (section 3.5), eq. 65, 66. (A1)(A2)(A3)(A2) (A3) First convert the inverse Fourier transform (eq. 66) into a Laplace transform. For this, consider the integral over the contour C in the complex plane:

$$I(z) = \frac{1}{2\pi} \int_C \frac{e^{zt}}{(1+z^H)(1+(-z)^H)} dz \quad (A14)$$

We take C to be the closed contour obtained by integrating along the imaginary axis (this part gives $R_H(t)$, eq. 66), and closing the contour along an (infinite) semicircle over the second and third quadrants. When $0 < H < 1$, there are no poles in these quadrants, but we must integrate around a branch cut on the -ve real axis. When $1 < H < 2$, we must take into account two new branch cuts and two new poles in the -ve real plane. In a polar representation $z = re^{i\theta}$, the additional branch cuts are along the rays $z = re^{\pm i\pi/H}$; $r > 1$, circling around the poles at $z = e^{\pm i\pi/H}$. The branch cuts give no net contribution, but the residues of the poles do make a contribution ($P_H \neq 0$ below). We can express both cases with the formula:

$$R_H(t) = -\frac{1}{\pi} \text{Im} \int_0^\infty \frac{e^{-xt}}{(1+x^H)(1+x^H e^{i\pi H})} dx + P_{H,+}(t); \quad t > 0 \quad (A25)$$

“Im” indicates the imaginary part and:

$$P_{H,\pm}(t) = 0; \quad 0 < H < 1$$

$$P_{H,\pm}(t) = -e^{t \cos(\frac{\pi}{H})} \frac{\sin\left(\pm \frac{\pi}{H} + \frac{H\pi}{2} + t \sin\left(\frac{\pi}{H}\right)\right)}{H \sin\left(\frac{\pi H}{2}\right)}; \quad 1 < H < 2 \quad (A36)$$

Formatted: Font: Italic

While the integral term is monotonic, the P_H term oscillates with frequency $\omega = 2\pi / \sin(\pi / H)$. P_H accounts for the oscillations visible in figs. 2, 3, 5b although since when $1 < H < 2$, $\cos(\pi/H) < 1$, they decay exponentially. When $H > 1$, this pole contribution dominates $R_H(t)$ for a wide range of t values around $t = 1$, although as we see below, eventually at large t , power law terms come to the fore. When $H = 1$, we obtain the classical

Ornstein-Uhlenbeck autocorrelation: $R_1(t) = \frac{1}{2} e^{-|t|}$.

A.2 Asymptotic expansions:

An advantage of writing $R_H(t)$ as a Laplace transform is that we can use Watson's lemma to obtain an asymptotic expansion (e.g. [Bender and Orszag, 1978]). The idea is that an expansion of eq. A.2 around $x = 0$ can be Laplace transformed term by term to yield an asymptotic expansion for large t . Defining the convenient coefficient:

$$D_n = (-1)^{n+1} \frac{\cos\left(\left(n - \frac{1}{2}\right)\pi H\right) - \cos\left(\frac{\pi H}{2}\right)}{2\pi \sin\left(\frac{\pi H}{2}\right)} = (-1)^n \frac{\sin\left(nH\frac{\pi}{2}\right) \sin\left((n-1)H\frac{\pi}{2}\right)}{\pi \sin\left(H\frac{\pi}{2}\right)} \quad (\text{A47})$$

The x expansion of the integrand can be expressed in terms of D_n as:

$$-\frac{1}{\pi} \text{Im} \frac{1}{(1+x^H)(1+x^H e^{iH\pi})} = -2 \sum_{n=1}^{\infty} D_{-n} x^{nH} \quad (\text{A58})$$

Therefore, taking the term by term Laplace transform and using Watson's lemma [Bender and Orszag, 1978]:

$$R_H(t) = -2 \sum_{n=1}^{\infty} D_{-n} \Gamma(1+nH) t^{-(1+nH)} + P_{H,+}(t); \quad t \gg 1 \quad (\text{A69})$$

Where we have used $\Gamma(1+Hn) \sin(nH\pi) = -\pi / \Gamma(-nH)$, and have included the exponentially decaying residue $P_{H,+}$ that contributes when $1 < H < 2$. The first two terms (without $P_{H,+}$) are explicitly:

$$R_H(t) = -\frac{1}{\Gamma(-H)} t^{-(1+H)} + \frac{2 + \sec(H\pi)}{2\Gamma(-2H)} t^{-(1+2H)} + \dots; \quad t \gg 1 \quad (\text{A740})$$

Note that for $0 < H < 1$ $\Gamma(-H) < 0$.

For the motions (fRm), we need the expansion of $V_H(t)$, it can be obtained by using

$R_H(t) = \frac{1}{2} \frac{d^2 V_H(t)}{dt^2}$ (eq. 35). Integrating R_H twice, we have:

$$V_H(t) = t + a_H - 4 \sum_{n=1}^{\infty} D_{-n} \Gamma(-1+nH) t^{1-nH} + 2P_{H,-}(t); \quad t \gg 1 \quad (\text{A844})$$

Formatted: Font: Italic

Formatted: MTDisplayEquation

Formatted: Font: Italic

Formatted: Font: Italic, Subscript

Where the $t + a_H$ terms come from the constants of integration and P_H from the poles when $1 < H < 2$. The unit coefficient of the leading t term is a consequence of $\lim_{t \rightarrow \infty} \frac{\partial V_H}{\partial t} = 1$. This can be shown by considering the derivative of V_H from eq. 24:

$$\frac{\partial V_H}{\partial t} = J(t) + G_{1,H}(t)^2; \quad J(t) = \int_t^\infty G_{0,H}(u) (G_{1,H}(u) - G_{1,H}(u-t)) du \quad (\text{A942})$$

Since for $0 < H < 2$, $G_{0,H}(t) > 0$ and $0 < G_{1,H}(t) < 2$ we obtain:

$$|J(t)| < \int_t^\infty G_{0,H}(u) |G_{1,H}(u) - G_{1,H}(u-t)| du < 2 \int_t^\infty G_{0,H}(u) du \quad (\text{A1043})$$

For large t , $G_{0,H}(t) \approx t^{1-H}$, $\lim_{t \rightarrow \infty} J(t) = 0$, in addition $\lim_{t \rightarrow \infty} G_{1,H}(t)^2 = 1$ so that $\lim_{t \rightarrow \infty} \frac{\partial V_H}{\partial t} = 1$

and to leading order $V_H(t) \approx t$ for large t . If needed, the constant term a_H can be obtained numerically.

A.3 Power series expansions about the origin:

For many applications one is interested in the behavior of $R_H(t)$ for scales of months which is typically less than the relaxation time, i.e. $t < 1$. It is therefore important to understand the small t behaviour. We again consider the Laplace integral for the $0 < H < 1$ case. In this case, we can divide the range of integration in two parts:

$$R_H(t) = -\frac{\text{Im}}{\pi} \int_0^1 \frac{e^{-xt} dx}{(1+x^H)(1+e^{i\pi H} x^H)} - \frac{\text{Im}}{\pi} \int_1^\infty \frac{e^{-xt} dx}{(1+x^H)(1+e^{i\pi H} x^H)} \quad (\text{A1144}).$$

and then use the binomial expansions:

$$\begin{aligned} \frac{1}{(1+x^H)(1+x^H e^{i\pi H})} &= \frac{1}{e^{i\pi H} - 1} \sum_{n=0}^{\infty} (-1)^n (e^{i\pi H} e^{i\pi H} - 1) x^{nH}; \quad x < 1 \\ \frac{1}{(1+x^H)(1+x^H e^{i\pi H})} &= -\frac{1}{e^{i\pi H} - 1} \sum_{n=1}^{\infty} (-1)^n (e^{-i\pi H} e^{i\pi H} - 1) x^{-nH}; \quad x > 1 \end{aligned} \quad (\text{A1245}).$$

We can now integrate each term separately using:

$$\begin{aligned} \int_0^1 e^{-xt} x^{nH} dx &= \sum_{j=1}^{\infty} \frac{(-1)^{j-1}}{(Hn+j)\Gamma(j)} t^{j-1} \\ \int_1^\infty e^{-xt} x^{-nH} dx &= E_{nH}(t) = \pi \frac{t^{-1+Hn}}{\sin(\pi nH)\Gamma(Hn)} + \sum_{j=1}^{\infty} \frac{(-1)^{j-1}}{(Hn-j)\Gamma(j)} t^{j-1} \end{aligned} \quad (\text{A1346})$$

Where E_{nH} is the exponential integral function. Adding the two integrals and summing over n , we obtain:

Formatted: Font: Italic

$$R_H(t) = \sum_{n=2}^{\infty} D_n \Gamma(1-Hn) t^{-1+Hn} + \sum_{j=1, \text{ odd}}^{\infty} F_j \frac{t^{j-1}}{\Gamma(j)} \quad (\text{A1417})$$

(note the appearance of D_n with $n>0$) and:

$$F_j = -\frac{1}{\pi} \cot\left(\frac{\pi H}{2}\right) \sum_{n=-\infty}^{\infty} \frac{(-1)^n}{nH+j} = -\frac{1}{\pi H} \cot\left(\frac{\pi H}{2}\right) \left(\Phi\left(-1, 1, 1-\frac{j}{H}\right) + \Phi\left(-1, 1, \frac{j}{H}\right) \right) \quad (\text{A1548})$$

where Φ is the Hurwitz-Lerch phi function $\Phi(z, s, a) = \sum_{n=0}^{\infty} z^n (n+a)^{-s}$.

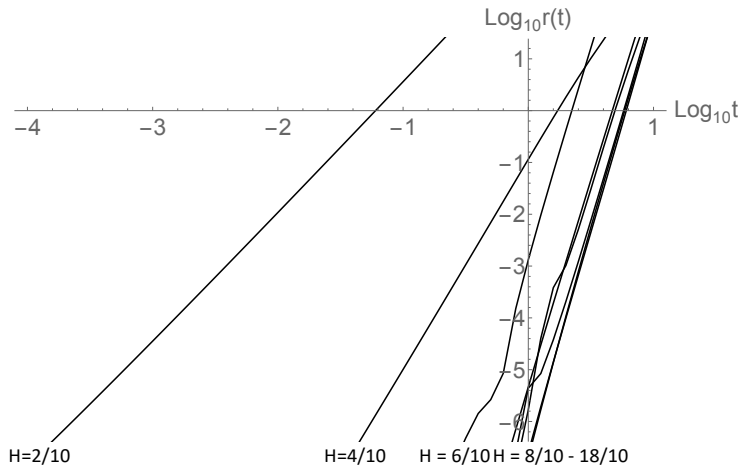


Fig. A1: This shows the logarithm of the relative error in the $R_H^{(10,10)}(t)$ approximation (i.e. with 10 fractional terms and 10 integer order terms) with respect to the deviation from the fGn $R_H(t)$ $r = \log_{10} \left| 1 - \left(R_H^{fGn}(t) - R_H^{(10,10)}(t) \right) / \left(R_H^{fGn}(t) - R_H(t) \right) \right|$. The lines are for $H = 2/10, 4/10, \dots, 16/10, 18/10$ (excluding the exponential case $H=1$), from left to right (note convergence is only for irrational H , therefore an extra 10^{-4} was added to each H). For the low H values the convergence is particularly slow, but is believed for H .

Comments:

1) These and the following formulae are for $t>0$; R_H is symmetric for $t \rightarrow -t$.

Formatted: Font: 11 pt

Formatted: Font: 11 pt

Formatted: Heading 3

2) Each integer term of the expansion F_j is itself obtained as an infinite sum, so that the overall result for $R_H(t)$ is effectively a doubly infinite sum. This procedure implicitly swaps the order of the summation and apparently explains the fact that while the expansions were derived for the case $0 < H < 1$, the final expansion is valid for the full range $0 < H < 2$: numerically, it accurately reproduces the oscillations when $H > 1$.

3) The fGn correlation function is given by the single $n = 2$ term:

$$R_H^{(fGn)}(t) = D_2 \Gamma(1-2H) t^{-1+2H} = \frac{\sin(H\pi)}{\pi} \Gamma(1-2H) t^{-1+2H} \quad (\text{A1649})$$

When $0 < H < 1/2$, it is divergent at the origin; since it corresponds to fGn, the normalization constant is $N_H^{-2} = K_H^{-2} = 2D_2 \Gamma(-1-2H)$. When $1/2 < H < 2$, it is still the leading term fractional term, but the constant F_1 dominates at small t .

4) The Hurwitz-Lerch phi function $\Phi\left(-1, 1, 1 - \frac{j}{H}\right)$ needed for F_j , diverges for $H = j/n$ where, n is an integer. The overall sum over all j thus diverges for all rational H . For irrational H , the convergence properties are not easy to establish, although due to the Γ functions, these series apparently converge for all $t > 0$, but the convergence is rather slow. Fig. A1 shows some numerical results showing the convergence of the 10th order fractional 10th order integer power approximation ($n_{max} = j_{max} = 10$). Since the fGn term diverges for small t when $H < 1/2$ it is more useful to consider the convergence of the difference with respect to the fGn term (i.e. $R_{fGn}(t) - R_{H,a}(t)$ is the sum in eq. A.15 from $n = 3$ to 10 and odd $j \leq 9$). Fig. A1 shows the logarithm of the ratio of the approximation with respect to the true value: $r = \log_{10} \left| 1 - \left(R_{fGn}(t) - R_{H,a}(t) \right) / \left(R_{fGn}(t) - R_H(t) \right) \right|$ (to avoid exact rationals, 10^{-4} was added to the H values). From the figure we see that the approximation is satisfactory except for small H , we return to this below.

5) For $H > 1/2$, when $t = 0$, the only nonzero term is from the constant F_1 : $R_H(0) = F_1$, this gives the normalization constant (section 3.2). Comparing with eq. 67, we therefore have:

$$\begin{aligned} R_H(0) &= \int_0^\infty G_{0,H}(s)^2 ds = F_1 \\ &= -\frac{1}{\pi H} \cot\left(\frac{\pi H}{2}\right) \left(\Phi\left(-1, 1, 1 - \frac{1}{H}\right) + \Phi\left(-1, 1, \frac{1}{H}\right) \right) \quad 1/2 < H < 2 \quad (\text{A1720}) \end{aligned}$$

Similarly, when $H > 3/2$, we can apply Parseval's theorem to the derivative $G'_{0,H}$, where it gives the coefficient of the t^2 term so that:

Formatted: Font: Italic

Formatted: Font: Not Italic

$$\int_0^{\infty} G'_{0,H}(s)^2 ds = -F_3 = \frac{1}{\pi H} \cot\left(\frac{\pi H}{2}\right) \left(\Phi\left(-1, 1, 1 - \frac{3}{H}\right) + \Phi\left(-1, 1, \frac{3}{H}\right) \right)$$

(A1821)

(when $H < 3/2$, the left hand side diverges while the right hand side remains finite).

6) The expression for $V_H(t)$ can be obtained by integrating twice noting that $V_H(0) = 0$, $V'_H(0) = 0$:

$$V_H(t) = 2 \sum_{n=2}^{\infty} D_n \Gamma(-1 - Hn) t^{1+Hn} + 2 \sum_{j=1, \text{ odd}}^{\infty} F_j \frac{t^{j+1}}{\Gamma(j+2)}; \quad 0 < H < 2$$

(A1922).

3.4 A Convenient approximation

The expansion for R_H is the sum of a fractional and an integer ordered series. Partial sums appear to converge (fig. A1), albeit slowly. Examination of partial sums shows that the integer ordered and fractional ordered terms tend to cancel, the difficulty due to the term $\Phi\left(-1, 1, 1 - \frac{j}{H}\right)$ that comes from the exponential integral. This suggests an alternative way of expressing the series:

$$R_H(t) = \sum_{n=2}^{\infty} D_n E_{nH}(t) + \sum_{j=1}^{\infty} C_j \frac{(-1)^{j-1}}{\Gamma(j)} t^{j-1}; \quad C_j = \sum_{n=2}^{\infty} \frac{D_n}{(Hn+j)}$$

(A2023)

Where D_n is given by eq. A.4 and the n sums start at $n = 2$ since $D_1 = 0$. C_j can be expressed as:

$$C_j = -\frac{ie^{-iH\pi}}{2\pi H(e^{iH\pi} - 1)} \left(-\left(e^{iH\pi} + e^{2iH\pi}\right) \Phi\left(-1, 1, 1 + \frac{j}{H}\right) + \Phi\left(e^{iH\pi}, 1, 1 + \frac{j}{H}\right) + e^{3iH\pi} \Phi\left(e^{-iH\pi}, 1, 1 + \frac{j}{H}\right) \right)$$

(A2124).

We can also expand the exponential integral:

$$E_{nH}(t) = \pi \frac{t^{-1+Hn}}{\sin(\pi nH) \Gamma(Hn)} + \sum_{j=1}^{\infty} \frac{(-1)^{j-1}}{(Hn-j) \Gamma(j)} t^{j-1}$$

(A2225).

For the j_{\max} and n_{\max} partial sums, we have:

$$R_{H, n_{\max}, j_{\max}}(t) = \sum_{n=2}^{n_{\max}} D_n \Gamma(1 - nH) t^{-1+Hn} + \sum_{j=1}^{j_{\max}} F_{j, n_{\max}} \frac{(-1)^{j-1}}{\Gamma(j)} t^{j-1}; \quad F_{j, n_{\max}} = C_j + \sum_{n=2}^{n_{\max}} \frac{D_n}{Hn-j}$$

(A2326)

Now define the (j_{\max}, n_{\max}) approximation by:

$$R_{H, n_{\max}, j_{\max}}(t) = \frac{R_H^{(n_{\max}+1, j_{\max})}(t) + R_H^{(n_{\max}, j_{\max})}(t)}{2}$$

(A2427).

Formatted: Heading 2

This has the effect of adding in half the next higher n term and is more accurate; overall, j_{max} and n_{max} may now be taken to be much smaller than in the previous approximation. For example putting $n_{max}=2, j_{max}=1$, we get with the partial sum:

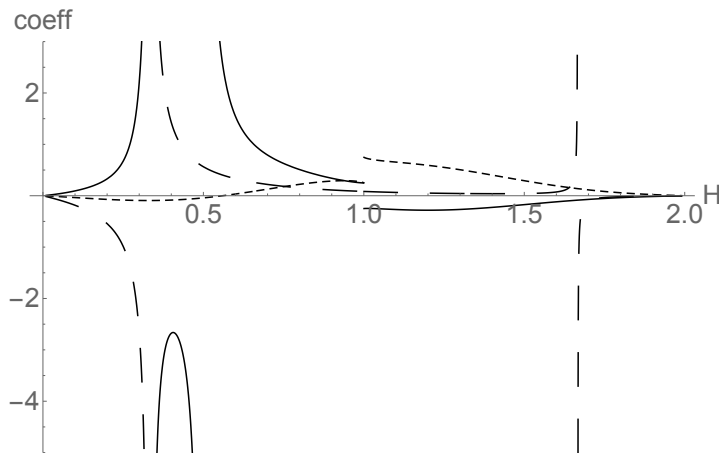
$$R_{H,2,1}(t) = R_H^{(fGn)}(t) + \frac{D_2}{2} \Gamma(1-3H) t^{-1+3H} + F_1 \quad (\text{A2528})$$

Where:

$$F_1 = C_1 + \frac{D_2}{2H-1} + \frac{D_3}{2(3H-1)}$$

$$D_2 = \frac{\sin(\pi H)}{\pi}; \quad D_3 = -\frac{\sin(\pi H)(1+2\cos(\pi H))}{\pi} \quad (\text{A2629})$$

To understand the behaviour, fig. A2 shows the behaviour of coefficient of the t^{-1+3H} term $\frac{D_2}{2} \Gamma(1-3H)$, the constant term F_1 and the coefficient of the next integer (linear in t) term $F_2 = C_2 + \frac{D_2}{2H-2} + \frac{D_3}{2(3H-2)}$. Up until the end of the fGn region ($H = 1/2$), the t^{-1+3H} and F_1 terms have opposite signs and tend to cancel. In addition, we see that for $t \approx 1$ and $H < 1$, they dominate over the (omitted) linear term. Fig. B3 shows that the $R_{H,2,1}$ approximation is surprisingly good for $H < 1$ and is still not so bad for $1 < H < 2$. This approximation is thus useful for monthly resolution macroweather temperature fields that have relaxation times of years or longer and where H is mostly over the range $0 < H < 1/2$, but over some tropical ocean regions can increase to as much as $H \approx 1.2$ ([Del Rio Amador and Lovejoy, 2020b]). Fig. A2 shows that the (2,1) approximation is reasonably accurate for $t \approx 1$, especially for $H < 1$.



Formatted: Indent: First line: 0 cm

Fig. A2: The solid line is the constant term F_1 , the long dashes are the coefficients $\frac{D_1}{2}\Gamma(1-3H)$ of the fractional power, the short dashes are the coefficients of the linear term: $F_2 = C_2 + \frac{D_2}{2H-2} + \frac{D_3}{2(3H-2)}$. We can see that the contribution of the linear term (used in the $R_{H,2,2}(t)$ approximation) for $H < 1$ and $t < 1$ is fairly small; whereas for $1 < H < 2$, it is larger and the $R_{H,2,2}(t)$ approximation is significantly better than the $R_{H,2,1}(t)$ approximation (see fig. B3).

Formatted: Font: 11 pt

Formatted: Font: 11 pt

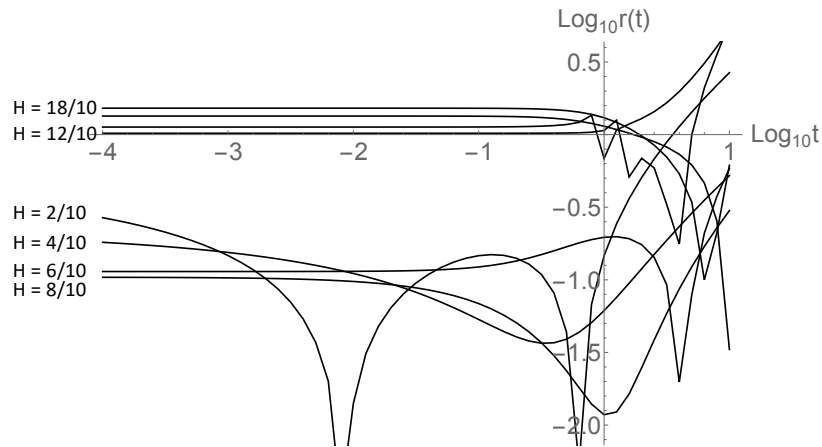


Fig. A3: This shows the logarithm of the relative error in the (2,1) approximation with respect to the deviation from the fGn $R_H(t)$ ($r = \log_{10} \left| 1 - \left(R_H^{fGn}(t) - R_{H,2,1}(t) \right) / \left(R_H^{fGn}(t) - R_H(t) \right) \right|$). For $H < 1$, $t < 0$ it is of the order $\approx 30\%$ whereas for $H > 1$, it is of the order 100% . The $H = 1$ (exponential) curve is not shown although when $t < 0$ the error is of order 60% .

Formatted: Font: 11 pt

Formatted: Font: 11 pt

Formatted: Font: 11 pt, Italic

Formatted: Font: 11 pt

Formatted: Font: 11 pt

B.1 Discussion

In section 2.3, we derived general statistical formulae for the auto-correlation functions of motions and noises defined in terms of Green's functions of fractional operators. Since the processes are Gaussian, autocorrelations fully determine the statistics. While the autocorrelations of fBm and fGn are well known (and discussed in section 3.1), those for fRm and fRn are new and are not so easy to deal with since they involve quadratic integrals of Mittag-Leffler functions:

In this appendix, we derive the leading terms in the basic small and large t expansions, including results of Padé approximants that provide accurate approximations to fRn at small times.

B.2 Small t behaviour

fRn statistics:

a) The range $0 < H < 1/2$:

Start with:

$$R_H(t) = N_H^2 \int_0^\infty G_{0,H}(t+s) G_{0,H}(s) ds \quad (90)$$

(eq. 34) and use the series expansion for $G_{0,H}$:

$$G_{0,H}(s) = \sum_{n=0}^\infty (-1)^{n+1} \frac{s^{(n+1)H-1}}{\Gamma(n+1)} \quad (91)$$

So that:

$$R_H(t) = N_H^2 \sum_{n,m=0}^\infty \frac{(-1)^{n+m}}{\Gamma(n+1)\Gamma(m+1)} \int_0^\infty (s+t)^{(n+1)H-1} s^{(m+1)H-1} ds \quad (92)$$

This can be written:

$$R_H(t) = N_H^2 t^{-1+2H} \sum_{n,m=0}^\infty A_{nm} t^{(m+n)H}; \quad A_{nm} = \frac{(-1)^{n+m}}{\Gamma(n+1)\Gamma(m+1)} \int_0^\infty (1+\xi)^{(n+1)H-1} \xi^{(m+1)H-1} d\xi \quad (93)$$

Evaluating the integral, and changing summation variables, we obtain:

$$A_{km} = \frac{(-1)^k \Gamma(1-H(k+2)) \sin(H\pi(m+1))}{\pi}; \quad k = m+n; \quad k < \left\lfloor \frac{1}{H} \right\rfloor - 2 \quad (94)$$

where we have taken $k = n + m$ and the square brackets indicate the integer part; beyond the indicated k range, the integrals diverge at infinity.

We can now sum over m :

$$R_H(t) = N_H^2 t^{-1+2H} \sum_{k=0}^{\left\lfloor \frac{1}{H} \right\rfloor - 2} B_k t^{kH}; \quad B_k = (-1)^k \frac{\Gamma(1-H(k+2)) \sin\left(H(k+1)\frac{\pi}{2}\right) \sin\left(H(k+2)\frac{\pi}{2}\right)}{\pi \sin\left(H\frac{\pi}{2}\right)} \quad (95)$$

where we have used:

$$\sum_{m=0}^{k+1} \sin(H\pi(m+1)) = \frac{\sin\left(H(k+1)\frac{\pi}{2}\right) \sin\left(H(k+2)\frac{\pi}{2}\right)}{\sin\left(H\frac{\pi}{2}\right)} \quad (96)$$

Finally, we can introduce the polynomial $f(z)$ and write:

$$R_H(t) = N_H^2 t^{-1+2H} f(t^H); \quad f(z) = \sum_{k=0}^{\left\lfloor \frac{1}{H} \right\rfloor - 2} B_k z^k \quad (97)$$

Taking the $k=0$ term only and using the $H < 1/2$ normalization $N_H = K_H$, we have

$K_H^2 B_0 = H(1+2H)$ and (as expected), we obtain the fGn result:

$$R_H(t) = H(1+2H) t^{-1+2H} + O(t^{-1+3H}); \quad t \ll 1; \quad 0 < H < 1/2 \quad (98)$$

(for t larger than the resolution τ).

Since the series is divergent, the accuracy decreases if we use more than one term in the sum. The series is nevertheless useful because the terms can be used to determine Padé approximants, and they can be quite accurate (see fig. B1 and the discussion below). The approximant of order 1, 2 was found to work very well over the whole range $0 < H < 3/2$.

b) The range $1/2 < H < 3/2$:

In this range, no terms in the expansion eq. 97 converge, however, the series still turns out to be useful. To see this use the identity:

$$2(1 - R_H(t)) = N_H^2 \int_0^\infty (G_{0,H}(s+t) - G_{0,H}(s))^2 ds + N_H^2 \int_0^t G_{0,H}(s)^2 ds; \quad N_H = C_H^{-1}; \quad H > 1/2$$

(99)

where we have used the $H > 1/2$ normalization $N_H = 1/C_H$.

It turns out that if we use this identity and substitute the series expansion for $G_{0,H}$, that the integrals converge up until order $m+n < [3/H] - 2$ (rather than $[1/H] - 2$), and the coefficients are identical. We obtain:

$$R_H(t) = 1 - N_H^2 t^{-1+2H} f(t^H); \quad f(z) = \sum_{k=0}^{\left[\frac{3}{H}\right]-1} B_k z^k; \quad 1/2 < H < 3/2 \quad (100)$$

where the B_k are the same as before. This formula is very close to the one for $0 < H < 1/2$ (eq. 97).

c) The range $3/2 < H < 2$:

Again using the identity eq. 99, we can make the approximation

$$G_{0,H}(s+t) - G_{0,H}(s) \approx t G'_{0,H}(s); \quad \text{this is useful since when } H > 3/2, \int_0^\infty G'_{0,H}(s)^2 ds < \infty \text{ and we}$$

obtain:

$$R_H(t) = 1 - \frac{t^2}{2C_H^2} \int_0^\infty G'_{0,H}(s)^2 ds + O(t^{2H-1}); \quad 3/2 < H < 2 \quad (101)$$

Padé:

Although the series (eqs. 97, 100) diverge, they can still be used to determine Padé approximants (see e.g. [Bender and Orszag, 1978]). Padé approximants are rational functions such that the first $N+M+1$ of their Taylor expansions of are the same as the first $N+M+1$ coefficients of the function f to which they approximate. The optimum (for $H < 1/4$) is the $N=1, M=2$ approximant ("Padé 12", denoted P_{12}). Applied to the function $f(z)$ in eq. 97, its first four terms are:

$$f(z) = B_0 + B_1 z + B_2 z^2 + B_3 z^3 \quad (102)$$

with approximant:

$$P_{12}(z) = \frac{B_0(B_1^2 - B_0B_2) + z(B_1^3 - 2B_0B_1B_2 + B_0^2B_3)}{B_0B_2 - B_1^2 + z(B_0B_3 - B_1B_2) + z^2(B_1B_3 - B_2^2)} \quad (103)$$

where the B_k are taken from the expansion eq. 95. Figures B1, B2 show that the approximants are especially accurate in the lower range of H values where the first term in the series (the fGn approximation) is particularly poor.

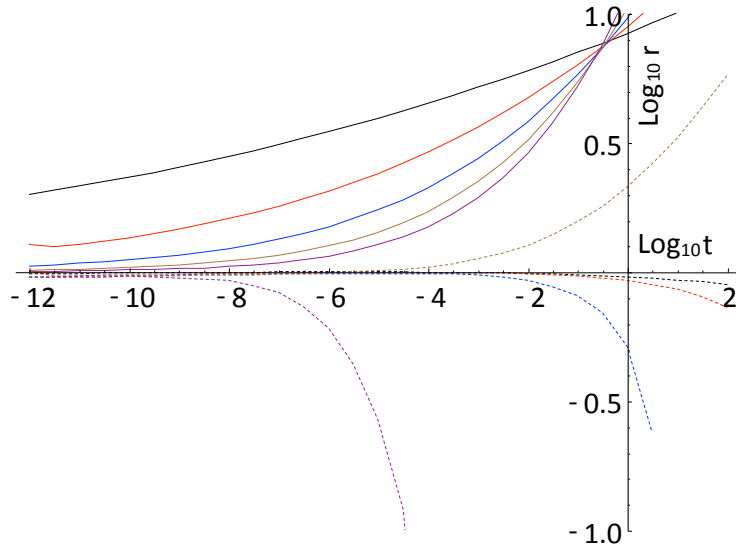


Fig. B1: The \log_{10} ratio of the fRn correlation function $R^{(fRn)}_{\mu}(t)$ to the fGn approximation $R^{(fGn)}_{\mu}(t)$ (solid) and to the Padé approximant $R^{(Padé)}_{\mu}(t)$ (dashed) for $H = 1/20$ (black), $2/20$ (red), $3/20$ (blue), $4/20$ (brown), $5/20$ (purple). The Padé approximant is the Padé12 polynomial (eq. 103). As H increases to 0.25, Padé gets worse, fGn gets better (see fig. B2).

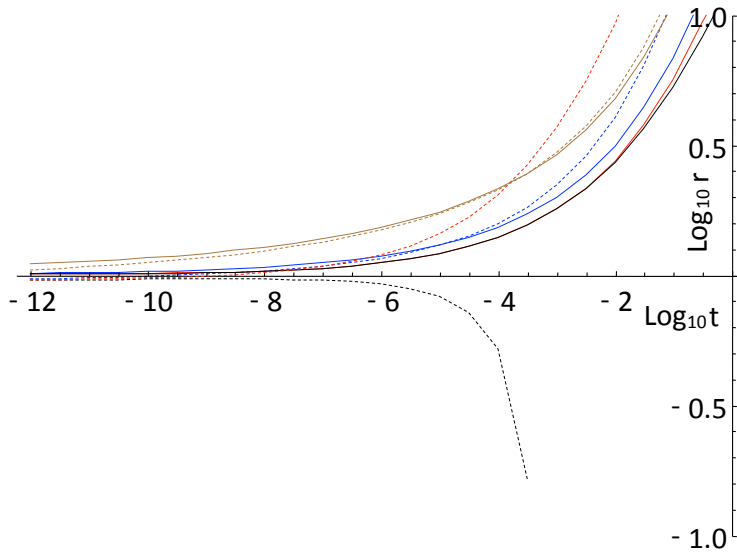


Fig. B2: The same as fig. B1 but for $H = 6/20$ (brown), $7/20$ (blue), $8/20$ (red), $9/20$ (black). The Padé12 approximant (dashed) is generally a bit worse than fGn approximation (solid).

fRm statistics:

For the small t behaviour of the motion fRm, it is simplest to integrate $R_H(t)$ twice:

$$V_H(t) = 2 \int_0^t \left(\int_0^s R_H(p) dp \right) ds \quad (104)$$

using the expansion eq. 95, we obtain:

$$V_H(t) = K_H^2 t^{1+2H} \sum_{k=0}^{\left[\frac{1}{H}\right]-2} \frac{B_k}{H(k+2)(1+H(k+2))} t^{kH} \quad ; \quad 0 < H < 1/2$$

$$V_H(t) = t^2 - C_H^{-2} t^{1+2H} \sum_{k=0}^{\left[\frac{3}{H}\right]-2} \frac{B_k}{H(k+2)(1+H(k+2))} t^{kH} \quad ; \quad 1/2 < H < 3/2$$

(105)

the leading terms are:

$$V_H(t) = t^{1+2H} + O(t^{1+3H}); \quad 0 < H < 1/2 \quad (t \ll 1) \quad (106)$$

and:

$$V_H(t) = t^2 - \frac{\Gamma(-1-2H)\sin(\pi H)}{\pi C_H^2} t^{1+2H} + O(t^{1+3H}); \quad 1/2 < H < 3/2 \quad (t \ll 1) \quad (107)$$

To find an expansion for the range $3/2 < H < 2$, we similarly integrate eq. 101:

$$V_H(t) = t^2 - \frac{t^4}{12C_H^2} \int_0^\infty G'_{0,H}(s)^2 ds + O(t^{2H+1}); \quad 3/2 < H < 2 \quad (108)$$

B.3 Large t behaviour:

When t is large, we can use the asymptotic t expansion:

$$(109)$$

to evaluate the first integral on the right in eq. 23. Using eq. 109 for the $G_{1,H}(s+t)$ term and the usual series expansion for the $G_{1,H}(s)$ we see that we obtain terms of the type:

$$\int_0^\infty (s+t)^{-mH} s^{nH} ds \propto t^{1-(m-n)H}; \quad (m-n)H > 1 \quad (110)$$

there will only be terms of decreasing order (the unit term has no t dependence).

Now consider the second integral in eq. 23:

$$I_2 = \int_0^t G_{1,H}(s)^2 ds \approx \int_0^t \left(1 - \frac{2s^{-H}}{\Gamma(1-H)} + \dots \right) ds \approx t - \frac{2t^{1-H}}{\Gamma(2-H)} + O(t^{1-2H}); \quad t \gg 1 \quad (111)$$

As long as $H < 1$, both of these terms will increase with t and will therefore dominate the first term: they will thus be the leading terms. We therefore obtain the expansion:

$$V_H(t) = N_H^2 \left[t - \frac{2t^{1-H}}{\Gamma(2-H)} + a_H + O(t^{1-2H}) \right] \quad (112)$$

where a_H is a constant term from the first integral. Putting the terms in leading order, depending on the value of H :

$$V_H(t) = N_H^2 \left[t - \frac{2t^{1-H}}{\Gamma(2-H)} + a_H + O(t^{1-2H}) \right]; \quad H < 1$$

$$V_H(t) = N_H^2 \left[t + a_H - \frac{2t^{1-H}}{\Gamma(2-H)} + O(t^{1-2H}) \right]; \quad H > 1 \quad (113)$$

To determine $R_H(t)$ we simply differentiate twice and multiply by $1/2$:

$$R_H(t) = -N_H^2 \left[\frac{t^{-1-H}}{\Gamma(-H)} + O(t^{-1-2H}) \right]; \quad 0 < H < 2 \quad (114)$$

Note that for $0 < H < 1$, $\Gamma(-H) < 0$ so that $R > 0$ over this range.

All the formulae for both the small and large t behaviours were verified numerically; see figs. 2, 3, 4.

1596

67

Formatted: Heading 1

Appendix CB: The $H=1/2$ special case:

When $H = 1/2$, the high frequency fGn limit is an exact “1/f noise”, (spectrum $\propto \omega^{-1}$) it has both high and low frequency divergences. The high frequency divergence can be tamed by averaging, but the not the low frequency divergence, so that fGn is only defined for $H < 1/2$. However, for the fRn, the low frequencies are convergent (appendix B) over the whole range $0 < H < 2$, and for $H = 1/2$ we find that the correlation function has a logarithmic dependence at both small and large scales. This is associated with particularly slow transitions from high to low frequency behaviours. The critical value $H = 1/2$ corresponds to the HEBE that was recently proposed [Lovejoy, 2020a; b] where it was shown that the value $H = 1/2$ could be derived analytically from the classical Budyko-Sellers energy balance equation.

is thus of intrinsic interest; and for fRn, it is possible to obtain exact analytic expressions for R_H , V_H and the Haar fluctuations; we develop these in this appendix, for some early results, see [Mainardi and Pironi, 1996]. For simplicity, we assume the normalization $N_H = 1$. [Hébert and Lovejoy, 2018; Lovejoy, 2019a; Mainardi and Pironi, 1996]

The starting point is the expression:

$$\begin{aligned} E_{1/2,1/2}(-z) &= \frac{1}{\sqrt{\pi}} - z e^{-z^2} \operatorname{erfc}(z) \\ E_{1/2,3/2}(-z) &= \frac{1 - e^{-z^2} \operatorname{erfc}(z)}{z} \end{aligned} \quad \operatorname{erfc}(z) = \frac{2}{\sqrt{\pi}} \int_z^\infty e^{-s^2} ds \quad (B1)$$

(e.g. [Podlubny, 1999]). From this, we obtain the impulse and step Green's functions:

$$\begin{aligned} G_{0,1/2}(t) &= \frac{1}{\sqrt{\pi t}} - e' \operatorname{erfc}(t^{1/2}) \\ G_{1,1/2}(t) &= 1 - e' \operatorname{erfc}(t^{1/2}) \end{aligned} \quad (B2)$$

(see eq. 16). The impulse response $G_{0,H}(t)$ can be written as a Laplace transform:

$$G_{0,1/2}(t) = \frac{1}{\pi} \int_0^\infty \frac{\sqrt{p}}{1+p} e^{-tp} dp \quad (B3)$$

Therefore, the correlation function is:

$$R_{1/2}(t) = \int_0^\infty G_{0,1/2}(t+s) G_{0,1/2}(s) ds = \frac{1}{\pi^2} \int_0^\infty ds e^{-s(p+q)} \int_0^\infty \int_0^\infty \frac{\sqrt{qp}}{(1+p)(1+q)} e^{-qt} dp dq \quad (B4)$$

Performing the s and p integrals we have:

$$R_{1/2}(t) = \frac{1}{2\pi} \int_0^\infty \left[\frac{1}{(1+q)} + \frac{\sqrt{q}}{(1+q)} - \frac{1}{(1+\sqrt{q})} \right] e^{-qt} dq \quad (B5)$$

Finally, this Laplace transform yields:

$$R_{1/2}(t) = \frac{1}{2} \left(e^{-t} \operatorname{erfi} \sqrt{t} - e' \operatorname{erfc} \sqrt{t} \right) - \frac{1}{2\pi} \left(e' \operatorname{Ei}(-t) + e^{-t} \operatorname{Ei}(t) \right) \quad (B6)$$

Formatted: Font: Italic

where:

$$Ei(z) = -\int_{-z}^{\infty} e^{-u} \frac{du}{u} \quad (B7)$$

and:

$$erfi(z) = -i(erf(iz)); \quad erf(z) = \frac{2}{\sqrt{\pi}} \int_0^z e^{-s^2} ds \quad (B8)$$

To obtain the corresponding V_H use:

$$V_{1/2}(t) = 2 \int_0^t \left(\int_0^s R_{1/2}(p) dp \right) ds \quad (B9)$$

The exact $V_{1/2}(t)$ is:

$$V_{1/2}(t) = G_{3,4}^{2,2} \left[t \begin{matrix} 2, & 2, & 5/2 \\ 2, & 2, & 0, & 5/2 \end{matrix} \right] + \frac{e^t}{\pi} (Shi(t) - Chi(t)) + (e^{-t} erfi(\sqrt{t}) - e^t erf(\sqrt{t})) \\ + t \left(1 + \frac{\gamma_E - 1}{\pi} \right) - 4\sqrt{\frac{t}{\pi}} + \frac{(1+t) \log t}{\pi} + 1 + \frac{\gamma_E}{\pi} \quad (B10)$$

where $G_{3,4}^{2,2}$ is the MeijerG function, Chi is the CoshIntegral function and Shi is the SinhIntegral function.

We can use these results to obtain small and large t expansions:

$$R_{1/2}(t) = -\left(\frac{2\gamma_E + \pi + 2 \log t}{2\pi} \right) + \frac{2\sqrt{t}}{\sqrt{\pi}} - \frac{t}{2} - \left(\frac{3 + 2\gamma_E + \pi + 2 \log t}{4\pi} \right) t^2 + O(t^{3/2}); \quad t \ll 1 \quad (B11)$$

$$R_{1/2}(t) = \frac{1}{2\sqrt{\pi}} t^{-3/2} - \frac{1}{\pi} t^{-2} + \frac{15}{8\sqrt{\pi}} t^{-7/2} + O(t^{-4}); \quad t \gg 1$$

where γ_E is Euler's constant = 0.57... and:

$$V_{1/2}(t) = -\frac{t^2 \log t}{\pi} + \frac{191 - 156\gamma_E - 78\pi}{144\pi} + \frac{16}{15\sqrt{\pi}} t^{5/2} - \frac{t^3}{6} - \frac{t^4 \log t}{12\pi} + O(t^{3/2}); \quad t \ll 1 \quad (B12)$$

$$V_{1/2}(t) = t + \frac{\pi + 2\gamma_E}{\pi} + \frac{2 \log t}{\pi} - \frac{4}{\sqrt{\pi}} t^{1/2} + \frac{1}{\sqrt{\pi}} t^{-1/2} - \frac{2}{\pi} t^{-2} + \frac{15}{4\sqrt{\pi}} t^{-3/2} + O(t^{-4}); \quad t \gg 1$$

We can also work out the variance of the Haar fluctuations:

$$\langle \Delta U_{1/2}^2(\Delta t) \rangle = \frac{\Delta t^2 \log \Delta t}{4\pi} + \frac{6\pi + 12\gamma_E - \log 16 + 960 \log 2}{240\pi} + \frac{512(\sqrt{2} - 2)}{240\sqrt{\pi}} \Delta t^{1/2} + \frac{\Delta t}{3} + O(\Delta t^{3/2}); \quad \Delta t \ll 1 \quad (B13)$$

Formatted: MTDisplayEquation

$$\langle \Delta U_{1/2}^2(\Delta t) \rangle = 4\Delta t^{-1} - \frac{32\sqrt{2}}{\sqrt{\pi}} \Delta t^{-3/2} + \frac{3t^{-2} \log \Delta t}{\pi} + O(\Delta t^{-2}); \quad \Delta t \gg 1$$

Figure C4-B1 shows numerical results for the fRn with $H = 1/2$, the transition between small and large t behaviour is extremely slow; the 9 orders of magnitude depicted in the figure are barely enough. The extreme low $(R_{1/2})^{1/2}$ (dashed) asymptotes at the left to a slope zero (a square root logarithmic limit, eq. 425B11), and to a $-3/4$ slope at the right. The RMS Haar fluctuation (black) changes slope from 0 to $-1/2$ (left to right). This is shown more clearly in fig. C2-B2 that shows the logarithmic derivative of the RMS Haar (black) compared to a regression estimate over two orders of magnitude in scale (blue; a factor 10 smaller and 10 larger than the indicated scale was used). This figure underlines the gradualness of the transition from $H = 0$ to $H = -1/2$. If empirical data were available only over a factor of 100 in scale, depending on where this scale was with respect to the relaxation time scale (unity in the plot), the RMS Haar fluctuations could have any slope in the range 0 to $-1/2$ with only small deviations.

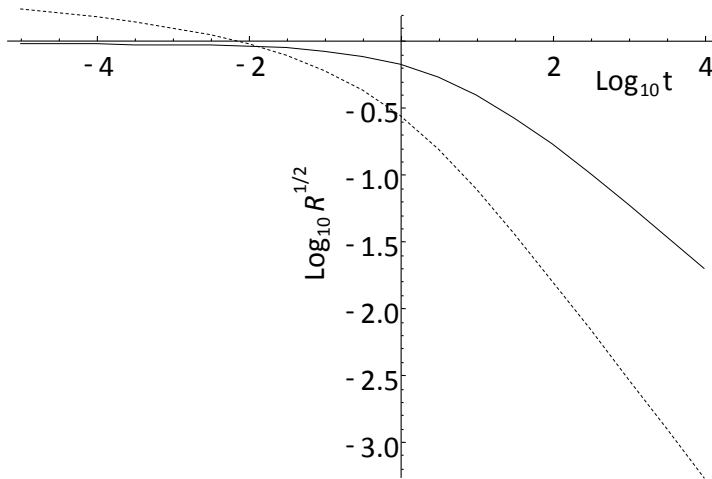
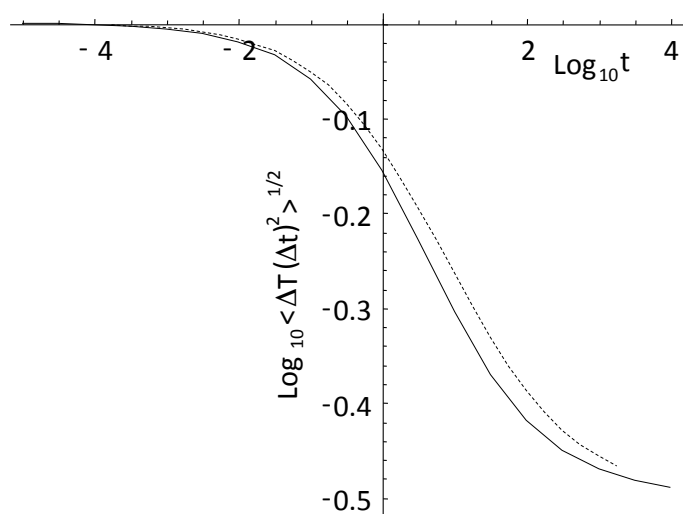


Fig. C4-B1: fRn statistics for $H = 1/2$: the solid line is the RMS Haar fluctuation, the dashed line is the root correlation function $(R_{1/2})^{1/2}$ (the normalization constant = 1, it has a logarithmic divergence at small t).

Formatted: Font: Times New Roman, 11 pt



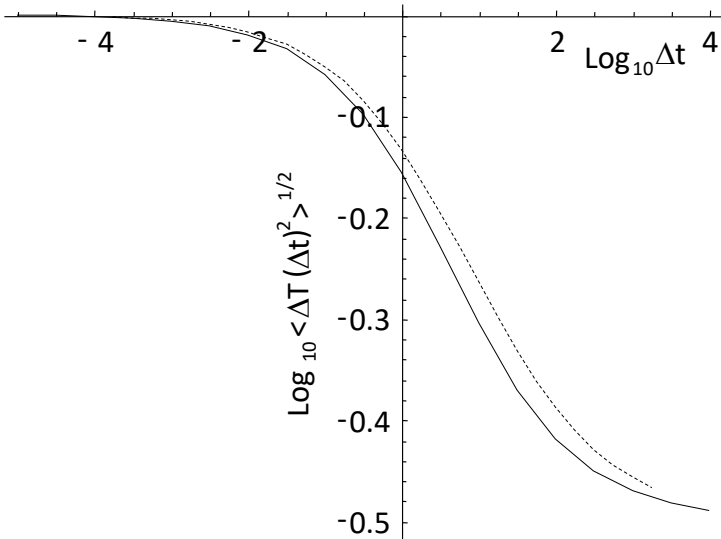


Fig. C2B2: The logarithmic derivative of the RMS Haar fluctuations (solid) in fig. C1-B1 compared to a regression estimate over two orders of magnitude in scale (dashed; a factor 10 smaller and 10 larger than the indicated scale was used). This plot underlines the gradualness of the transition from $H = 0$ to $H = -1/2$: over range of 100 or so in scale there is approximate scaling but with exponents that depend on the range of scales covered by the data. If data were available only over a factor of 100 in scale, the RMS Haar fluctuations could have any slope in the fGn range 0 to $-1/2$ with only small deviations.

Formatted: Font: 11 pt

References:

- Atanackovic, M., Pilipovic, S., Stankovic, B., and Zorica, D., *Fractional Calculus with applications in mechanics: variations and diffusion processes*, 313 pp., Wiley, 2014.
- Bender, C. M., and Orszag, S. A., *Advanced mathematical methods for scientists and engineers*, Mc Graw Hill, 1978.
- Biagini, F., Hu, Y., Øksendal, B., and Zhang, T., *Stochastic Calculus for Fractional Brownian Motion and Applications*, Springer-Verlag, 2008.
- Budyko, M. I., The effect of solar radiation variations on the climate of the earth, *Tellus*, 21, 611-619, 1969.
- Buizza, R., Miller, M., and Palmer, T. N., Stochastic representation of model uncertainties in the ECMWF Ensemble Prediction System, *Q. J. Roy. Meteor. Soc.*, 125, 2887-2908, 1999.
- Chekroun, M. D., Simonnet, E., and Ghil, M., Stochastic Climate Dynamics: Random Attractors and Time-dependent Invariant Measures *Physica D*, 240, 1685-1700 2010.
- Coffey, W. T., Kalmykov, Y. P., and Titov, S. V., Characteristic times of anomalous diffusion in a potential, in *Fractional Dynamics: Recent Advances*, edited by J. Klafter, S. Lim and R. Metzler, pp. 51-76, World Scientific, 2012.
- Del Rio Amador, L., and Lovejoy, S., Predicting the global temperature with the Stochastic Seasonal to Interannual Prediction System (StocSIPS) *Clim. Dyn.* doi: org/10.1007/s00382-019-04791-4, 2019.
- Del Rio Amador, L., and Lovejoy, S., Long-range Forecasting as a Past Value Problem: Using Scaling to Untangle Correlations and Causality *Geophys. Res. Lett.*, (submitted, Nov. 2020), 2020a.
- Del Rio Amador, L., and Lovejoy, S., Using scaling for seasonal global surface temperature forecasts: StocSIPS *Clim. Dyn.*, under review, 2020b.
- Dijkstra, H., *Nonlinear Climate Dynamics*, 357 pp., Cambridge University Press, 2013.
- Franzke, C., and O'Kane, T. (Eds.), *Nonlinear and Stochastic Climate Dynamics*, Cambridge University Press, Cambridge, 2017.
- Gripenberg, G., and Norros, I., On the Prediction of Fractional Brownian Motion *J. Appl. Prob.*, 33, 400-410, 1996.
- Hasselmann, K., Stochastic Climate models, part I: Theory, *Tellus*, 28, 473-485, 1976.
- Hebert, R. (2017), A Scaling Model for the Forced Climate Variability in the Anthropocene, MSc thesis, McGill University, Montreal.
- Hébert, R., and Lovejoy, S., Regional Climate Sensitivity and Historical Based Projections to 2100, *Geophys Res Lett.*, 45, 4248-4254 doi: 10.1002/2017GL076649, 2018.
- Hébert, R., Lovejoy, S., and Tremblay, B., An Observation-based Scaling Model for Climate Sensitivity Estimates and Global Projections to 2100, *Climate Dynamics*, (in press), 2020.
- Herrmann, R., *Fractional Calculus: an Introduction for Physicists*, World Scientific, 2011.
- Hilfer, R. (Ed.), *Applications of Fractional Calculus in Physics* World Scientific, 2000.

- 1717 Hipel, K. W., and McLeod, A. I., *Time series modelling of water resources and*
 1718 *environmental systems*, 1st edn. ed., Elsevier, 1994.
- 1719 Hurst, H. E., Long-term storage capacity of reservoirs, *Transactions of the American*
 1720 *Society of Civil Engineers*, 116, 770-808, 1951.
- 1721 IPCC, *Climate Change 2013: The Physical Science Basis. Contribution of Working Group*
 1722 *I to the Fifth Assessment Report of the Intergovernmental Panel on Climate Change*,
 1723 Cambridge University Press: Cambridge, 2013.
- 1724 Jumarie, G., Stochastic differential equations with fractional Brownian motion inputs,
 1725 *Int. J. Systems. Sci.*, 24, 1113, 1993.
- 1726 Karczewska, A., and Lizama, C., Solutions to stochastic fractional relaxation equations,
 1727 *Phys. Scr.*, T136 7pp doi: 10.1088/0031-8949/2009/T136/014030 2009.
- 1728 Kobelev, V., and Romanov, E., Fractional Langevin Equation to Describe Anomalous
 1729 Diffusion *Prog. of Theor. Physics Supp.*, 139, 470-476, 2000a.
- 1730 Kobelev, V., and Romanov, E., Fractional Langevin Equation to Describe Anomalous
 1731 Diffusion, *Progress of Theoretical Physics Supplement*, 139, 470-476, 2000b.
- 1732 Kou, S. C., and Sunney Xie, X., Generalized Langevin Equation with Fractional Gaussian
 1733 Noise: Subdiffusion within a Single Protein Molecule, *Phys. Rev. Lett.*, 93, 4 doi:
 1734 10.1103/PhysRevLett.93.180603, 2004.
- 1735 Lovejoy, S., Using scaling for macroweather forecasting including the pause, *Geophys.*
 1736 *Res. Lett.*, 42, 7148-7155 doi: DOI: 10.1002/2015GL065665, 2015.
- 1737 Lovejoy, S., The spectra, intermittency and extremes of weather, macroweather and
 1738 climate, *Nature Scientific Reports*, 8, 1-13 doi: 10.1038/s41598-018-30829-4, 2018.
- 1739 Lovejoy, S., The half-order energy balance equation, *J. Geophys. Res. (Atmos.)*,
 1740 (submitted, Nov. 2019), 2019a.
- 1741 Lovejoy, S., *Weather, Macroweather and Climate: our random yet predictable*
 1742 *atmosphere*, 334 pp., Oxford U. Press, 2019b.
- 1743 Lovejoy, S., The Half-order Energy Balance Equation, Part 1: The homogeneous HEBE
 1744 and long memories, *Earth Syst. Dyn. Disc.* doi: <https://doi.org/10.5194/esd-2020-12>,
 1745 2020a.
- 1746 Lovejoy, S., The Half-order Energy Balance Equation, Part 2: The inhomogeneous
 1747 HEBE and 2D energy balance models, *Earth Sys. Dyn. Disc.* doi:
 1748 <https://doi.org/10.5194/esd-2020-13>, 2020b.
- 1749 Lovejoy, S., *Weather, Macroweather and Climate: our random yet predictable*
 1750 *atmosphere* Oxford U. press, 2019c.
- 1751 Lovejoy, S., and Schertzer, D., *The Weather and Climate: Emergent Laws and*
 1752 *Multifractal Cascades*, 496 pp., Cambridge University Press, 2013.
- 1753 Lovejoy, S., Del Rio Amador, L., and Hébert, R., Harnessing butterflies: theory and
 1754 practice of the Stochastic Seasonal to Interannual Prediction System (StocSIPS), , in
 1755 *Nonlinear Advances in Geosciences*, , edited by A. A. Tsonis, pp. 305-355, Springer
 1756 Nature, 2017.
- 1757 Lovejoy, S., del Rio Amador, L., and Hébert, R., The ScaLIng Macroweather Model
 1758 (SLIMM): using scaling to forecast global-scale macroweather from months to
 1759 Decades, *Earth Syst. Dynam.*, 6, 1-22 doi: www.earth-syst-dynam.net/6/1/2015/,
 1760 doi:10.5194/esd-6-1-2015, 2015.
- 1761 Lovejoy, S., Procyk, R., del Rio Amador, L., and Hébert, R., The fractional Energy
 1762 Balance Equation, *Quart. J. Roy. Meteor. Soc.*, under review, 2020a.

- 1763 Lovejoy, S., Procyk, R., Hébert, R., and del Rio Amador, L., The Fractional Energy
 1764 Balance Equation, *Quart. J. Roy. Met. Soc.*, (under revision), 2020b.
- 1765 Lutz, E., Fractional Langevin equation, *Physical Review E*, 64, 4 doi:
 1766 10.1103/PhysRevE.64.051106, 2001.
- 1767 Mainardi, F., and Pironi, P., The Fractional Langevin Equation: Brownian Motion
 1768 Revisited, *Extracta Mathematicae* 10 140–154, 1996.
- 1769 Mandelbrot, B. B., *The Fractal Geometry of Nature*, Freeman, 1982.
- 1770 Mandelbrot, B. B., and Van Ness, J. W., Fractional Brownian motions, fractional noises
 1771 and applications, *SIAM Review*, 10, 422-450, 1968.
- 1772 Mandelbrot, B. B., and Wallis, J. R., Computer Experiments with fractional gaussian
 1773 noises: part 3, mathematical appendix, *Water Resour Res*, 5, 260–267 doi:
 1774 org/10.1029/WR005i001p00260, 1969.
- 1775 Metzler, R., and Klafter, J., The Random Walks Guide To Anomalous Diffusion: A
 1776 Fractional Dynamics Approach, *Physics Reports*, 339, 1-77, 2000.
- 1777 Miller, K. S., and Ross, B., *An introduction to the fractional calculus and fractional*
 1778 *differential equations*, 366 pp., John Wiley and Sons, 1993.
- 1779 Newman, M., An Empirical Benchmark for Decadal Forecasts of Global Surface
 1780 Temperature Anomalies, *J. of Clim.*, 26, 5260-5269 doi: DOI: 10.1175/JCLI-D-12-
 1781 00590.1, 2013.
- 1782 Nonnenmacher, T. F., and Metzler, R., Applications of fractional calculus techniques to
 1783 problems in biophysics, in *Fractional Calculus in physics*, edited by R. Hilfer, pp. 377-
 1784 427, World Scientific, 2000.
- 1785 Palma, W., *Long-memory time series*, Wiley, 2007.
- 1786 Palmer, T. N., and Williams, P. (Eds.), *Stochastic physics and Climate models*, 480 pp.,
 1787 Cambridge University Press, Cambridge, 2010.
- 1788 Papoulis, A., *Probability, Random Variables and Stochastic Processes*, Mc Graw Hill,
 1789 1965.
- 1790 Penland, C., A stochastic model of IndoPacific sea surface temperature anomalies
 1791 *Physica D*, 98, 534-558, 1996.
- 1792 Penland, C., and Magorian, T., Prediction of Nino 3 sea surface temperatures using
 1793 linear inverse modeling, *J. Climate*, 6, 1067–1076, 1993.
- 1794 Podlubny, I., *Fractional Differential Equations*, 340 pp., Academic Press, 1999.
- 1795 Procyk, R., Lovejoy, S., and Hébert, R., The Fractional Energy Balance Equation for
 1796 Climate projections through 2100, *Earth Sys. Dyn. Disc.*, under review doi:
 1797 org/10.5194/esd-2020-48 2020.
- 1798 Rypdal, K., Global temperature response to radiative forcing: Solar cycle versus
 1799 volcanic eruptions, *J. Geophys. Res.*, 117, D06115 doi: 10.1029/2011JD017283, 2012.
- 1800 Sardeshmukh, P., Compo, G. P., and Penland, C., Changes in probability associated with
 1801 El Nino, *J. Climate*, 13, 4268-4286, 2000.
- 1802 Sardeshmukh, P. D., and Sura, P., Reconciling non-gaussian climate statistics with
 1803 linear dynamics, *J. of Climate*, 22, 1193-1207, 2009.
- 1804 Schertzer, D., and Lovejoy, S., Physical modeling and Analysis of Rain and Clouds by
 1805 Anisotropic Scaling of Multiplicative Processes, *Journal of Geophysical Research*, 92,
 1806 9693-9714, 1987.

- 1807 Schertzer, D., Larchevue, M., Duan, J., Yanovsky, V. V., and Lovejoy, S., Fractional
1808 Fokker-Planck equation for nonlinear stochastic differential equation driven by non-
1809 Gaussian Levy stable noises, *J. of Math. Physics*, 42, 200-212, 2001.
- 1810 Schiessel, H., Friedrich, C., and Blumen, A., Applications to problems in polymer
1811 physics and rheology, in *Fractional Calculus in physics*, edited by R. Hilfer, pp. 331-376,
1812 World Scientific, 2000.
- 1813 Sellers, W. D., A global climate model based on the energy balance of the earth-
1814 atmosphere system, *J. Appl. Meteorol.*, 8, 392-400, 1969.
- 1815 van Hateren, J. H., A fractal climate response function can simulate global average
1816 temperature trends of the modern era and the past millennium, *Clim. Dyn.* , 40, 2651
1817 doi: <https://doi.org/10.1007/s00382-012-1375-3>, 2013.
- 1818 Vojta, T., Skinner, S., and Metzler, R., Probability density of the fractional Langevin
1819 equation with reflecting walls, *Phys. Rev. E* 100, , 042142 doi:
1820 10.1103/PhysRevE.100.042142, 2019.
- 1821 Watkins, N., Fractional Stochastic Models for Heavy Tailed, and Long-Range
1822 Dependent, Fluctuations in Physical Systems, in *Nonlinear and Stochastic Climate*
1823 *Dynamics*, edited by C. Franzke and O. K. T., pp. 340-368, Cambridge University Press,
1824 2017.
- 1825 Watkins, N., chapman, s., Klages, R., Chechkin, A., Ford, I., and stainforth, d.,
1826 Generalised Langevin Equations and the Climate Response Problem, *Earth and Space*
1827 *Science Open Archive* doi: doi:10.1002/essoar.10501367.1, 2019.
- 1828 Watkins, N. W., Chapman, S. C., Chechkin, A., Ford, I., Klages, R., and Stainforth, D. A.,
1829 On Generalized Langevin Dynamics and the Modelling of Global Mean Temperature,
1830 *arXiv:2007.06464v1*, [cond-mat.stat-mech] 2020.
- 1831 West, B. J., Bologna, M., and Grigolini, P., *Physics of Fractal Operators*, 354 pp., Springer,
1832 2003.
- 1833